An experimental and computational investigation of organic molecular cocrystals

by

Thalia Carstens

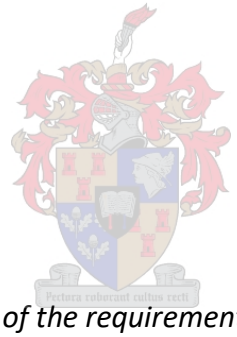

Thesis presented in partial fulfilment of the requirements for the degree of Master of Science in chemistry at Stellenbosch University

Supervisor: Prof. Delia A. Haynes
Co-supervisor: Dr. Vincent J. Smith
Faculty of Science
Department of Chemistry and Polymer Science

December 2017

Declaration

By submitting this thesis electronically, I declare that the entirety of the work contained therein is my own, original work, that I am the sole author thereof (save to the extent explicitly otherwise stated), that reproduction and publication thereof by Stellenbosch University will not infringe any third-party rights and that I have not previously in its entirety or in part submitted it for obtaining any qualification.

December 2017

Abstract

Cocrystals have historically provided a unique platform for studying and tuning structure-property relationships of materials. In this study, co-crystallisation was specifically investigated as a possible way to prevent unwanted dimerisation in dithiadiazolyl (DTDA) radicals. Attempts were made to co-crystallise DTDAs with one another, as well as with TEMPO radical, *p*-benzoquinone (BQ) and 2,3-dichloro-5,6-dicyanobenzoquinone (CCBQ). A cocrystal between the TEMPO radical and CCBQ, {TEMPO}{CCBQ}, was successfully obtained by both co-grinding of the co-formers and recrystallisation from methanol.

Molecular gas-phase and periodic binding energy calculations on the three known DTDA cocrystals showed that the heterodimers (cocrystals) were consistently more stable than the homodimers of the co-formers. Using the known cocrystal results as a benchmark, similar calculations carried out on a series of experimentally attempted co-former combinations indicated that some combinations may warrant further investigation. The DTDA radical 4′-(2,6-difluorophenyl)-DTDA (**3)** is known to be polymorphic, and conversion between these polymorphs was observed in this study. Differential scanning calorimetry (DSC) identified a phase change from **3γ** to **3β** upon heating, and a transformation of **3α** to **3γ** was observed over time at room temperature, however this has not yet been observed using thermal analysis.

The effect of a change in halogen substituent on the structures of a series of {*p*-halophenol}{*p*-benzoquinone} ({XP}{BQ}, where X is a halogen) cocrystals has been investigated. Two new cocrystals, {4-fluorophenol}{BQ} ({FP}{BQ}) and {4-iodophenol}{BQ} ({IP}{BQ}), were found in this study, where the chloro- and bromo-derivatives are previously known. Both 1:1 and 2:1 cocrystals of {FP}{BQ} was obtained concomitantly. The 1:1 form, {1FP}{BQ}, also has two polymorphs where **α**-{1FP}{BQ} and **β**-{1FP}{BQ} were obtained by

recrystallisation and sublimation, respectively. {IP}{BQ} was only found to crystallise as the 2:1 form. This form also has two polymorphs, with **α**-{2IP}{BQ} and **β**-{2IP}{BQ} obtained from recrystallisation and sublimation, respectively. Although the previously-known cocrystals were found to be isostructural to one another, none of the newly obtained forms or polymorphs were isostructural to each other or to the known cocrystals.

Uittreksel

Kokristalle het histories ’n unieke platform geskep vir die bestudering en afstemming van materiale se struktuur-eienskap verhoudings. In hierdie studie is kokristallisasie spesifiek ondersoek as 'n moontlike manier om ongewenste dimerisasie in dithiadiazolyl radikale (DTDA) te voorkom. Daar is gepoog om DTDA's met mekaar te kristalliseer, sowel as met TEMPO radikaal, p-bensokinoon (BQ) en 2,3-dichloor-5,6-disiano bensokinoon (CCBQ). 'n Kokristal tussen die TEMPO radikaal en CCBQ {TEMPO}{CCBQ} is suksesvol verkry deur beide mede-maling van die mede-vormers, en herkristallisasie uit metanol.

Molekulêre gasfase en periodiese bindingsenergie berekenings op die drie bekende DTDA-kokristalle het getoon dat die heterodimere (kokristalle) konsekwent meer stabiel is as die homodimere van die mede-vormers. Deur gebruik te maak van die bekende kokristal resultate as 'n maatstaf, het soortgelyke berekenings wat uitgevoer is op 'n reeks eksperimentele kokristal pogings aangedui dat sommige van dié kombinasies verdere ondersoek kan regverdig. Die DTDA radikaal 4’-(2,6-difluorofeniel)-DTDA (**3**) word geken om polimorfies te wees, en in hierdie studie is die verandering tussen dié polimorfe waargeneem. Differensiële skanderingskalorimetrie (DSK) het 'n faseverandering van **3γ** tot **3β** geïdentifiseer tydens verwarming, en 'n transformasie van **3α** tot **3γ** is mettertyd waargeneem by kamertemperatuur. Maar laasgenoemde is nog nie met behulp van termiese analise bevestig nie.

Die effek van 'n verandering in halogeensubstituent op die strukture van 'n reeks {p-halofenol}{p-benzoquinone} ({XP}{BQ}, waar X 'n halogeen is) kokristalle is ondersoek. Twee nuwe kokristalle, {4-fluorofenol}{BQ} ({FP}{BQ}) en {4-jodofenol}{BQ} ({IP}{BQ}), is in hierdie studie gevind waar die chloor- en broomderivate vooraf bekend is. Beide 1:1 en 2:1 kokristalle van {FP}{BQ} is gelyktydig verkry. Twee polimorfe van die 1:1-vorm, {1FP} {BQ}, het ook verskyn,

waar α-{1FP}{BQ} en β-{1FP}{BQ} onderskeidelik deur herkristallisasie en sublimasie verkry is. {IP}{BQ} het slegs gekristalliseer as die 2:1-vorm. Hierdie vorm het ook twee polimorfe, waar α-{2IP}{BQ} en β-{2IP}{BQ} onderskeidelik verkry is uit herkristallisasie en sublimasie. Alhoewel die voorheen bekende kokristalle bevind is om isostruktureel te wees teenoor mekaar, was geen van die nuut verkrygde vorms of polimorfe bevind om isostruktureel teenoor mekaar, of teenoor die voorheen bekende kokristalle te wees nie.

Acknowledgements

Firstly, I would like to thank my two supervisors, Prof. Delia Haynes and Dr. Vincent Smith. Thank you to Delia for introducing me to supramolecular chemistry in undergraduate, for allowing me creative freedom to make my project my own, for helping to provide the resources I needed to undertake the project, and for being involved. Thank you to Vincent for your consistent interest in my work, even though a large part of it is not related to your specific field of research. Thank you for patiently showing me the ropes on so many instruments and listening to the rants of the late-night crew in the office.

Secondly, a huge thank you to my family, whom I love dearly. To my parents for their endless support, without which I would not have been completing a masters degree now, and to my brother for being my friend and always having my back. To my extended family who have supported me and walked a close journey with me throughout my years at university, thank you. I would also like to extend a thank you to my friends not involved in my project or anything chemistry related, for keeping me in touch with the world beyond the chemistry lab and for the support and companionship.

Thank you to the Supramolecular Chemistry group, whom I have not only had the pleasure of sharing office and lab space with, but many journeys including conferences, wine tastings, wine festivals, cheese and wines, and all things wine-related. Thank you to Charl, Dewald and Bernard for introducing me to computational chemistry and being a constant help, and a special thank you to Dewald for answering my computational questions, even whilst burning the midnight oil. Thank you also to Leigh, for selflessly sharing your knowledge.

Finally, I would like to thank the support staff for their service in and around the labs, Elsa at NMR, and Malcolm for making the specialised glassware for this project. A big thank you also to Stellenbosch University for providing me with the facilities for this project, as well as the National Research Foundation for funding.

Publications and Posters

Conferences

Part of this work was presented at three conferences:

10th national Centre for High Performance Computing conference, 5-9 December 2016, East London: *Dithiadiazolyl radicals – A theoretical investigation of cocrystal formation*

23rd International Conference on the Chemistry of the Organic Solid State, 2-7 April 2017, Stellenbosch: *Dithiadiazolyl radicals – A theoretical investigation of cocrystal formation*

24th Congress of the International Union of Crystallography, 21-28 August 2017 Hyderabad, India: *Multicomponent dithiadiazolyl crystals as a route to novel magnetic materials*

List of abbreviations

χ_i	KS one-electron spin orbitals
∇^2	Laplacian operator
4-CNDTDA	4'-(4-cyanoperfluorophenyl)-1,2,3,5-dithiadiazolyl
BQ	p-benzoquinone
BrP	4-bromophenol
CCBQ	2,3-dichloro-5,6-dicyanobenzoquinone
ClP	4-chlorophenol
DFT	Density Functional Theory
DSC	Differential Scanning Calorimetry
DTDA	dithiadiazolyl radicals
E_0	ground state energy of a system
F_2DTDA	4'-(2,6-difluorophenyl)-1,2,3,5-dithiadiazolyl
FP	4-fluorophenol
GGA	general gradient approximation
GUI	graphical user interface
ħ	Planck's constant
HF	Hartree-Fock
HMDS	hexamethyldisilazane
IP	4-iodophenol
IR	Infrared Spectroscopy
KS	Kohn-Sham
LAG	liquid-assisted grinding
LDA, LSDA	local (spin) density approximation
MS	mass Spectrometry
NMR	nuclear magnetic resonance
PhDTDA	4-phenyl-1,2,3,5-dithiadiazolyl
p-NPNN	p-nitrophenyl nitronyl nitroxide
PXRD, VT-PXRD	(variable temperature) powder X-ray diffractometry
QM	quantum mechanics
RHF	Restricted Hartree-Fock
ROHF	Restricted Open-shell Hartree-Fock

SCF	self-consistent field
SOMO	singly occupied molecular orbital
SP	single point
TCNE	tetracyanoethylene
TEMPO	(2,2,6,6-tetramethylpiperidin-1-yl)oxyl radical
TGA	thermogravimetric analysis
UHF	Unrestricted Hartree-Fock
α, β	spin functions (HF)
φ	spatial orbital
Ψ	wave function
$\hat{H}$	Hamiltonian operator
δ_{ij}	Kronecker delta
$\phi_i(\vec{x}_i)$	one-electron spin orbitals

Table of Contents

This thesis is dedicated to my grandfather,
Pieter Carstens

Chapter 1

Introduction

ONLY A FOOL KNOWS EVERYTHING.
--THE CHEMIST ANALYST, SEPTEMBER 1946

The compounds studied during this project are related to the field of molecular magnetism in that they are either organic radicals, or could possibly form radical compounds. They also exhibited a wide range of solid-state phenomena that include polymorphism, cocrystal formation, and a range of intermolecular interactions. This chapter will introduce and address these properties as well as give some background to quantum mechanical methods applied in this study.

1.1 Supramolecular chemistry

Over the years the field of "supramolecular chemistry" has taken a number of forms[1], all of which agree on some main aspects: it is the chemistry aimed at developing increasingly complex systems with some specific properties, explicitly through focus on non-covalent interactions. The blanket term of *supramolecular chemistry* includes host-guest chemistry, self-assembly, soft/smart materials, crystal engineering, nanotechnology, supramolecular devices and, at the interface with the biological sciences, biological chemistry (see for example Figure 1.1).

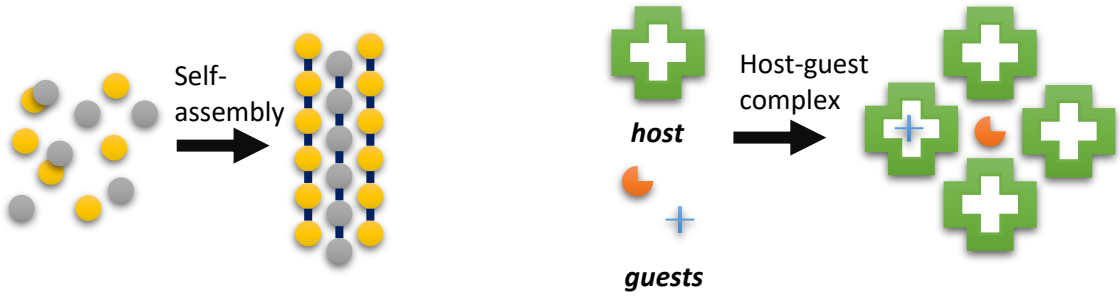

Figure 1.1. Simple example of left) molecular self-assembly, and right) a host-guest system.

Fundamentally, research in the subfields of supramolecular chemistry is concerned with the interactions between molecules and the relationship of these with the properties of the resulting materials.

1.1.1 Supramolecular synthons

Understanding the interactions in crystal packing is an essential step towards the modification and prediction of packing motifs as well as physical properties of materials. Crystal structures often contain patterns of functional groups involved in common interactions that, from a

crystal engineering* perspective, can be a useful tool for solid-state modification. These common interactions were described by Desiraju[2] as *supramolecular synthons*, defined as

> *"structural units within supermolecules which can be formed and/or assembled by known or conceivable synthetic operations involving intermolecular interactions."*

Some familiar groups of supramolecular synthons include hydrogen bonds, halogen bonds (including halogen-halogen contacts[3]) and π-stacking (Figure 1.4). These are commonly occurring supramolecular synthons in organic magnetic materials and were explicitly exploited during this project.[4–6]

1.1.1.1 van der Waals interactions

At infinite separation, two atoms have no interactions between them. However, as they approach one another the atoms start interacting due to the correlated motion of electrons. These interaction forces are commonly referred to as *dispersion*, *London* forces, or *van der Waals* forces. Interactions in this class are generally quite weak and not very structure-directing[1], however, they play an important role in the packing of molecules in the solid state as well as in biological systems.[7]

1.1.1.2 Hydrogen bonding

Pauling introduced the concept of hydrogen bonding (H-bond)[8], however, since then a number of definitions have arisen. An accepted definition seems to be when a hydrogen atom, H, that is covalently bound to an electronegative atom X, is involved in an attractive electrostatic interaction with another electronegative atom, Y, nearby such that X-H···Y-Z.[9] Y may also be a charged atom, then it is termed a charge-assisted H-bond. The X-H···Y angle of

* Crystal engineering looks at understanding intermolecular interactions and molecular recognition in the context of crystal packing, to establish a connection between molecular and supramolecular structures of materials.[2]

a hydrogen bond is typically around 180°, and the interaction may decrease in strength as it deviates from this angle.[9] H-bonds strongly influence packing modes since they add directionality in the packing, making them potentially important supramolecular synthons in supramolecular self-assembly and general structure prediction (see Figure 1.2 for examples of H-bonding).

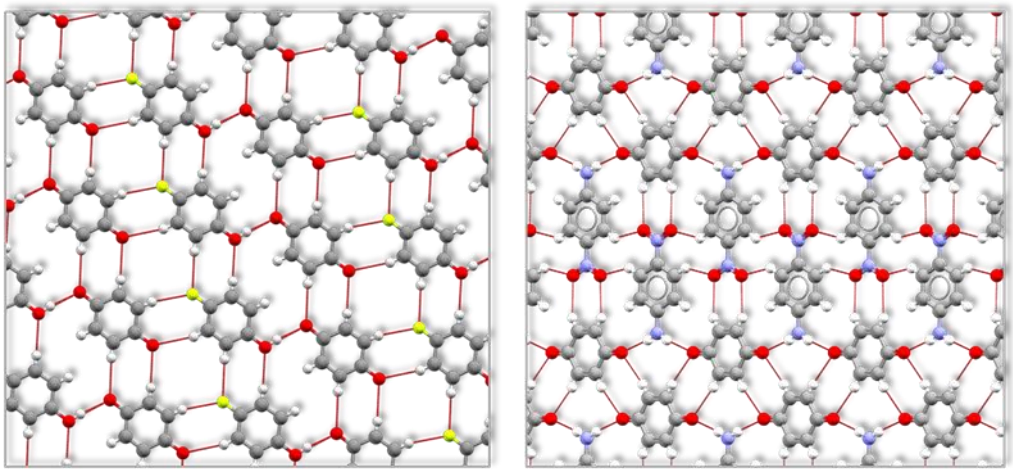

Figure 1.2. Two examples of hydrogen bonds in a crystal structure. Left: {FP}{BQ} cocrystal, which will be discussed in chapter 5; Right) REFCODE: BAPMAH[10]. Hydrogen bonds are displayed in red.

1.1.1.3 Halogen bonding

Another very important structure-directing interaction in supramolecular chemistry is the halogen bond. Politzer *et al.* defined the halogen bond as an electrostatically-driven, noncovalent interaction between a region of positive electrostatic potential on a halogen atom X in R-X and a negative site on atom B (R-X···B), where B can be the lone pair on a Lewis base of the π-system on an unsaturated molecule.[11,12] The directionality of the halogen bond arises due to the positive electrostatic potential along the extension of the R-X bond, created due to the σ-hole – an area of charge-depletion on the half-filled *p*-orbital of the *X* atom involved in covalent bonding. Some would argue that halogen bonding is counterintuitive since covalently-bound halogen atoms themselves are typically negative. However, others have argued that atoms can have regions of both positive and negative character on the same atom,

in different areas, supporting the argument for the existence of the noncovalent halogen bond.[13] There has also been some debate around whether halogen-halogen (X-X') contacts can be classified as halogen bonds or simply fall within the broader scheme of intermolecular interactions. However, to distinguish supramolecular differences, X-X' contacts have been classified into two groups – type I and type II contacts. Type II contacts, which are classified as X-bonds, involve the interaction of electrophilic and nucleophilic areas on two *X* atoms, whereas type I contacts simply minimise electrostatic repulsion by interaction with neutral areas on the surface of an *X* atom (Figure 1.3).[3]

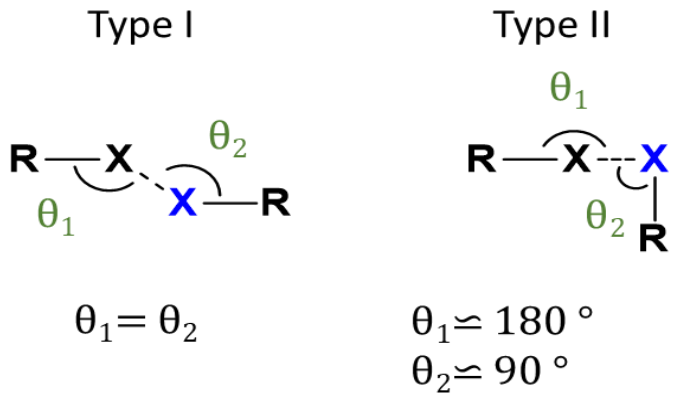

Figure 1.3. Typical type I (left) and type II (right) X-X' contacts. Type I: $\theta_1 \cong \theta_2 \cong 180^{\circ}$; Type II: $\theta_1 \cong 180^{\circ}, \theta_2 \cong 90^{\circ}$. Figure adapted from ref. 3.

1.1.1.4 π-stacking

One of the most prominent noncovalent interactions in the solid state is π-stacking. The simplest example of this interaction is the benzene dimer (Figure 1.4), with the three most stable geometries being parallel-displaced, T-shaped and face-to-face. These interactions have been calculated to be typically of the range of -1 to -6 kcal/mol, and depending on the substituents on the ring; interplanar distances typically range between 3.2 and 3.8 Å.[14–17]

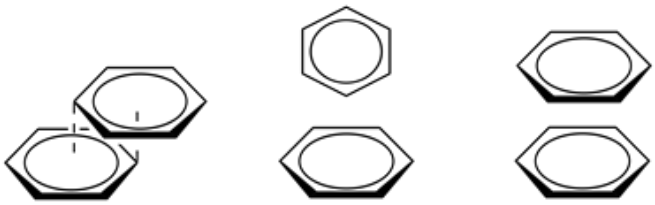

Figure 1.4. The three most stable π-π interaction geometries. Left) parallel-displaced; middle) T-shaped; right) face-to-face (sandwiched) (adapted from ref. 15).

Long-range dispersion interactions are mainly responsible for the binding of π-stacked dimers, and this is due to instantaneous/induced multipole fluctuations.[17,18]

1.2 Cocrystals

Research in the field of supramolecular assembly of molecular materials has recently focused more on multicomponent materials. Although there is some debate as to the definition of a cocrystal, and even around the term "cocrystal" and its adequacy[19,20], a cocrystal can broadly be described as a crystalline material with unique physical properties, that is made up of two or more components in in the solid state.[21] These components could be atoms, ionic compounds or molecules and as such hydrates, solvates and clathrates could *technically* all be considered cocrystals. However, for the purpose of this study, a cocrystal will refer to a multicomponent material, where the components are neutral molecules (specifically organics) and pack in stoichiometric ratios in the solid state.

Cocrystals are very important in the fields of crystal engineering as well as in pharmaceutical chemistry[22,23]. For example, cocrystals have been used to stabilise inherently unstable compounds, as a unique method for the purification of compounds, as well as a way of extracting important compounds from very dilute solutions.[22] Co-crystallisation also provides a unique opportunity to introduce specific physical properties into a material via a

second (or even third) co-former. This co-former could also bear different, and possibly structure-directing, functional groups that could be exploited during molecular self-assembly.[24] So far, very little is understood about the thermodynamics and formation of cocrystals, and other multicomponent systems. However, although cocrystals have been extensively studied experimentally and theoretically, the fundamentals behind the stability of a binary system over a single component material, or *vice versa*, remains poorly understood. For more information on this specific topic, see Chapters 3 and 5.

1.3 Polymorphism

The packing mode of molecules in the solid state is controlled by thermodynamic and kinetic driving forces. As a result, a compound may have more than one crystalline solid phase. This phenomenon of multiple solid phases is called *polymorphism*. Polymorphism has historically been a profoundly difficult term to define although the basic idea is well understood, however, a broadly acceptable definition seems to be the existence of different crystal structures for the same chemical compound.[25,26] Polymorphism has quickly become an essential area of research due to the fact that different polymorphs exhibit a host of different physical properties including thermodynamic, packing motifs, spectroscopic, kinetic, surface and mechanical properties.[27]

Polymorphs may undergo transformation processes whereby one phase converts to another either reversibly (enantiotropic) or irreversibly (monotropic).[28] These phase transformations may be induced by a number of factors including pressure, temperature, humidity or even time. Reports of "disappearing polymorphs" have also surfaced with greater frequency, as common polymorphs become impossible to make again or phase transformations occur after which the first phase is never seen again, or only after many years

of trial and error.[29,30] In this way, polymorphism has piqued the interest of more and more researchers in the area of supramolecular assembly and crystal engineering, since the fundamental understanding and prediction of polymorphism remains elusive. For more information on this specific topic, see Chapters 4 and 5.

1.4 Molecular magnets

Conventional magnets have been known for millennia and are generally composed of metals, metal oxides, or intermetallics[†], with electron spins residing in d-(metallics) and f-orbitals (intermetallics and lanthanides). However, the first case of a molecular magnet (a magnet composed of molecular species, or polymers, prepared by relatively soft synthetic methods)[31] was reported in 1987 with the discovery of $[Fe(C_5Me_5)_2]^+[TCNE]^{\bullet-}$ (TCNE=tetracyanoethylene)[32,33]. This was followed by the discovery of a purely organic ferromagnet in the β-phase of *p*-nitrophenyl nitronyl nitroxide (*p*-NPNN) in 1991, which displayed the magnetic capabilities of organic molecular materials with electron spins in the p-orbitals.[34] The majority of organic molecular magnets known to date order below liquid helium temperatures, with some exceptions[35,36], but it was soon realised that heavier p-block elements such as S and Se have the potential for stronger exchange- as well as spin-orbit coupling due to the more diffuse orbitals associated with them.[37] Organic nitroxide and nitrophenyl nitroxides (N- and O-centered spin) as well as thia- and selena-azolyl (S/Se- and N-centered spin) compounds have since been investigated as potential molecular magnetic materials with ordering temperatures above liquid helium temperature[36,38]. Molecular magnets can thus enable more flexible tuning of magnetic properties, combining magnetic properties

[†] Intermetallics are solid-state compounds with defined stoichiometry, exhibiting metallic bonding (i.e. Co_5Sm).

with other structural properties such as electrical and optical properties, as well as being simpler to synthesise.

1.5 Organic radicals

Organic radical compounds are open-shell molecules[‡] generally made up of H, C, N, O and S. Due to the electronic nature of these compounds (the unpaired electron), they tend to be quite reactive and are prone to dimerisation in many cases, leading to spin-pairing of the single electron. The design of organic radicals relies heavily on both the stabilisation of the radical, as well as controlling the electronic structure, and by extension the intermolecular interactions that govern the physical properties of the material.

A number of methods have been implemented as measures to prevent this dimerisation and guide intermolecular interactions, their success depending on the type of system. [39–41] Bulky substituents have been used to protect the atom where the radical resides from taking part in reactions, and have been used on systems such as the polychlorinated trityl radicals[42]. Aromaticity of the radical has also been used as a means to prevent dimerisation, where the electron is delocalised over the entire molecule, or a part of it. Some examples of delocalised radical systems include nitroxides and nitronyl nitroxides[43], verdazyls[41] and dithiadiazolyls[44] (DTDAs).

[‡] In molecular orbital theory, open-shell molecules are molecules with a valence shell that is not completely filled. This generally implies an unpaired electron (radical) in molecules, resulting in a singly-occupied molecular orbital (SOMO).

1.5.1 Chemistry of nitroxide radicals

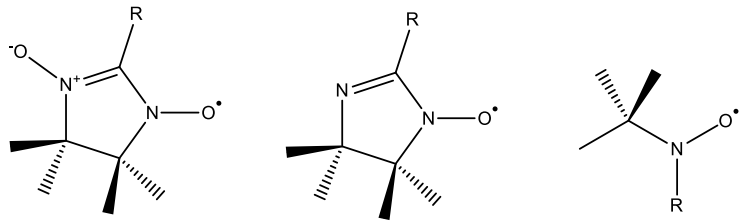

Figure 1.5. Some examples of nitroxide radicals, adapted from ref. 45.

Nitroxide and nitronyl nitroxide radicals were the first to be used in the field of organic magnetic materials.[43,45,46] The first case of spontaneous magnetisation was in the β-phase of *p*-NPNN, however, its magnetic ordering temperature of 0.48 K was problematic.[34] Nitroxides are persistent radicals, being mostly air and chemically stable. This is demonstrated by the 2,2,6,6-tetramethylpiperidin-1-yl)oxyl radical (TEMPO), which is often employed in organic synthesis as catalyst for oxidation reactions.[47] The stability has been attributed to both electron delocalisation as well as steric encumberment around the radical centre. The heteroatoms on these radicals can be used as binding sites that can coordinate to metal ions, creating strong exchange interactions between the radical compound and the metal centre.[46] Nevertheless, the low magnetic ordering temperatures of these materials make them unfavourable options for practical organic magnet applications.

1.5.2 Chemistry of dithiadiazolyl radicals

Another important family of organic radicals is the 1,2,3,5-dithiadiazolyl radicals (DTDAs) (Figure 1.6). As stated earlier, they are known to order at higher temperatures than nitroxides and nitronyl nitroxides, making them a more attractive choice as building blocks for organic magnetic materials.[46] DTDAs are neutral radicals with 7 π electrons, where the unpaired electron resides mostly on the sulfur and nitrogen atoms. The singly-occupied molecular orbital (SOMO, where the single electron/radical resides) on the heterocycle of the DTDAs is nodal at

the carbon atom, which is an important observation since the molecules can be fine-tuned through the R-group without influencing the electronics of the heterocycle.[44]

Although these compounds have more desirable magnetic ordering temperatures, they have a strong tendency to dimerise upon assembly in the solid state, losing their magnetic properties in the process[48] (see Figure 1.6 for dimerisation modes). To date, there are only 6 known monomeric (undimerised) DTDA radicals[36,38,49–52]. The first DTDA to be characterised was PhDTDA, which packs as a *cis*-oid dimer[53]. However, with the subsequent discovery and characterisation of many more dimeric DTDAs, it was soon realised that more care will need to be taken in order to tune the functionalities on these materials for specific physical properties (such as magnetism and conductivity).[44] A strong supramolecular synthon, which is often exploited in these systems as a structure-direction interaction, is the CN···S-S interaction, along with other more general N···S contacts.

A lot of effort has been put into preventing the dimerisation process, one method being co-crystallisation of these radicals. Three DTDA cocrystals are known[5,54], all which are also dimeric in nature. To our knowledge, there are no known examples of DTDA radicals co-crystallised with other families of radicals or even with neutral organic molecules.

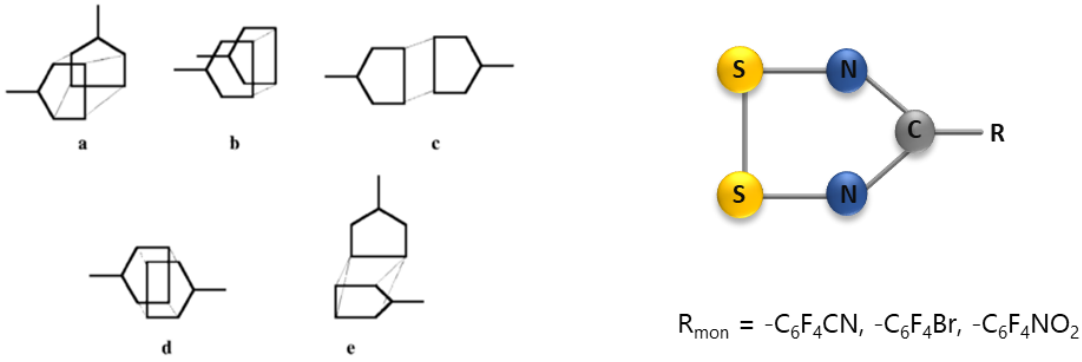

Figure 1.6. Left) Common dimerisation modes of DTDA radicals, taken with permission from ref. 43. a) twisted, b) *cis*-cofacial, c) *trans*-antarafacial, d) *trans*-cofacial and e) orthogonal; Right) basic structure of the DTDA heterocycle, where the *R*-group can be varied. The R_{mon} listed are the known monomeric DTDAs.

1.6 Quantum mechanics and computational chemistry

This section will present information and equations found in Cramer[55] as well as additional references, where required.

Quantum mechanics has laid the foundation for the prediction of chemical properties in microscopic systems, historically based on macroscopic analogues, from first principles. The fundamentals of quantum mechanics state that microscopic (or subatomic) systems are best described by *wave functions* describing the physical properties of a system, and each of these physical properties has a quantum *operator* associated with it which, if applied to a wave function, allows for the prediction of these physical properties. Through this, predicting the probability of finding a system exhibiting a specific property within a certain range of values became possible.

Many known chemical models, however, did not find their existence in connection with quantum mechanics but were rather based on intuition and experimentation. From a non-intuitive stand point, a model may be more easily understood if explained from the point of view of an intuitive chemical model rather than the more complex quantum mechanical description. This section will introduce the quantum mechanical concepts that brought about some better-known chemical models, some of which were used in during this project. It will focus on some of the basics of wave function theory, Hartree-Fock (HF), and finally Density Functional Theory (DFT) without delving very deeply into the mathematics of the quantum mechanics.

1.6.1 The wave function

During the very early 1900s, physicists and chemists realised that perhaps the description of microscopic systems and macroscopic models should differ quite substantially, as opposed to modelling microscopic systems after their macroscopic analogues. Soon it was discovered that microscopic systems could be quantised. This was an extreme suggestion at the time, since quantisation is not only a characteristic of wave-like systems, but also particles of matter. This idea announced the arrival of quantum mechanics (QM) – a way in which to describe matter exhibiting both wave- and particle-like properties.

The wavefunction, denoted by $\boldsymbol{\Psi}$, is the fundamental postulate of quantum mechanics. This is said to exist for any chemical system, and any operator or function acting on $\boldsymbol{\Psi}$ will return the observable property of the system, asked for by the operator. The wavefunction is expressed as:

$$\nu\Psi = E\Psi \qquad \text{(Eq. 1.1)}$$

where ν is an operator represented as an N x N square matrix, and E is an eigenvalue of the eigenfunction, $\boldsymbol{\Psi}$. The product of the wavefunction, $\boldsymbol{\Psi}$, with its complex conjugate, $|\boldsymbol{\Psi}^*\boldsymbol{\Psi}|$, represents a probability density. As a result, working with non-complex systems, this product becomes $|\boldsymbol{\Psi}|^2$, and then the integral of this product over a region of space will give the probability that the electron will be within that specific region of multi-dimensional space.

1.6.2 The Hamiltonian operator

The first, and probably most important operator that will be introduced is the Hamiltonian, which returns E – the energy of a system:

$$\hat{\mathrm{H}}\Psi = E\Psi \qquad \text{(Eq. 1.2)}$$

where *v* is now replaced by the Hamiltonian, *H*. This equation is known as the Schrödinger equation. The Hamiltonian contains five contributions towards the total energy of a system, and is represented mathematically as:

$$\hat{\mathrm{H}} = -\sum_i \frac{\hbar^2}{2m_e}\nabla_i^2 - \sum_k \frac{\hbar^2}{2m_k}\nabla_k^2 - \sum_i \sum_k \frac{e^2 Z_k}{r_{ik}} + \sum_{i<j} \frac{e^2}{r_{ij}} + \sum_{k<l} \frac{e^2 Z_k Z_l}{r_{kl}}. \qquad \text{(Eq. 1.3)}$$

Here, the first two terms are the kinetic energies of the electrons and the nuclei, the third is the attraction of the electrons to the nuclei, and the last two terms represent the interelectronic and internuclear repulsions, respectively. The first two terms are the kinetic terms, and the final three are the potential terms as they appear in classical mechanics. Electrons are denoted by *i* and *j*, nuclei by *k* and *l*, ħ is Planck's constant divided by 2π, m_e and m_k are the masses of electrons and nuclei respectively, *e* is the charge on an electron and *Z* the atomic number, ∇^2 is the Laplacian operator and *r* represents the distance between two atoms (*i* and *j* for example). The Laplacian

$$\nabla^2 = \frac{\partial^2}{\partial x_i^2} + \frac{\partial^2}{\partial y_i^2} + \frac{\partial^2}{\partial z_i^2} \qquad \text{(Eq. 1.4)}$$

takes this form when working in Cartesian coordinates. For simplification, we assume that the wave functions are orthonormal, and hence for a one electron system:

$$\iiint \Psi_i \Psi_j dx dy dz = \delta_{ij} \qquad \text{(Eq. 1.5)}$$

or

$$\int \Psi_i \Psi_j d\boldsymbol{r} = \delta_{ij}. \qquad \text{(Eq. 1.6)}$$

Here, the multiple integrals over all space were simply replaced with a simplified integral over *3n*-dimensional volume, ***r***, and δ_{ij} is the Kronecker delta. The Kronecker delta is equal to 1 if *i=j* and zero otherwise. The assumption of an orthonormal wave function has two qualities associated with it. The first is *orthogonality*, which states that the integral is zero if *i≠j*, and the second being *normal*, which means when *i=j* then the integral is equal to 1.

Applying this to the Schrödinger equation (Eq. 1.2) will eventually provide the molecular energy of a system:

$$\int \Psi_j \hat{\mathrm{H}} \Psi_i d\boldsymbol{r} = \int \Psi_j E_i \Psi_i d\boldsymbol{r} \qquad \text{(Eq. 1.7)}$$

but E is scalar, so it can be removed from the integral and Eq. 1.6 can be applied such that

$$\int \Psi_j \hat{\mathrm{H}} \Psi_i d\boldsymbol{r} = E_i \delta_{ij}. \qquad \text{(Eq. 1.8)}$$

However, the Schrödinger equation cannot be solved exactly for a many-electron system. As a result, some approximations have to be made, which will be discussed below.

1.6.3 The Born-Oppenheimer approximation

As stated above, the Schrödinger equation cannot be solved for a many-electron system. This is due to interdependency between the behaviour of the motion of particles – no particle moves independently of the others. The Born-Oppenheimer approximation provides a way to somewhat simplify this problem. In simple terms, this approximation says that the motion of electrons and nuclei in a molecule can be separated, and as a result, computing the energy and wavefunction of an average-sized system becomes possible.

In a molecule, the atomic nuclei and electrons are moving at enormously different rates. This is due to the fact that protons and neutrons weigh about 1800 times that of an

electron and as a result, move slower. Also recall the Hamiltonian (Eq. 1.3), and the mass variable in the denominator of the kinetic terms. For practical application then, the nuclear positions are "fixed" and the electronic energies are calculated for these fixed nuclear positions. The nuclear kinetic energy term is then evaluated independently of the electrons, nuclear-electron correlation is eliminated, and the nuclear-nuclear repulsion is constant for a specific geometry. Since the nuclear kinetic energy terms can be neglected, the *electronic* Schrödinger equation can be written as:

$$\hat{\mathrm{H}}_{elec}(r,R)\Psi_{el}(r,R) = E_{el}(R)\Psi_{el}(r,R) \qquad \text{(Eq. 1.9)}$$

where the resulting wavefunction is called the Born-Oppenheimer wavefunction. Although the nuclear kinetic terms are neglected, the nuclei can still occupy different positions, **R**, and this variation is taken into account in the Born-Oppenheimer approximation. The nuclear repulsion term is not part of the electronic Hamiltonian, it should be added to E_{el} to give the E_{tot}

$$E_{tot} = E_{el} + E_{nuc}. \qquad \text{(Eq. 1.10)}$$

The wavefunction is not an actual observable quantity. However, since we are assuming orthonormality of the wavefunction, taking the square of the wavefunction will allow the determination of the probability of finding electrons in the range i = 1-N in the volume defined by $dr_1 \ldots dr_N$.

1.6.4 The variation principle

In order to get to a position to solve the many-electron Schrödinger equation, a good approximation of the wavefunction, Ψ_{el}, is necessary. This is done with the variation principle, which allows for the approximation of the lowest energy ground states, some excited states, and finally the wavefunction. The variation principle makes use of a trial wavefunction, Ψ_{trial},

and states that the energy of this approximated wavefunction, E_{trial}, will always be greater than or equal to the real ground state energy, E_0, of a particular system, thus providing an upper bound on the true ground state energy of a system. Mathematically it can be represented as:

$$\int \Psi_{trial} \hat{\mathrm{H}} \Psi_{trial} d\boldsymbol{r} = E_{trial} \geq E_0 = \int \Psi_0 \hat{\mathrm{H}} \Psi_0 d\boldsymbol{r}. \qquad \text{(Eq. 1.11)}$$

The way in which the variation principle then approximates the ground state wavefunction, Ψ_0, is by picking an initial trial wavefunction, Ψ_{trial}, and then varying it until E_{trial} is minimised. Through this, an approximate to the wavefunction and ground state of a system is found.

1.6.5 The Hartree-Fock approximation

As stated above, a trial wavefunction has to be approximated in order to obtain a description of the ground state wavefunction, Ψ_0, to ultimately find the ground state energy, E_0, of a many-electron system. However, to do this a starting point is needed, and this starting point is determined using a Slater determinant. This is known as the Hartree-Fock (HF) method. Antisymmetric wavefunctions, that is to say, wavefunctions of a many-electron system that do not change sign upon exchange of two electrons

$$\Psi_e(\vec{x}_1, \vec{x}_2) = -\Psi_e(\vec{x}_2, \vec{x}_1) \qquad \text{(Eq. 1.12)}$$

are constructed using a Slater determinant. For an *N*-electron system, the Slater determinant, Φ_{SD}, consists of *N* one-electron spin orbitals denoted by $\phi_i(\vec{x}_i)$

$$\Phi_{SD} = \frac{1}{\sqrt{N!}} \begin{vmatrix} \phi_1(\vec{x}_1) & \phi_2(\vec{x}_1) & \cdots & \phi_N(\vec{x}_1) \\ \phi_1(\vec{x}_2) & \phi_2(\vec{x}_2) & \cdots & \phi_N(\vec{x}_2) \\ \vdots & \vdots & \ddots & \vdots \\ \phi_1(\vec{x}_N) & \phi_2(\vec{x}_N) & \cdots & \phi_N(\vec{x}_N) \end{vmatrix}. \qquad \text{(Eq. 1.13)}$$

The spin orbitals are constructed by multiplying a spatial orbital φ by a spin function, and this contains information about spin up (α) and spin down (β) functions. The determinant can then be written as

$$\Phi_{SD} = \frac{1}{\sqrt{N!}}\det\{\phi_1(\vec{x}_1)\phi_2(\vec{x}_2) \dots \phi_N(\vec{x}_N)\}. \qquad \text{(Eq. 1.14)}$$

Due to the antisymmetrical properties, the determinant changes sign if two rows are interchanged (and hence two electrons), and it is zero if two are the same. The mathematics of the Hartree-Fock method is more extensive and complex, but will not be discussed further. The only final comment is that the HF approximation employs a self-consistent field (SCF) method for determining expressions for the spin orbitals. Since the spin orbital operator ϕ_i is dependent on all other N-1 ϕ_j spin orbitals, the HF equations are applied in an iterative fashion until a set of self -consistent orbitals is found. This means that the input and resulting spin orbitals differ by less than a specific cut-off tolerance.

1.6.6 Restricted and unrestricted Hartree-Fock

So far, only situations where all spatial orbitals are occupied by two electrons with opposite spin – also called closed shell systems, have been accounted for. Although this may describe most molecular systems, it is not the case for all systems, for example radical compounds with a singly occupied molecular orbital (SOMO), or where a system has an odd number of electrons and one orbital is occupied by a single electron. The way that most molecular systems are treated, where two electrons occupy each orbital, is by the *Restricted Hartree-Fock* (RHF) method. In the case of an odd number of electrons, when all orbitals have paired electrons and one orbital contains the last lone electron, the *Restricted Open Hartree-Fock* (ROHF) method is applied, and when all electrons are allowed to occupy different spatial orbitals we apply the *Unrestricted Hartree-Fock* (UHF) method (Figure 1.7).

However, a sometimes unrealistic lowering of energy is often observed for UHF methods. The UHF wavefunctions are generally not eigenfunctions of the spin operator $\hat{S}^2$,

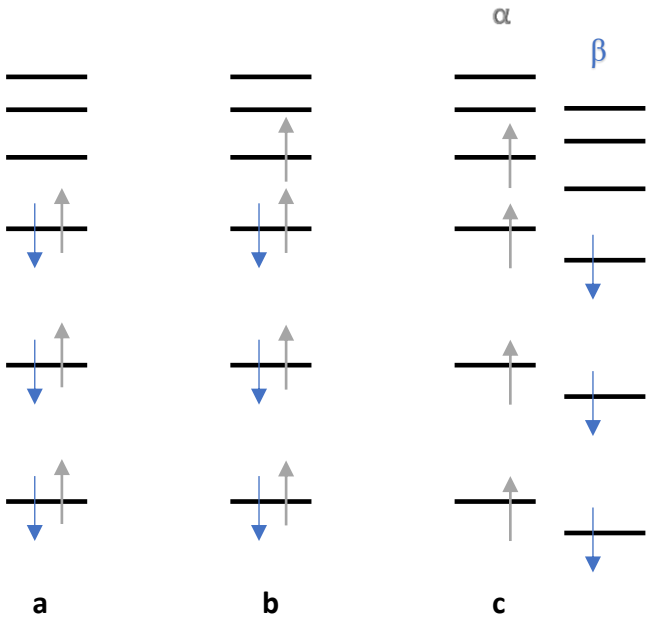

Figure 1.7. Graphical example of the energy levels of a) RHF, b) ROHF and c) UHF with the α and β spins.

whereas the solution to the Schrödinger equation should be.[§] This is called spin contamination, and implies that the UHF wavefunction is contaminated with higher spin states. Simply put, doublets are contaminated by quartets, sextets, octets, etc., and triplets are contaminated by pentets, heptets and nonets. So, if the value of $< \hat{S}^2 >$ differs from that of S(S+1), it can be said that spin contamination is present. This spin contamination is an unfortunate price to be paid when working with the UHF method, if a lower energy description of the system needs to be obtained.

The HF method offers an exact treatment of exchange but it does not, however, account for electron correlation (or dispersion interactions) – caused by instantaneous dipoles that interact due to fluctuations in the electron density. This is where density functional theory (DFT) steps in (see next section). The main difference between HF and DFT lies in the fact that HF calculates energy from orbitals, whereas DFT calculates energy as a function of electron density.

1.7 Density Functional Theory

The wavefunction itself is, for the most part, a non-intuitive concept for a many-electron system. Even though the wavefunction can be expressed in the form of the Slater determinant of one-electron orbitals, it is does not necessarily provide the best expression of the wavefunction, and it is essentially uninterpretable.

The question of whether a more intuitive approach could be used sparked the development of density functional theory. It was suggested that a physical observable may be

[§] A well-behaved wavefunction should be an eigenfunction of the total spin operator, $\hat{S}^2$, which when applied to a wavefunction, should look like: $\hat{S}^2\Psi_0 = S(S+1)\,\Psi_0$. Here, S(S+1) are the values of the eigenfunctions, where S is 0 for a singlet, ½ for a doublet, and 1 for a triplet.

a more intuitive approach to calculating some physical properties of molecules – the only question was, which observable? Since the Hamiltonian is constructed with dependence on 1) atomic positions of nuclei, 2) number of nuclei, and 3) total number of electrons, the most obvious option became electron density.[56] The number of electrons is found by integrating the electron density over all space (Eq. 1.15),

$$N = \int \rho(\boldsymbol{r}) d\boldsymbol{r}. \qquad \text{(Eq. 1.15)}$$

Nuclei, being point charges, correspond to maxima in the electron density, and then the atomic numbers can be found since each nucleus is located at a maximum in the electron density;

$$\left.\frac{\partial \bar{\rho}(r_i)}{\partial r_i}\right|_{r_i=0} = -2Z_i \rho(\boldsymbol{r_i}) \qquad \text{(Eq. 1.16)}$$

where i is a nucleus, $\bar{\rho}$ is spherically averaged electron density, r_i is the radial distance from nucleus i, and Z_i is the nuclear atomic number. With this information, one can then construct the Hamiltonian, solve the Schrödinger equation, and calculate the wavefunctions. Since DFT uses electron density as its fundamental property, unlike HF which deals directly with the wavefunction, the electron density is known as the *functional* of DFT. In this case, DFT uses the electron density to describe the total energy of a system.

Since the development of DFT, many descriptors of the total energy of a system have been developed by researchers in the field, and these are also referred to as *functionals*. Since they contain kinetic, potential and in some cases exchange-correlation terms, which are all functions of the electron density, they can be termed *functionals*. Many of these functionals will be mentioned below, and they are generally named as abbreviations of the surnames of the authors that developed them. See the review by Zhao and Truhlar[57] for a list of *some* functionals developed to date.

1.7.1 Kohn-Sham methodology

Similar to the Hamiltonian in Eq. 1.3, the DFT electronic energy is expressed using a kinetic term $E_T(\rho)$, a nuclear-electron term $E_{ne}(\rho)$, and an electron-electron term $E_{ee}(\rho)$ (Eq. 1.17). The DFT energy is, however, expressed as a function of the electron density; here $E_{xc}(\rho)$ is the exchange-correlation energy. The exchange energy comes from the Pauli exclusion principle stating that two electrons with parallel spin cannot be in the same position at the same time, resulting in a repulsion between electrons with parallel spin; the correlation comes from the same principle, and simply states that there is some correlated motion between electrons with opposite spins due to their inherent Coulombic repulsion. The precise description of the E_{xc} term remains elusive, but is described using approximations like LDA and GGA (vide infra). This expression, the Kohn-Sham approach (KS)[58],

$$E_e^{DFT}(\rho) = E_T(\rho) + E_{ne}(\rho) + E_{ee}(\rho) + E_{xc}(\rho) \qquad \text{(Eq. 1.17)}$$

was proposed by Kohn and Sham in 1965.[59] It came about due to the realisation that many difficulties arise with electron-electron interactions in the Hamiltonian, whereafter a system of fictitious *non-interacting* electrons was proposed to be simpler. Herein, the electron density is described by a set of one-electron spin-orbitals – known as the Kohn-Sham approach to the implementation of DFT. So now we can find the orbitals, χ_i, that minimise the energy as a function of electron density:

$$\hat{\mathrm{H}}_i^{KS}\chi_i = \epsilon_i\chi_i \qquad \text{(Eq. 1.18)}$$

where

$$\hat{\mathrm{H}}_i^{KS} = -\frac{\hbar^2}{2m_e}\nabla_i^2 - \frac{e^2}{4\pi\varepsilon_0}\sum_k^M \frac{Z_k}{r_{ik}} + \frac{e^2}{4\pi\varepsilon_0}\int \frac{\rho(\vec{r}_j)}{r_{ij}}d\vec{r}_j + V_{xc}(\vec{r}_i)\,.$$

This operator shares similarities with the Hamiltonian (Eq. 1.3) in that the first three terms are defined in the same way, the only difference being the exchange-correlation (XC) term, V_{xc}. No true, comprehensive expression exists for this term, but it can be represented as

$$V_{xc} = \frac{\partial E_{xc}}{\partial \rho}. \qquad \text{(Eq. 1.19)}$$

Here, V_{xc} is called a functional derivative - a one-electron operator for which the expectation value is E_{xc}. The one-electron spin orbitals mentioned above, χ_i, are used to calculate the electron density by using them to construct a Slater determinant, similar to that used in HF theory. However, the KS approach is an iterative process since, although solving the secular equation[**] from the DFT Slater determinant yields the electron density, the electron density is also required to calculate the matrix elements of the secular equation. So, minimisation of the electronic energy is achieved by matrix manipulation of the Slater determinant until self-consistency of the electron density is achieved. The equations need to be solved self-consistently, where V_{xc} is calculated in each cycle with a good approximation for E_{xc} (Eq. 1.19).

Finally, the principal difference between HF and DFT lies in that, contrary to the HF approximations, DFT is an exact method – DFT contains no approximations. Cramer[55] describes it as follows:

> *"…HF is a deliberately* approximate *theory, whose development was in part motivated by an ability to solve the relevant equations* exactly, *while DFT is an* exact *theory, but the relevant equations must be solved* approximately*…"*

[**] The secular equations are obtained by equating the Slater determinant to zero. In the case of DFT, the Slater determinant uses Kohn-Sham orbitals.

1.7.2 Exchange-correlation energy, E_{xc}

Since one would ideally want to be performing KS calculations, it is important first to find a way to describe the exchange-correlation term, E_{xc}. Although DFT is an exact method, a number of approximations for E_{xc} have to be made, since no true description for this term is known. Hartree-Fock gives an exact treatment of the exchange, although it scales with molecular size making it expensive for larger systems.[60] HF does not, however, have a very good description for correlation energy at all. Since the E_{xc} term is simply a summation of the two-body *exchange* and *correlation* contributions, dependent on the electron density ρ, it can be separated as $E_{xc}[\rho] = E_x[\rho] + E_c[\rho]$. In terms of the dependence of E_{xc} on the electron density, it can be expressed as an interaction between the electron density and an energy density, denoted by ε_{xc}, that is dependent on the electron density

$$E_{xc}[\rho] = \int \rho\varepsilon_{xc}[\rho]d\boldsymbol{r} \qquad \text{(Eq. 1.20)}$$

where

$$\varepsilon_{xc} = -\frac{9\alpha}{8}\left(\frac{3}{\pi}\right)^{1/3}\rho^{1/3}(\boldsymbol{r}). \qquad \text{(Eq. 1.21)}$$

The energy density, ε_{xc}, is a unit of electron density per particle density, not electron density per volume density. The correlation part of the E_{xc} term is not as simple to explicitly express, but some parameterisations are available. Spin is easily implemented in DFT by using separate functionals for the α and β spin densities. The spin densities at any point can be determined by

$$\zeta(\boldsymbol{r}) = \frac{\rho^{\alpha}(\boldsymbol{r}) - \rho^{\beta}(\boldsymbol{r})}{\rho(\boldsymbol{r})} \qquad \text{(Eq. 1.22)}$$

where $\zeta(\boldsymbol{r})$ is the normalised spin polarisation, the α spin density is equal to $\frac{\rho_{total}\times(\zeta+1)}{2}$, and the β spin density is equal to the difference between that value and ρ_{total}.

1.7.3 Local density approximations (LDA)

Local density approximation (LDA) is a term that refers to any DFT method that exclusively uses the density at some specific point **r**, or the *local* density, to compute ε_{xc} at that position. In other words, the density must be single-valued at every point, but may behave differently otherwise. The exchange energy can be computed as with eq. 1.20 where, in the case of the LDA approach, the value of α is equal to $\frac{2}{3}$. Unpolarised systems have $\zeta = 0$, however, for systems with spin polarisation, a spin-polarised formalism has to be used. This is often distinguished from LDA by referring to it as *local spin density approximation* (LSDA). LDA is a relatively simple and easy method to employ but, like all methods, it does have its limitations: 1) it overestimates binding energies, 2) it does not deal well with magnetic materials, 3) it underestimates lattice parameters, and 4) it struggles with the energetics of chemical reactions.[55,61] However, since the contribution from the exchange is so much larger than that of the correlation, it has been suggested that the exchange be treated exactly, as with HF, and the correlation be estimated with LSDA. So then, E_x is the energy of the Slater determinant of the Kohn-Sham orbitals, and E_c is everything else. In that way, attempts to more accurately describe the exchange-correlation energy have been made by combining exact exchange and local density approximations.[60,62]

Again, for the correlation energy density, even for a simple system, an analytical derivation has proved impossible. Some examples of work done on this front include work by Ceperley[63] and Vosko[64] in 1980.

1.7.4 Generalised gradient approximation (GGA)

Since the electron density in a molecular system is hardly ever spatially uniform, LDA has some limitations. A way to solve this in terms of the correlation functional is to make it depend both on the local density as well as the gradient of the density – the extent to which the density changes. This is referred to as the *generalised gradient approximation* (GGA), as it is a gradient-corrected method. The GGA approach has also helped solve some of the issues in LDA, stated above. Most GGA functionals simply have a correction added onto the LDA functional:

$$\varepsilon_{x/c}^{GGA}[\rho] = \varepsilon_{\substack{x \\ c}}^{LSDA}[\rho] + \Delta\varepsilon_{x/c}\left[\frac{|\nabla\rho(\boldsymbol{r})|}{\rho^{4/3}(\boldsymbol{r})}\right]. \qquad \text{(Eq. 1.23)}$$

The first well-known GGA functional was introduced by Becke[65], and was referred to simply as "B" which has very good long-range energy density asymptotic behaviour. Other similar examples of GGA functionals include FT97[66,67], PW[68], *m*PW[69] and X[70], where X (X being a functional) is a combination of B88[71] and PW91[72] in order to improve performance of the functionals. In terms of functionals that do not have empirical parameters, some examples include B86[73], PBE[74] and *m*PBE[75], and amongst those correlation functionals which provide some corrections to the correlation energy density are B88, P86[76], PW91 and LYP[77].

Conventionally, in order to completely describe the exchange and correlation parts, the acronyms for each are concatenated. For example, the BLYP functional is composed of the GGA exchange functional B and the correlation functional LYP.

1.7.5 Hybrid functionals

It was in 1993 that Becke introduced the idea of mixing HF and local DFT theories in an attempt to improve the accuracy of previous methods and lay the groundwork for further development.[60,78] This is a more computationally expensive method, but it performs very well.

The clear reason why this was done was to exploit the best parts of both methods – the exact exchange of HF with the exchange and correlation from empirical or *ab initio* sources. The value of this lies in that the exchange energy, $E_x(\rho)$, is normally significantly larger than the correlation energy, making this a key term. The exact exchange energy is described by

$$E_x^{exact} = -\frac{1}{2}\sum_{i,j}^{N}\iint \chi_i^*(\vec{x}_1)\,\chi_j^*(\vec{x}_2)\frac{1}{\boldsymbol{r_{ij}}}\chi_i(\vec{x}_2)\chi_j(\vec{x}_1)d\vec{x}_1 d\vec{x}_2 \qquad \text{(Eq. 1.24)}$$

and a portion of this is included in hybrid functionals like:

$$E_x = E_x(\rho) + a_x E_x^{exact} \qquad \text{(Eq. 1.25)}$$

where a_x is found by fitting to accurate experimental data. Some popular hybrid functionals include PBE0[79], HSE, and B3LYP. The B3LYP functional, for example, is a concatenation of Becke's exchange functional B and the correlation functional of Lee, Yang and Parr.

1.8 The dispersion energy problem

The van der Waals, or dispersion, interactions play a key role in chemical systems in that they control for example, the binding of proteins, the packing of crystals, formation of aggregates, host-guest systems and the orientation of molecules on surfaces. Although methods like HF and hybrid DFT functionals include exact exchange, which, along with electrostatics describe the dispersion interaction, these methods still overestimate binding energies and underestimate equilibrium distances between molecules. A way to overcome this is by introducing a dispersion correction to the mean-field (HF or DFT) energy

$$E_{MF-D} = E_{MF} + E_{disp} \qquad \text{(Eq. 1.26)}$$

where E_{disp} is an empirical dispersion correction. Since the early 2000s, a number of corrections and revisions have been introduced, from multipole expansion approximation to preventing potential *double counting* of short-range correlation by introducing a damping factor.[61] However, certainly the most popular form of the dispersion correction was the DFT-D scheme introduced by Grimme.[80] There have since been two revisions of this DFT-D correction – second generation (or GD2) and third generation (GD3); they will be discussed in more detail below.

1.8.1 DFT-D development

KS-DFT does include electron correlation in an approximated manner, but dispersion is still very poorly accounted for in DFT. Early methods to solve this problem included modifying and/or combining functionals, for example the X3LYP[70] functional. However, the use of many of these functionals does not extend much further than the limited systems they were initially tested on. Then, in 2004 Grimme introduced a practical new dispersion correction given by[80,81]

$$E_{disp} = -s_6 \sum_{i=1}^{N_{at}-1} \sum_{j=i+1}^{N_{at}} \frac{C_6^{ij}}{R_{ij}^6} f_{damp}(R_{ij}) \qquad \text{(Eq. 1.27)}$$

where N_{at} is the number of atoms, R_{ij} is the interatomic distance, C_6^{ij} is a dispersion coefficient for the atom pair *ij* taking on the form $C_6^{ij} = 2\frac{C_6^i C_6^j}{C_6^i + C_6^j}$, and s_6 is a global scaling factor. The C_6 coefficients are taken from ref. 78. However, as mentioned above, at short ranges dispersion interactions are negligible and covalent interactions dominate. As a result, dispersion corrections applied at short-range could count the contribution twice. A damping factor, f_{damp}, that tends to zero fast enough at small *R* values such that the dispersion correction is negligible, is included. It is expressed as

$$f_{damp}(R) = \frac{1}{1 + e^{-\alpha(R/R_0 - 1)}} \qquad \text{(Eq. 1.28)}$$

where R_0 is the sum of the van der Waals radii. Grimme tested this DFT-D correction with BLYP, BP86 and PBE and the correction performed best in combination with PBE and BLYP. Results on geometries and binding energies were very promising, but due to lack of reliable experimental data, the accuracy of the results was difficult to judge.

Two years later, Grimme introduced a new GGA density functional, B97-D[61], with atom-pairwise dispersion correction of the form C_6R^{-6} included. He reported parameters for elements up to xenon and scaling factors for the functionals BLYP, PBE, TPSS and B3LYP – three GGAs and a hybrid functional, respectively. Three main factors were addressed with this new correction: 1) C_6 coefficients are only known for elements H, C-Ne, and ideally chemists want atomic parameters for the entire periodic table, 2) molecules with third-row elements had problematic results, and 3) inconsistencies in thermochemical results were seen when adding dispersion correction to the KS-DFT energy. This modified approach treated short-range correlation with the density functional description and a damping factor, C_6R^{-6}, was added for medium to long range correlation. This new correction, also termed GD2, has the same dispersion description as seen in Eq. 1.27, however, modifications were made to the damping factor. The value of α, which was previously 23[80], was reduced to a value of 20 which results in better corrections for mid-range interactions. The C_6^{ij} also now takes on the form $C_6^{ij} = \sqrt{C_6^i C_6^j}$. The C_6 coefficient here was calculated in a very non-empirical way from atomic ionisation potentials (I_p) and dipole polarisabilities, α,

$$C_6 = 0.05 N I_p \alpha. \qquad \text{(Eq. 1.29)}$$

Here, *N* is equal to 2, 10, 18, 36 and 54 for the atoms in the rows 1-5 on the periodic table. This slight modification showed improved accuracy over the first generation DFT-D model.

1.9 Project aims

This project focused on studying multicomponent materials of neutral organic molecules, both experimentally and computationally, in order to rationalise their properties, thus adding to the arsenal of information available on the driving forces behind cocrystal formation. Two main groups of compounds were used to this end, 1) neutral organic radical compounds, due to their potential as organic magnetic materials, and 2) neutral organic charge transfer compounds. Computational methods were employed to complement the experimental studies.

The focus of this project was the dithiadiazolyl (DTDA) family of radicals. These were chosen since the research group is very familiar with DTDAs and the chemistry related to these compounds. Nitroxide radicals were also explored due to their chemical and thermal stability, and potential as co-formers to the DTDAs. The specific DTDA radicals used in this project were chosen because for various reasons, they were thought to be more likely to crystallise as monomers. The first choice of radicals were ones that are already monomeric in the solid state, including the fluorinated 4′(4-bromoperfluorophenyl)-DTDA and 4′(4-chloroperfluorophenyl)-DTDA. These were chosen as they already crystallise as monomers and thus might form cocrystals containing monomers. A second group of DTDAs were chosen based on the presence of a halogen ortho-substituent, which results in a larger twist angle between the DTDA and aromatic R-group that could hinder dimerisation. In addition to the two monomeric

radicals already listed above, the 4'(2,6-difluorophenyl)-DTDA, 4'(2-chlorophenyl)-DTDA and 4'(2,5-dichlorophenyl)-DTDA. Additionally, the chlorinated radicals have slightly longer intradimer S···S contact distances [82]. The 2,6-difluoro-DTDA radical is polymorphic, with ***γ***-phase being 50% monomeric[83], so this DTDA falls somewhere between the first and second group. The last group of radicals chosen were oxygen-centred radicals, namely *p*-nitrophenyl nitronyl nitroxide (*p*-NPNN) and TEMPO. These O-centred radicals are known to be more stable to contact with oxygen and moisture[84,85], and the *p*-NPNN carries a nitro functionality, which could be a strong supramolecular synthon for co-crystallisation purposes.

Cocrystals of benzoquinone and some of its derivatives, with a series of *p*-halophenols were also investigated as neutral organic co-formers. Quinones are known to form semiquinones[86], and do not show the potential to dimerise favourably with DTDA radicals (as is a common and undesired occurrence amongst DTDA radicals). Halophenols show the potential for strong halogen bonding, which was introduced as a strong synthon for the supramolecular assembly of these materials.[3] These systems were investigated to study the effect of a halogen substituent on the structure of a series of cocrystals.

The computational work pursued during this project entailed studying the known DTDA cocrystals, both in the gas phase as well as periodically, in order to look for any observable trends, and then comparing these results with similar computational studies done on seemingly unsuccessful co-crystallisation combinations. Through this we aimed to gain insight into the formation of cocrystals so that research can move to an area less driven by serendipity, and more towards the prediction of viable co-former combinations (partners).

1.10 References

1 J. W. Steed and J. L. Atwood, *Supramolecur Chemistry*, John Wiley & Sons, Ltd, Hoboken, United States, 2nd edn., 2009.
2 G. R. Desiraju, *Angew. Chem. Int. Ed. Engl.*, 1995, **34**, 2311–2327.
3 P. Metrangolo and G. Resnati, *IUCrJ*, 2014, **1**, 5–7.
4 N. Bricklebank, S. Hargreaves and S. E. Spey, *Polyhedron*, 2000, **19**, 1163–1166.
5 S. W. Robinson, D. A. Haynes and J. M. Rawson, *CrystEngComm*, 2013, **15**, 10205–10211.
6 K. V Shuvaev, A. Decken, F. Grein, T. S. M. Abedin, L. K. Thompson and J. Passmore, *Dalt. Trans.*, 2008, 4029–4037.
7 B. Brutschy and P. Hobza, *Chem. Rev.*, 2000, **100**, 3861–3862.
8 L. Pauling, *The Nature of the Chemical Bond*, Cornell University Press, Ithaca, NY, 1939.
9 E. Arunan, G. R. Desiraju, R. A. Klein, J. Sadlej, S. Scheiner, I. Alkorta, D. C. Clary, R. H. Crabtree, J. J. Dannenberg, P. Hobza, H. G. Kjaergaard, A. C. Legon, B. Mennucci and D. J. Nesbitt, *Pure Appl. Chem.*, 2011, **83**, 1637–1641.
10 C. R. Groom, I. J. Bruno, M. P. Lightfoot and S. C. Ward, *Acta Cryst.*, 2016, **B72**, 171–179.
11 P. Politzer, J. S. Murray and T. Clark, *Phys. Chem. Chem. Phys.*, 2010, **12**, 7748–7757.
12 G. R. Desiraju, P. S. Ho, L. Kloo, A. C. Legon, R. Marquardt, P. Metrangolo, P. Politzer, G. Resnati and K. Rissanen, *Pure Appl. Chem.*, 2013, **85**, 1711–1713.
13 P. Politzer, J. S. Murray and M. C. Concha, *J. Mol. Model.*, 2008, **14**, 659–665.
14 S. Tsuzuki, in *Intermolecular Forces and Clusters I*, ed. D. J. Wales, Springer Berlin Heidelberg, Berlin, Heidelberg, 2005, pp. 149–193.
15 M. O. Sinnokrot, E. F. Valeev and C. D. Sherrill, *J. Am. Chem. Soc.*, 2002, **124**, 10887–10893.
16 L. M. Salonen, M. Ellermann and F. Diederich, *Angew. Chem. Int. Ed.*, 2011, **50**, 4808–4842.
17 S. Tsuzuki, T. Uchimaru, M. K, M. Mikami and K. Tanabe, *Chem. Phys. Lett.*, 2000, **319**, 547–554.
18 S. Grimme, *Angew. Chem. Int. Ed.*, 2008, **47**, 3430–3434.
19 A. D. Bond, *CrystEngComm*, 2007, **9**, 833–834.
20 G. R. Desiraju, *Cryst. Growth Des.*, 2003, **5**, 466–467.
21 G. P. Stahly, *Cryst. Growth Des.*, 2009, **9**, 4212–4229.
22 N. Qiao, M. Li, W. Schlindwein, N. Malek, A. Davies and G. Trappitt, *Int. J. Pharm.*, 2011, **419**, 1–11.
23 C. B. Aakeroy, S. Forbes and J. Desper, *J. Am. Chem. Soc.*, 2009, **131**, 17048–17049.
24 D. Braga, F. Grepioni and L. Maini, *Chem. Commun.*, 2010, **46**, 6232–6242.
25 T. L. Threlfall, *Analyst*, 1995, **120**, 2435–2460.
26 G. R. Desiraju, *Cryst. Growth Des.*, 2008, **8**, 3–5.
27 H. G. Brittain, Ed., *Polymorphism in Pharmaceutical Solids*, Informa Healthcare USA, Inc., New York, 2009, vol. 192.
28 D. Giron, *Eng. Life Sci.*, 2003, **3**, 103–112.
29 J. D. Dunitz and J. Bernstein, *Acc. Chem. Res.*, 1995, **28**, 193–200.
30 Y. Beldjoudi, A. Arauzo, F. Palacio, M. Pilkington and J. M. Rawson, *J. Am. Chem. Soc.*, 2016, **138**, 4–11.
31 J. S. Miller and A. J. Epstein, *Angew. Chem. Int. Ed. Engl.*, 1994, **33**, 385–415.
32 J. S. Miller, J. C. Calabrese, H. Rommelmann, S. R. Chittipeddi, J. H. Zhang, W. M. Reiff and A. J. Epstein, *J. Am. Chem. Soc.*, 1987, **109**, 769–781.
33 J. S. Miller, *J. Mater. Chem.*, 2010, **20**, 1821–2040.
34 M. Tamura, Y. Nakazawa, D. Shiomi, K. Nozawa, Y. Hosokoshi, M. Ishikawa, M. Takahashi and M. Kinoshita, *Chem. Phys. Lett.*, 1991, **186**, 401–404.
35 P. M. Allemand, K. C. Khemani, A. Koch, F. Wudl, K. Holczer, S. Donovan, G. Gruner and J. D. Thompson, *Science (80-.).*, 1991, **253**, 301–302.

36 A. J. Banister, N. Bricklebank, I. Lavender, J. M. Rawson, C. I. Gregory, B. K. Tanner, W. Clegg, M. R. J. Elsegood and F. Palacio, *Angew. Chem. Int. Ed. Engl.*, 1996, **35**, 2533–2535.
37 R. I. Thomson, C. M. Pask, G. O. Lloyd, M. Mito and J. M. Rawson, *Chem. Eur. J.*, 2012, 1–6.
38 G. Antorrena, J. E. Davies, M. Hartley, F. Palacio, M. Jeremy, J. Nicholas, B. Smith and A. Steiner, *Chem. Commun.*, 1999, 1393–1394.
39 R. A. Beekman, R. T. Boeré, K. H. Moock and M. Parvez, *Can. J. Chem.*, 1998, **93**, 85–93.
40 J. M. Rawson, J. Luzon and F. Palacio, *Coord. Chem. Rev.*, 2005, 2631–2641.
41 R. G. Hicks, *Can. J. Chem.*, 2004, **82**, 1119–1127.
42 O. Armet, J. Veciana, C. Rovira, J. Riera, J. Castaner, E. Molins, J. Rius, C. Miravitlles, S. Olivella and J. Brichfeus, *J. Phys. Chem.*, 1987, **91**, 5608–5616.
43 J. H. Osiecki and E. F. Ullman, *J. Am. Chem. Soc.*, 1968, **2300**, 1078–1079.
44 D. A. Haynes, *CrystEngComm*, 2011, **13**, 4793–4805.
45 P. M. Allemand, C. Fite, G. Srdanov, N. Keder, F. Wudl and P. Canfield, *Synth. Mater.*, 1991, **41**–**43**, 3291–3295.
46 I. Ratera and J. Veciana, *Chem. Soc. Rev.*, 2012, **41**, 303–349.
47 M. Angelin, M. Hermansson, H. Dong and O. Ramstrom, *Eur. J. Org. Chem.*, 2006, 4323–4326.
48 A. J. Banister, A. S. Batsanov, O. G. Dawe, P. L. Herbertson, J. A. K. Howard, S. Lynn, I. May, J. N. B. Smith, J. M. Rawson, T. E. Rogers, B. K. Tanner, G. Antorrena and F. Palacio, *Dalt. Trans.*, 1997, 2539–2541.
49 A. Alberola, R. J. Less, C. M. Pask, J. M. Rawson, F. Palacio, P. Oliete, C. Paulsen, A. Yamaguchi, R. D. Farley and D. M. Murphy, *Angew. Chem. Int. Ed.*, 2003, **42**, 4782–4785.
50 W. V. F. Brooks, N. Burford, J. Passmore, M. J. Schriver and L. H. Sutcliffe, *Chem. Commun.*, 1987, 69–71.
51 A. Alberola, R. J. Less, F. Palacio, C. M. Pask and J. M. Rawson, *Molecules*, 2004, **9**, 771–781.
52 A. Alberola, C. S. Clarke, D. A. Haynes, S. I. Pascu and J. M. Rawson, *Chem. Comm.*, 2005, **3**, 4726–4728.
53 A. Vegas, A. Perez-Salazar, A. J. Banister and R. G. Hey, *J. Chem. Soc. Dalt. Trans.*, 1980, 1812–1815.
54 C. Allen, D. A. Haynes, C. M. Pask and J. M. Rawson, *CrystEngComm*, 2009, **11**, 2048–2050.
55 C. J. Cramer, *Essentials of Computational Chemistry*, 2004.
56 P. Hohenberg and W. Kohn, *Phys. Rev. B.*, 1964, **136**, 864–871.
57 Y. Zhao and D. G. Truhlar, *Acc. Chem. Res.*, 2008, **41**, 157–167.
58 W. Kohn, A. D. Becke and R. G. Parr, *J. Phys. Chem.*, 1996, **100**, 12974–12980.
59 W. Kohn and L. J. Sham, *Phys. Rev.*, 1965, **140**, 1133–1138.
60 A. D. Becke, *J. Chem. Phys.*, 1993, **98**, 1372–1377.
61 S. Grimme, *J. Comput. Chem.*, 2006, **27**, 1787–1799.
62 A. D. Becke, *J. Chem. Phys.*, 1993, **98**, 5648–5652.
63 D. M. Ceperley and B. J. Alder, *Phys. Rev. Lett.*, 1980, **45**, 566–569.
64 S. H. Vosko, L. Wilk and M. Nusair, *Can. J. Chem.*, 1980, **58**, 1200–1211.
65 A. D. Becke, *J. Chem. Phys.*, 1997, **107**, 8554–8560.
66 M. Filatov and W. Thiel, *Mol. Phys.*, 1997, **91**, 847–859.
67 M. Filatov and W. Thiel, *Int. J. Quant. Chem.*, 1997, **62**, 603–616.
68 J. P. Perdew and Y. Wang, *Phys. Rev. B.*, 1986, **33**, 8800.
69 C. Adamo and V. Barone, *J. Chem. Phys.*, 1998, **108**, 664–675.
70 X. Xu and W. A. Goddard III, *PNAS*, 2004, **101**, 2673–2677.
71 A. D. Becke, *Phys. Rev. A.*, 1988, **38**, 3098–3100.
72 J. P. Perdew, J. A. Chevary, S. H. Vosko, K. A. Jackson, M. R. Pederson, D. J. Singh and C. Fiolhais, *Phys. Rev. B.*, 1992, **46**, 6671–6687.
73 A. D. Becke, *J. Chem. Phys.*, 1986, **4524**, 4524–4529.
74 J. P. Perdew, K. Burke and M. Ernzerhof, *Phys. Rev. Lett.*, 1996, **77**, 3865–3868.
75 C. Adamo and V. Barone, *J. Chem. Phys.*, 2002, **116**, 5933–5940.

76 J. P. Perdew, *Phys. Rev. B.*, 1986, **33**, 8822–8824.
77 C. Lee, W. Yang and R. G. Parr, *Phys. Rev. B.*, 1988, **37**, 785–789.
78 J. P. Perdew, M. Ernzerhof and K. Burke, *J. Chem. Phys.*, 1996, **105**, 9982–9985.
79 C. Adamo and V. Barone, *J. Chem. Phys.*, 1999, **110**, 6158–6170.
80 S. Grimme, *J. Comput. Chem.*, 2004, **25**, 1463–1473.
81 Q. Wu and W. Yang, *J. Chem. Phys.*, 2002, **116**, 515–524.
82 A. Alberola, E. Carter, C. P. Constantinides, D. J. Eisler, D. M. Murphy and J. M. Rawson, *Chem. Commun.*, 2011, **47**, 2532–2534.
83 E. M. Fatila, M. C. Jennings, J. Goodreid and K. E. Preuss, *Acta Cryst.*, 2010, **C66**, 260–264.
84 D. G. B. Boocock and E. F. Ullman, *J. Am. Chem. Soc.*, 1968, 6873–6874.
85 C. Hirel, K. E. Vostrikova, J. Pecaut, V. I. Ovcharenko and P. Rey, *Chem. Eur. J*, 2001, **7**, 2007–2014.
86 R. M. Buchanan and C. G. Pierpont, *J. Am. Chem. Soc.*, 1980, **102**, 4951.

Chapter 2

Materials and Methods

WE MIGHT AS WELL ATTEMPT TO INTRODUCE A NEW PLANET
INTO THE SOLAR SYSTEM, OR TO ANNIHILATE ONE ALREADY IN EXISTENCE,
AS TO CREATE OR DESTROY A PARTICLE OF HYDROGEN.
ALL THE CHANGES WE CAN PRODUCE CONSIST IN SEPARATING PARTICLES
THAT ARE IN A STATE OF … COMBINATION, AND JOINING
THOSE THAT WERE PREVIOUSLY AT A DISTANCE.

-- JOHN DALTON, 1810

This chapter contains a detailed discussion of the synthesis of some dithiadiazolyl (DTDA) as well as nitroxide radicals, as well as their characterisation. Synthesis of radical cocrystals, polymorphs and charge transfer complexes will be discussed in the relevant chapters 3, 4 and 5 respectively. Computational methods as well as problems encountered and solutions employed will also be discussed in this chapter. However, more detailed methods and results related to specific models and systems will be presented and discussed in their relevant sections in this thesis.

2.1 Experimental techniques and methods

2.1.1 Materials

Except where specifically otherwise stated, all starting materials for synthesis were purchased either from Sigma Aldrich, FluoroChem or LGC Chemicals (SA branch for Alfa Aesar) and were used as is. Solvents used for synthesis were purchased from Sigma Aldrich whereas crystallisation solvents as well as diethyl ether were purchased from Kimix. Diethyl ether was dried over molecular sieves that were activated in a furnace for 48 hours, and ethyl acetate and *n*-hexanes were purified by distillation before use. All other solvents were used as received.

2.1.2 Instrumentation

2.1.2.1 Single crystal X-ray diffraction (SCXRD)

Crystals of the desired size and quality were coated in paratone oil and mounted on a MiTeGen mount of appropriate size. The mount was then placed on a goniometer head of a single crystal x-ray diffractometer.

X-ray data were collected on a Bruker D8 Venture or Bruker SMART Apex diffractometer under the software control of Apex2 or Apex3. The D8 Venture is equipped with a microfocus MoKα sealed tube X-ray source as well as a Photon II detector. It is fitted with an Oxford Cryostream 800 Series cryostat, used to control the temperature for data collection at 100 K. Data reduction and absorption corrections were done using SAINT[1] and SADABS[2], respectively. The SMART Apex is equipped with a Mo-Kα fine-focus sealed tube Iμs X-ray source, multilayer-monochromator 0.5 mm collimator and an Apex II detector. It is fitted with an Oxford Cryostream 700 Series cryostat, used to control the temperature for data collection. The structures were solved with the aid of the X-Seed[3] graphical user interface with SHELXS-97[4] using direct methods, and subsequently refined with SHELXL-2014[5], SHELXD-97[6] or using least squares minimisation or solved with SHELXT[7]. Non-

hydrogen atoms were refined anisotropically. Mixed hydrogen treatment was employed, with non-hydroxyl hydrogens placed at calculated positions using riding models. Hydroxyl hydrogens were found in Fourier difference maps and refined isotropically.

2.1.2.2 Thermal analysis

Thermogravimetric analysis (TGA) was performed by measuring the mass loss as the sample was heated at a constant rate. A TA Instruments Q500 thermogravimetric analyser was used. Samples of about 2-6 mg were placed in an open aluminium pan, placed inside the furnace and the temperature was ramped from room temperature to 600 °C at a constant heating rate of 10 °C/min. N_2 gas flowing at a rate of 50 ml min^{-1} was used to purge the furnace.

Differential Scanning Calorimetry (DSC) was performed on a TA Instruments Q20 system attached to a cooling unit, under N_2 purge with a flow rate of 50 ml min^{-1}. Samples were typically powders or crystalline material of about 1-4 mg, placed in hermetically or non-hermitically sealed aluminium pans with non-vented lids. Reference pans were prepared in the same manner. Non-vented lids were chosen since all compounds used in this project sublime, and an open lid would have resulted in unwanted material loss during the DSC runs. A standard procedure was used on all samples initially, with subsequent modification where necessary. Samples were initially allowed to equilibrate at 30 °C. The temperature was then decreased to -80 °C (either 5 or 10 °C/min), followed by an increase in temperature to 120 °C (10 °C /min) in the case of the DTDA radicals, and possibly higher in the case of compounds with higher melting points and/or degradation temperatures. The upper temperature limit was determined by the degradation temperature indicated on the TGA of each sample. Where no thermal events were seen, sample procedures were modified such that temperatures were decreased to -20 °C followed by an increase to either 80 or 100 °C. Each of these procedures was cycled at least twice for each sample. DSC runs modified more specifically to certain samples will be described in the relevant section.

For hot stage microscopy, a Linkam DSC600 hot stage equipped with a T95-System Controller was used. Depending on the sample, either aluminium or sapphire pans were used to hold the samples, which were subjected to cooling/heating cycles analogous to the DSC runs, except at a heating rate of 5 °C/min. Final data was processed using the Linksys32 software.

2.1.2.3 Powder X-ray diffraction

Variable temperature powder X-ray diffraction experiments were carried out on a PANalytical X'Pert PRO instrument using Bragg-Brentano geometry. Intensity data were collected using an X'Celerator detector and 2θ scans (Cu Kα radiation, λ = 1.5418 Å) were carried out in the range of 5-50° at 45 kV and 40 mA, with exposure time ranging from 150 to 180 s/step, depending on the peak intensities. Powder samples were placed in 0.5 or 1.5 mm capillaries and mounted on a goniometer head of the diffractometer, using a gas-cell apparatus (Figure 2.1).[8,9]

The setup consists of a brass gas cell with a threaded valve. A glass capillary containing powdered sample is inserted into the gas cell and mounted onto a goniometer head that oscillates around 180°

Figure 2.1. Gas cell setup

Ambient temperature powder patterns were collected using a Bruker D2 Phaser diffractometer with (Bragg Brentano geometry) using CuKα radiation (λ = 1.5418 Å) at 30 kV and 10 mA. The instrument is equipped with a Lynxeye detector with 2θ scans performed in the range 4-50° with a 0.016° step size. Samples were spun at 30 revolutions per minute.

2.1.2.4 Spectroscopy and spectrometry

Nuclear Magnetic Resonance (NMR) spectroscopy was used as characterisation tool. All samples (20-30 mg) were prepared using deuterated dimethylsulfoxide (DMSO-d_6). Analysis was carried out at the Central Analytical Facility of the University of Stellenbosch on a VNMRS Agilent (300/400 MHz) or an Inova Agilent (600 MHz) NMR spectrometer for both ^{1}H-NMR and ^{13}C-NMR.

Infrared spectroscopy (IR) was also used as a fingerprinting characterisation tool. Analysis was performed on a Bruker ALPHA FTIR spectrometer, complete with attenuated total reflection (ATR) capabilities for the analysis of powders, solids, liquids and pastes.

2.2 Synthesis and characterisation of dithiadiazolyl (DTDA) radicals

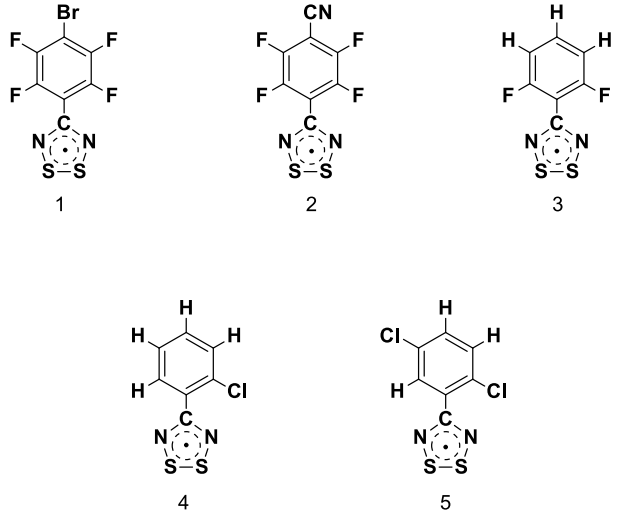

Figure 2.2. List of the DTDA radicals synthesised for the purpose of this project.

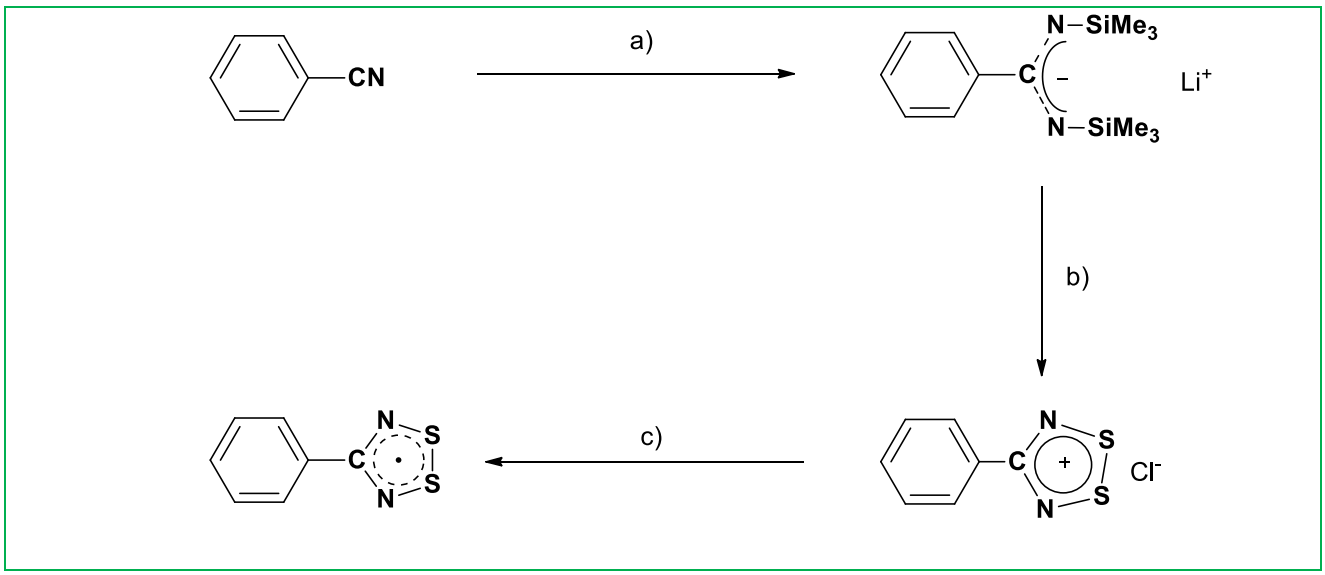

Scheme 2.1. General synthetic route for the multistep synthesis of dithiadiazolyl radicals. a) HMDS (1 eq.), n-BuLi (1 eq.), Et_2O, stir overnight, b) S_2Cl_2 or SCl_2 (excess), 1-3 hrs, c) $SbPh_3$ (0.7 eq.), 60 °C, overnight.

The procedure followed for the synthesis of the DTDA radicals (Figure 2.2) is modified from a well-established literature procedure.[10,11] This modified procedure involves the reaction of a parent nitrile,

bearing a chosen R-functionality, with hexamethyldisilazane (HMDS) forming lithium bis(HMDS) *in situ*. This is followed by condensation with SCl_2 or S_2Cl_2 and, finally, triphenylantimony ($SbPh_3$) reducing agent (Scheme 2.1). Radicals are then purified by sublimation under vacuum, onto a water-cooled cold finger. The SCl_2/S_2Cl_2 is synthesised in house by careful reaction of pure Cl_2 (g) with sulphur powder, and a final distillation to purify the SCl_2. The entire procedure is performed under inert conditions using standard Schlenk techniques.

2.2.1 Synthesis of SCl_2

Powdered sufur (100 g, 3.12 mol.) was placed in a 500 ml round-bottom flask (RB). A flow of chlorine gas was then bubble over the sulfur powder at ~1 bubble per second. The atmosphere inside the RB changes to a cloudy yellow after a few minutes. The flow of chlorine is then increased to ~2 bubbles per second, whereafter the sulfur powder changes colour to orange-brown. Yellow droplets start forming on the side of the RB and orange-brown liquid starts forming along the edges of the sulfur powder. At this point, stirring is started. Stirring increases the Cl_2 consumption, so the flow rate has to be adjusted accordingly. After about 10 minutes, the entire contents of the RB is liquid. As reaction with the Cl_2 proceeds, the colour of the liquid changes from bright yellow, to bright orange, to dark red. The dark red colour appears after about 1 hour. Iron trichloride ($FeCl_3$, 0.1 g, 0.6 mmol.) was added to the solution, the flask placed in a water bath, and stirring continued for an additional hour.

The next step of the synthesis involved distillation of the SCl_2. Phosphorus trichloride (PCl_3, 2 ml, 0.023 mol.) was added to the solution before heating, and the SCl_2 fraction collected between 55-60 °C as a dark cherry red liquid.

2.2.2 Synthesis of 4-bromoperfluorobenzonitrile

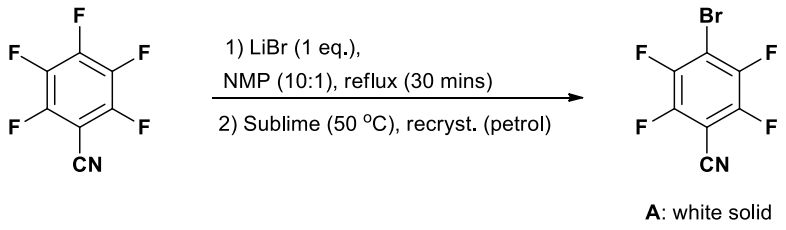

Scheme 2.2. The synthesis of 4-bromo-2,3,5,6-tetrafluorobenzonitirile from pentafluorobenzonitrile

Although the parent 4-bromo-2,3,5,6-tetrafluorobenzonitirile used for the synthesis of **1** can be bought from a number of chemical stores, it is expensive, and its synthesis is very simple. As a result, we chose to synthesise this starting nitrile in the lab. The procedure is a two-step synthesis. The first step involved refluxing pentafluorobenzonitrile (0.956 g, 4.95 mmol.) along with 1 eq. of lithium bromide (0.43 g, 4.95 mmol.) in 10 eq. N-methyl-2-pyrrolidone (NMP, 0.0495 mol, 4.8 ml) for 30 minutes. The solution becomes dark brown in colour, and towards the end of the reflux, a dark precipitate clearly starts forming. The reaction was quenched with 20 ml H_2O whereafter the dark brown precipitate was filtered off. The product was sublimed at 55 °C onto a cold finger under static vacuum in a Schlenk. The crystals of **A** that formed on the cold finger were white of colour (0.58 g, 46%).

Compound **A** was compared to commercially-bought 4-bromoperfluorobenzonitrile purchased from Sigma Aldrich in order to compare efficacy and yield during the synthesis of radical **1**. The yields using the in-house synthesised nitrile compares very well with commercially-bought nitrile (see Appendix A).

2.2.3 Synthesis of 4-(4′-bromoperfluorophenyl)-1,2,3,5-dithiadiazolyl (1)

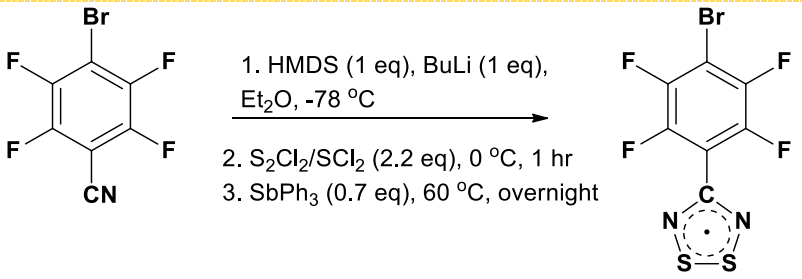

Scheme 2.3. The synthesis of 4-(4′-bromoperfluorophenyl)-1,2,3,5-dithiadiazolyl radical.

Dry diethyl ether (30 ml) was added to a Schlenk under constant N_2 atmosphere, and cooled to -78 °C. Hexamethyldisilazane (HMDS, 0.414 ml, 0.319 g, 1.97 mmol) and *n*-butyllithium (BuLi, 1.6 M solution in hexanes, 1.232 ml, 1.97 mmol) were added to the cooled solvent, follow by the addition of 4-bromobenzonitrile (0.5 g, 1.97 mmol). The reaction was warmed to room temperature as it proceeds to form the lithiated intermediate, LiHMDS. As the HMDS and BuLi react, the solution turns milky white in colour. Once this solution has gone clear and was warmed to room temperature, nitrile was added, when an immediate colour change to a pale yellow colour was observed – this turned orange/brown after a few hours. This was allowed to stir at room temperature overnight, followed by cooling the solution to 0 °C and adding the SCl_2 (2.2 eq., 0.27 ml, 0.437 g). Immediately, an orange precipitate formed. This was left to stir at room temperature for 1 hour, after which it was filtered using a cannula filter, and washed with 2 x 15 ml Et_2O. The resulting orange/brown salt was dried *in vacuo* for an additional 1-2 hours to ensure all solvent had been removed. The final step in the synthesis was the solvent-free reduction using $SbPh_3$ (0.7 eq., 1.38 mmol, 0.487 g). The white powder was added to the salt and mixed well to increase contact surface area, and was heated to 60 °C overnight. After a few minutes, a colour change from orange to dark brown/black was observed, indicating successful reduction of the salt. Once all the salt was reduced, the radical was purified by sublimation onto a cold finger under static vacuum between 90-100 °C and was collected as dark brown/black thin needles and plates (0.11 g, 17%).

2.2.4 Synthesis of 4-(4′-cyanoperfluorophenyl)-1,2,3,5-dithiadiazolyl (2)

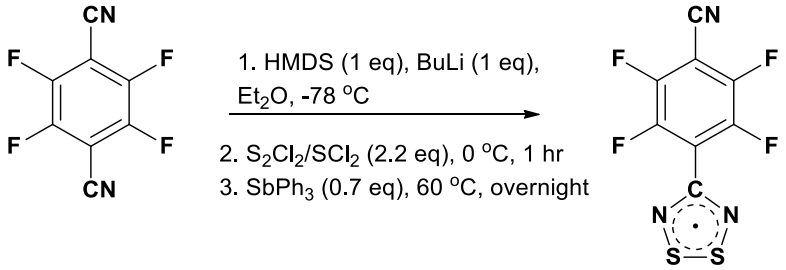

Scheme 2.4. Synthetic route for the synthesis of 4-(4′-cyanoperfluorophenyl)-1,2,3,5-dithiadiazolyl radical.[12]

HMDS (1 eq., 1.03 ml, 0.793 g, 4.92 mmol) and *n*-BuLi (1 eq., 3.07 ml, 0.315 g, 4.92 mmol) were added to Et_2O (40 ml) cooled to -78 °C. The solution was removed from the slurry and allowed to warm to room temperature, again turning milky as the formation of LiHMDS proceeds. After 20 minutes, the solution had gone clear, and the 1,4-dicyano-2,3,5,6-tetrafluorobenzonitrile (1 g, 4.92 mmol) was added and allowed to stir overnight. An immediate colour change to bright yellow was observed, and after about an hour the solution was a clear dark brown/red. The next step included the addition of SCl_2 (2.5 eq., 0.782 ml, 1.26 g, 0.012 mol) which resulted in an immediate brown precipitate*.

After an hour, the salt was washed with 2 x 15 ml Et_2O and filtered using a cannula filter. The salt was dried *in vacuo*. The brown/orange salt was reduced using $SbPh_3$ (0.7 eq., 3.44 mmol, 1.21 g) between 60 -70 °C overnight, resulting in a dark brown/black solid. The radical was purified by sublimation onto a cold finger between 100-120 °C and collected† as black needles (0.36 g, 26%). **MS ESI**$^+$: $[M+H]^+$ 277.9464 g/mol, calculated for $C_8F_4N_3S_2$ 277.2251 g/mol.

* after making this radical a number of times, using both SCl_2 and S_2Cl_2, lower yields were noticed when using S_2Cl_2 as well as a decrease in yield when the salt-formation step is left to stir for longer than 1/1.5 hrs.

† the sublimation temperature of this radical is quite high, and close to that of $SbPh_3$. When increasing sublimation temperature above 115 °C you often get $SbPh_3$ co-subliming with the radical onto the cold finger, which is undesirable. Additionally, it was noticed that this radical is temperature sensitive and degrades after longer exposure to elevated temperatures. Ideally crystals should be collected within 24 hours of starting the sublimation for best quality crystals and minimisation of degradation due to heat. Out of all the radicals used in this project, this one is also the most air sensitive – with signs of degradation only moments after being exposed to air.

2.2.5 Synthesis of 4-(2',6'-difluorophenyl)-1,2,3,5-dithiadiazolyl (3)

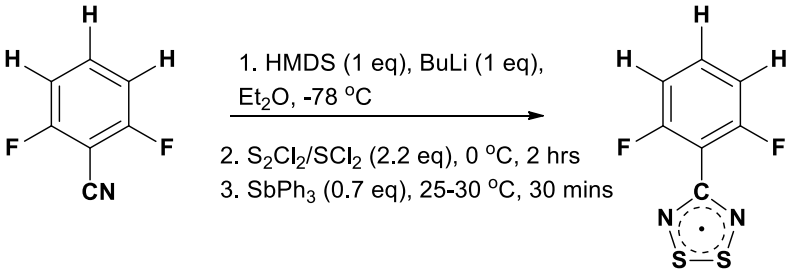

Scheme 2.5. Synthetic route for the synthesis of 4-(2',6'-difluorophenyl)-1,2,3,5-dithiadiazolyl radical.[13]

HMDS (1 eq., 1.50 ml, 7.18 mmol, 1.16 g) and *n*-BuLi (1 eq., 4.48 ml, 7.18 mmol, 0.46 g) were added to Et_2O (40ml) at -78 °C, resulting in a cloudy solution. After warming to room temperature and stirring for about 20 minutes, the solution went clear and the 2,6-difluorobenzonitrile (1 g, 7.18 mmol) was added. An immediate colour change from yellow, to orange to brown/green was observed. This solution was allowed to stir at room temperature overnight. Subsequent addition of SCl_2 (2.5 eq., 1.14 ml, 1.84 g, 0.018 mol) resulted in a dark orange precipitate which was left to stir for 2 hours. The resulting brown/orange salt was washed with 2 x 15 ml Et_2O and dried *in vacuo*. The reduction of this salt with $SbPh_3$ proceeded slightly differently to the rest of the radicals, in that it happens at room temperature conditions, very quickly. Upon adding the $SbPh_3$ (0.7 eq., 4.16 mmol, 1.47 g), reduction started immediately, evident by the salt immediately changing colour to dark brown/black. The reduction was completed within 30 minutes between 25-30 °C. The radical was purified by sublimation onto a cold finger between 35-100 °C as a mixture of morphologies, ranging from green/gold, to purple/gold to black/gold blocks and needles in 8-25% yield. This radical has 3 known polymorphs, each having a different sublimation temperature, so the resulting product collected from the cold finger is a mixture of 3 polymorphs (refer to Chapter 3 for this polymorph study). **MS ESI$^+$**: $[M+H]^+$ 216.9707 g/mol, calculated for $C_7H_3F_2N_2S_2$ 216.2348 g/mol.

2.2.6 Synthesis of 4-(2'-chlorophenyl)-1,2,3,5-dithiadiazolyl (4)

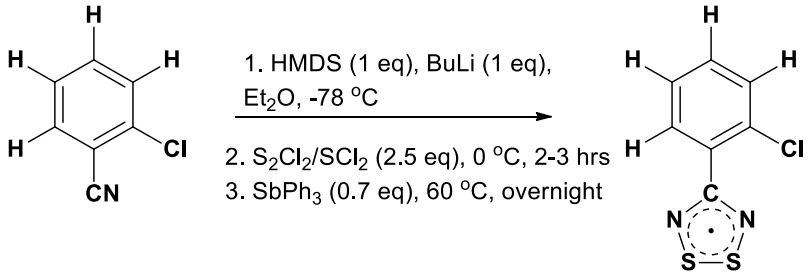

Scheme 2.6. Synthetic route for the synthesis of 4-(2'-chlorophenyl)-1,2,3,5-dithiadiazolyl radical.[14]

HMDS (1 eq., 1.52 ml, 1.17 g, 7.26 mmol) and *n*-BuLi (1 eq., 4.54 ml, 0.47 g, 7.26 mmol) were added to Et_2O (30ml) at -78 °C, resulting in a cloudy solution. After warming to room temperature and stirring for about 20 minutes, the solution went clear and 2-chlorobenzonitrile (1 g, 7.26 mmol.) was added. An immediate colour change to dark orange was observed, and the resulting solution was allowed to stir at room temperature After a few hours, the solution appeared more red/orange. Addition of S_2Cl_2 (2.5 eq., 1.15 ml, 1.87 g, 0.018 mol) resulted in a yellow/orange precipitate, and the resulting mixture was left to stir for 2-3 hours. The salt was filtered, washed with 2 x 15 ml Et_2O and dried in *in vacuo*. Reduction of the salt with $SbPh_3$ (0.7 eq., 5.08 mmol. 1.8 g) followed, whereafter the mixture was heated to 60 °C and left to reduce overnight. The resulting reduced salt was dark red/black in colour. The radical was purified by sublimation onto a cold finger at 80 °C and collected as black blocks/powder over 2 to 3 days (0.28 g, 18%). **MS ESI$^+$**: $[M+H]^+$ 214.9494 g/mol, calculated for $C_7H_4ClN_2S_2$ 214.6997 g/mol.

2.2.7 Synthesis of 4-(2',5'-dichlorophenyl)-1,2,3,5-dithiadiazolyl (5)

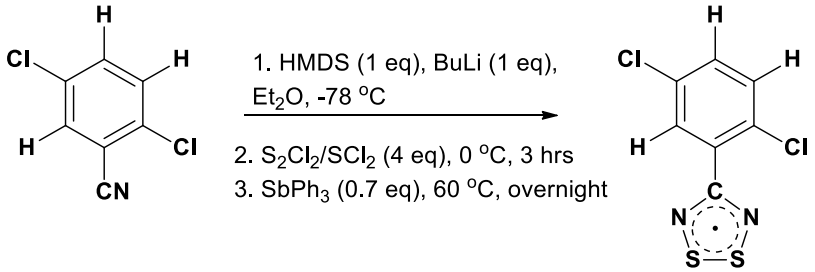

Scheme 2.7. Synthetic route for the synthesis of 4-(2',5'-dichlorophenyl)-1,2,3,5-dithiadiazolyl radical.[14]

HMDS (1 eq., 1.22 ml, 0.94 g, 5.81 mmol) and *n*-BuLi (1 eq., 3.64 ml, 0.37 g, 5.81 mmol) were added to Et_2O (30ml) at -78 °C, resulting in a cloudy solution. After warming to room temperature and stirring for about 15 minutes, the solution went clear and 2,5-dichlorobenzonitrile (1 g, 5.81 mmol.) was added. The solution turned a blue/green colour, which is unusual for these types of radicals, however this was allowed to stir at room temperature overnight. Addition of S_2Cl_2 (4 eq., 1.94 ml, 3.14 g, 0.02 mol) resulted in a yellow precipitate, which was left to stir for 3 hours.[‡] The salt was washed with 3 x 15 ml Et_2O and dried in *in vacuo*. The reduction step followed, with the addition of $SbPh_3$ (0.7 eq., 4.07 mmol., 1.43 g) and the mixture was heated to 60 °C and left to reduce overnight. The radical was purified from the resulting red/black salt by sublimation onto a cold finger at 90-110 °C and collected as black blocks/powder (0.35 g, 24%). **MS ESI$^+$**: $[M+H]^+$ 249.9180 g/mol, calculated for $C_7H_3Cl_2N_2S_2$ 249.1448 g/mol.

2.3 Attempted synthesis of a nitroxide radical

As mentioned in chapter 1, a lot of research has focused on co-crystallising DTDA radicals with one another, however, whether the dimerisation might be more effectively prevented by attempting co-crystallisation of DTDA radicals with non-sulphur based radicals, like the group of nitroxide radicals

[‡] The chlorinated radicals react at a slower rate with the S_2Cl_2/SCl_2 and hence stirred for 3 hours as opposed to the 1-2 hours for the fluorinated radicals.

(oxygen-based radicals), was investigated. The synthesis of nitroxides is a well-established multi-step route commonly referred to as the Ullman procedure[15], however the first step of this synthetic route posed a number of issues. These issues, mostly stemming from the challenging reduction of an aliphatic nitro functionality, did not only arise in our own attempts to synthesise this radical, but is a common problem in the literature as well[16]. Alternative synthetic procedures for the reduction of aliphatic nitro groups are rare in literature, and as a result, most attempted synthetic procedures were designed for aromatic nitros, and were unsuccessful. The most common synthesis of *p*-nitrophenyl nitronyl nitroxide (*p*-NPNN) entails reduction of the nitro, followed by condensation with an aldehyde bearing the desired functional group and, finally, oxidation to get the desired radical.

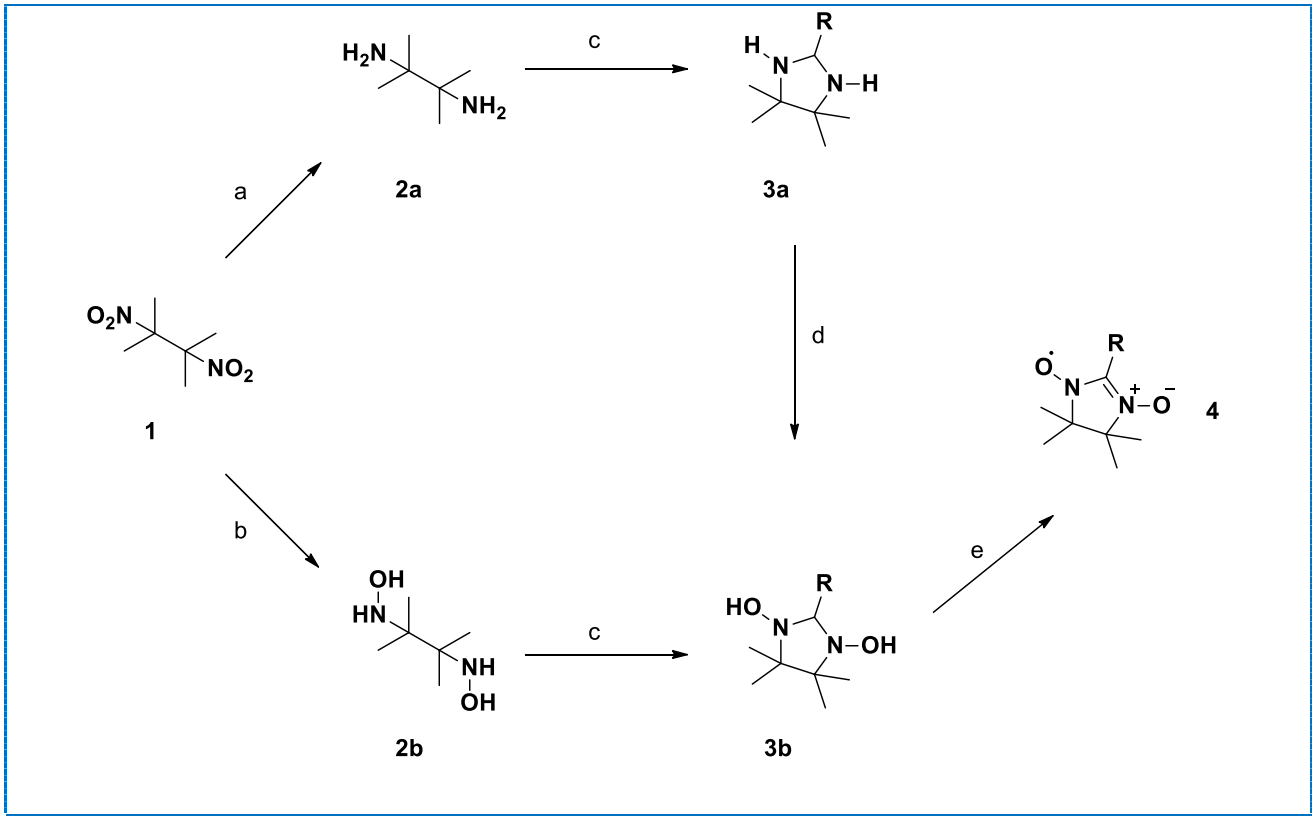

Scheme 2.8. Multi-step synthetic route towards *p*-NPNN. a) Zn/NH_4, THF/H_2O, b) Sn, OR Zn, c) RHCO, methanol, $CHCl_3$, d) *m*-chloroperbenzoic acid/ CH_2Cl_2, e) $NaIO_4$ or MnO_2, CH_2Cl_2/H_2O.

2.3.1 Synthesis of dimethyldiaminobutane DMDA (2a)

The first attempted reduction of the nitro followed the synthesis put forward by Hirel *et al.* in 2001, using tin (Sn) as catalyst. Dimethyldinitrobutane (DMDN, 0.2 g, 1.13 mmol) was initially suspended

in conc. HCl (5 ml) at room temperature and consequently refluxed, which yielded no product. Instead, in subsequent reactions the DMDN was added to conc. HCl at 60 °C. Granular Sn (1.07 g, 9.04 mmol) was added in small portions with constant stirring, and once all the Sn had been added, the reaction refluxed for 4 hours. The final clear reaction solution was quenched with 30 ml Et_2O and the water layer carefully basified to pH≈10 using conc. NaOH; the aqueous layer turns milky around pH=3. The fine white solid was centrifuged out of the aqueous layer. Analysis by NMR showed no product formation.

Table 2.1. Summary of reactants and equivalents used for the attempted synthesis of dimethyldiaminobutane from dimethyldinitrobutane.

	Reactant	**Equivalent**	**Mass/Vol**	**mmol**
Attempt 1	DMDN	1	0.2 g	1.13
	Sn (granular)	8	1.07	9.04
	HCl (conc.)		5 ml	
Attempt 2	DMDN	1	1.5 g	8.52
	NH_4Cl	24	10.9 g	204
	Zn (elemental)	6	3.3 g	
	Solvent:	**MeOH (1):H_2O (1):AcCN (2)**		

The second attempted reduction of the nitro to an amine was done using Zn metal as catalyst. The DMDN (1 eq., 1.5 g) and NH_4Cl (24 eq., 10.9 g) were added to a 2:1 mixture of H_2O:AcCN (18.8 ml H_2O, 35.8 ml AcCN) in a 2-necked round bottom flask. Two immiscible layers were present, and the layers became miscible with the final addition of MeOH (18.8 ml). This mixture was stirred at room temperature. After an hour the solution went pink, and after 2 hours this pink solution was filtered to remove the excess solid and washed with MeOH. The filtrate was washed with 3 x 20 ml EtOAc, where after the bright pink organic layer was washed with 40 ml brine, dried over $MgSO_4$, and the solvent removed *in vacuo*. However, after obtaining no product in the form of liquid or solid after removal of the solvent, it became apparent that the small aliphatic amine is partially soluble in both the organic and aqueous phases and this poses a problem for liquid-liquid extraction. It was also later discovered that the pink colour presented by the organic phase was possibly due to the

presence of small amounts of nitroxide radical. The bis(hydroxyamine) formed first, which then oxidises alcohols (in this case the MeOH) into aldehydes, where the bis(hydroxyamine) is then air oxidised into the nitroxide[16]. Instead, the reaction was tried again, using THF as solvent.

2.3.2 Synthesis of bis-(dihydroxyamino)butane (2b)

The synthesis of the bis-(dihydroxyamino)butane is the more common Ullman route referred to above, with some minor adjustments. Although it is not explicitly stated in the procedure to do so, as a precaution this reaction was performed under strictly inert conditions since the bis-(dihydroxy) isn't stable to air. DMDN (0.5 g, 1 eq.) was dissolved in 15 ml THF, whilst NH_4Cl (1.22 g, 5.3 M) was separately dissolved in 8 ml H_2O. The NH_4Cl solution was then added to the THF mixture in a Schlenk, under a blanket of Argon gas. The reaction was cooled to 8-12 °C, with Ar(g) bubbling through the reaction mixture to rid it of any oxygen. While the reaction was kept at 8-12 °C, Zn (granular, 0.801 g) was added in portions over 1 hour, and then stirred for a further 2 hours. The Schlenk was sealed under Ar(g) and kept in the fridge at 4 °C overnight. The reaction solution was filtered and washed with 5 x 50 ml THF. The organic layer was isolated, dried over $MgSO_4$ and the solvent removed *in vacuo*. An oil was obtained, but analysis by NMR indicated no product formation.

In the end, the *p*-NPNN radical could not be successfully synthesised, and was not attempted further for use in this project

2.4 Computational Methods

In this section, a brief overview of the manner in which calculations were performed and visualisation done will be given. Details specific to certain areas of this project will be reiterated and discussed in the relevant chapters, with reference to methods and computational software tools discussed in this section as well as chapter 1.

2.4.1 Visualisation tools

For the visualisation of geometry optimisations and vibrational energies, as well as building the models which will be discussed in chapter 6, the program ChemCraft v1.8, authored by Grigoriy Adrienko was used[17]. It is a simple and powerful open-source visualisation tool for quantum chemistry computations, and is well suited to visualise the output files produced by Gaussian09. In addition to being a powerful visualisation tool, it also supports tools for constructing and manipulating molecular structures and building Z-matrices for easy input file construction, without requiring additional graphical acceleration. The software suite used for the periodic calculations (which will be discussed later) has its own built-in visualisation graphical user interface (GUI).

2.4.2 Gas-phase computation

As mentioned in chapter 1, the computational aspect of this project essentially entails two parts: a) studying the systems in the gas phase to gain some insight into the stability and favourability of the dimers in the gas phase, and b) studying the systems periodically, to compare the effects of packing interactions and their role on the dimer interactions. This section will discuss the computational methods employed for the gas-phase calculations. Except where explicitly stated otherwise, all final values which will be presented were corrected for the zero-point vibrational energy contribution.

The software package employed for 0 K gas-phase computation was Gaussian09 revision D.01, a software suite for computational chemistry.[18] Gaussian09 has a wide spectrum of capabilities, including molecular mechanics (MM), semi-empirical methods, Hartree-Fock (HF), Møller-Plesset perturbation theory (MP) and density functional theory (DFT), to name a few.

2.4.2.1 Hydrogen treatment

Except in cases where full geometry optimisations were performed (which is explicitly stated, where relevant), all hydrogens were optimised to neutron distances. This was done using a very simple

method in Gaussian whereby all non-hydrogen atoms are assigned the number *-1* whilst all hydrogens were assigned the number *0*. Along with the keyword NoSymm, this allows for easy H-atom optimisation.

2.4.2.2 Basis sets and functionals

The B3LYP[19] DFT functional was used for all gas-phase calculations, including geometry optimisations as well as single point energy calculations. This functional is known to be a trusted general purpose functional[20,21], and is said to describe electrostatics and predict minimum energy geometries quite well[22,23,24], however it does not account for dispersion interactions. As a result, Grimme's third generation dispersion correction, GD3, was applied to all calculations[25]. The all-electron basis set 6-311++G(d,p)[26] (also sometimes denoted 6-311++G**) was used for all calculations. Although this is a large basis set and generally computationally very expensive, the systems worked with in this project are all organic and small and so the expense was not an issue. Calculations on similar systems in the literature have been performed using the same basis set, or 6-31G(d,p), which is smaller than the one used in this project[27].

2.4.2.3 List of important keywords

Calculations were initially performed using simple redundant internal coordinates specified by Gaussian. Initially, no integration grid was specified and no special keywords used. It became apparent very soon that there were issues with the way Gaussian defines certain torsion angles between the monomer units of a dimer, so Opt=Cartesian was used to solve this problem. In this way, Gaussian defines the model using Cartesian coordinates instead of a creating a redundant internal coordinate system. Using Cartesian coordinates in Gaussian does not allow one to perform partial optimisations or freeze atoms with ModRedundant, which had to be done for some select cases which will be discussed in the relevant sections. In those cases, Opt=ModRedundant was used for the partial optimisation.

Along with noticing problems with the coordinate system used by Gaussian for some models in this project, many of the optimisations showed convergence issues. In order to solve this issue, SCF=XQC along with a very fine integration grid was used by way of the keyword Integral(Grid=UltraFine). The QC keyword allows for the use of quadratically convergent methods in the SCF process[28]. In this way, when the model is far from convergence a steepest descent method[29] is employed, whereas, unless the energy goes up, Newton-Raphson steps are used when close to convergence. In the event that the first-order SCF has not converged, XQC adds an extra SCF=QC step, and as a result this method is more computationally expensive than a simple SCF. The dispersion correction was added to all calculations using EmpiricalDispersion=GD3.

2.4.3 Periodic systems

The second aspect of the computational portion of this project entailed looking at the known radical cocrystals, and their co-formers, in the solid state. In addition to studying the dimer pair interactions in the gas phase, it was speculated that additional answers might stem from studying the solid-state packing. To our knowledge, these radicals have not been studied periodically, or at least, results of periodic calculations on these radicals have not been published. The reason for this is quite simple: computationally, radicals are complicated. The periodic calculations performed on these systems are by no means straight forward, since finding a way to work around the singlet or triplet state multiplicity of these systems makes manipulating the periodic model more complicated, and this was not completely resolved during this project. However, some interesting results were found and will be presented nonetheless. Again, this section will cover the overarching methods used for the periodic calculations; computation specific to certain areas will be presented in the relevant chapter.

The periodic calculations were carried out using the Materials Studio 2016 (MS16) computation chemistry software suite, using the CASTEP[30] and DMol[3(31,32)] modules and DFT calculations. MS16 also has its own built-in visualiser for visualisation of all properties calculated.

2.4.4 Hydrogen treatment

As with the gas-phase calculations, all hydrogens in all structures were optimised to neutron distances prior to any property calculations. This was easily done in MS16 by applying constraints to the coordinates of all non-hydrogen atoms, and optimisation was then done using the CASTEP module. Grimme's second generation dispersion correction GD2[33] was applied to all calculations. Although this dispersion correction is not as accurate in its attempt to account for non-covalent interactions, as is the case for the GD3, the GD3 correction is not implemented in MS16. However, although GD3 shows slight improvements in accuracy for "light" molecules and weak interactions, it performs very similar to GD2 in conjunction with the PBE functional, as shown by Grimme *et al.* in 2010.[25]

2.4.4.1 Lattice energy calculations

Lattice energies were calculated for the periodic structures, and not lattice enthalpies. This was done since, for an accurate description of the thermodynamic properties, the structures need to preferably be in a global energy minimum providing no imaginary frequencies. However, since the idea is to study the structures as they are in the solid state, and not optimise beyond the hydrogens, not all the structures are in global energy minima, especially not completely fluorinated structures where no optimisations were done. Hence an accurate description of the thermodynamics cannot be calculated due to the presence of imaginary frequencies. Lattice energies were calculated as follows:

$$E_{latt=} \frac{E_{cryst}}{Z} - \sum_{i=1}^{N} E_i^{mol} \qquad \text{(Eq. 2.1)}$$

where E_{cryst} is calculated as the energy of the unit cell, N is the number of crystallographically unique molecular units in the unit cell, and E_i^{mol} is the molecular unit – so, the energy calculated for one

unique molecule. Then $\sum_{i=1}^{N} E_i^{mol}$ is simply a summation of the energies of all unique molecules, which is the accounted for by adjusting the *Z* value.

2.4.4.2 Functionals and basis sets

For all periodic calculations, the PBE[34] functional was used, which performs well for solid-state structures in both the CASTEP and DMol[3] modules [32] and is a reasonably inexpensive functional. For the small non-radical, organic compound calculations the TNP[35] basis set in the DMol[3] module was used. This is a triple-numerical basis set with polarisation functions on both light and heavy atoms, and although it is expensive, it is very accurate. For radicals, the larger DNP+ functional was used, which has additional diffuse functions. It is costlier in terms of computing power and time, but better at describing systems where long-range effects are non-negligible.

2.5 References

1 Bruker (2009), *SAINT*.
2 R. Blessing, *Acta Cryst.*, 1995, **A51**, 33–38.
3 L. J. Barbour, *J. Supramol. Chem.*, 2001, **1**, 189–191.
4 G. M. Sheldrick, *Acta Cryst.*, 2008, **A64**, 112–122.
5 G. M. Sheldrick, *Acta Crystallogr. Sect. C Struct. Chem.*, 2015, **71**, 3–8.
6 T. R. Schneider and G. M. Sheldrick, *Acta Cryst.*, 2002, **D58**, 1772–1779.
7 G. M. Sheldrick, *Acta Crystallogr. Sect. A Found. Crystallogr.*, 2015, **71**, 3–8.
8 D. S. Yufit and J. A. K. Howard, *J. Appl. Cryst.*, 2005, **38**, 583–586.
9 J. E. Warren, R. G. Pritchard, D. Abram, H. M. Davies, T. L. Savarese, R. J. Cash, P. R. Raithby, R. Morris, R. H. Jones and S. J. Teat, *J. Appl. Cryst.*, 2009, **42**, 457–460.
10 A. Alberola, R. J. Less, F. Palacio, C. M. Pask and J. M. Rawson, *Molecules*, 2004, **9**, 771–781.
11 A. Alberola, R. J. Less, C. M. Pask, J. M. Rawson, F. Palacio, P. Oliete, C. Paulsen, A. Yamaguchi, R. D. Farley and D. M. Murphy, *Angew. Chem. Int. Ed.*, 2003, **42**, 4782–4785.
12 A. J. Banister, N. Bricklebank, W. Clegg, M. R. J. Elsegood, C. I. Gregory, I. Lavender, J. M. Rawson and B. K. Tanner, *Chem. Commun.*, 1995, 679–680.
13 C. S. Clarke, D. A. Haynes, J. N. B. Smith, A. S. Batsanov, J. A. K. Howard, S. I. Pascu and J. M. Rawson, *CrystEngComm*, 2010, **12**, 172–185.
14 A. Alberola, E. Carter, C. P. Constantinides, D. J. Eisler, D. M. Murphy and J. M. Rawson, *Chem. Commun.*, 2011, **47**, 2532–2534.
15 J. H. Osiecki and E. F. Ullman, *J. Am. Chem. Soc.*, 1968, **2300**, 1078–1079.
16 C. Hirel, K. E. Vostrikova, J. Pecaut, V. I. Ovcharenko and P. Rey, *Chem. Eur. J*, 2001, **7**, 2007–2014.
17 G. Adrienko, ChemCraft.
18 Gaussian 09, Revision D.01, M. J. Frisch, G. W. Trucks, H. B. Schlegel, G. E. Scuseria, M. A. Robb, J. R. Cheeseman, G. Scalmani, V. Barone, G. A. Petersson, H. Nakatsuji, X. Li, M. Caricato, A. Marenich, J. Bloino, B. G. Janesko, R. Gomperts, B. Mennucci, H. P. Hratchian, J. V. Ortiz, A. F. Izmaylov, J. L. Sonnenberg, D. Williams-Young, F. Ding, F. Lipparini, F. Egidi, J. Goings, B. Peng, A. Petrone, T. Henderson, D. Ranasinghe, V. G. Zakrzewski, J. Gao, N. Rega, G. Zheng, W. Liang, M. Hada, M. Ehara,

K. Toyota, R. Fukuda, J. Hasegawa, M. Ishida, T. Nakajima, Y. Honda, O. Kitao, H. Nakai, T. Vreven, K. Throssell, J. A. Montgomery, Jr., J. E. Peralta, F. Ogliaro, M. Bearpark, J. J. Heyd, E. Brothers, K. N. Kudin, V. N. Staroverov, T. Keith, R. Kobayashi, J. Normand, K. Raghavachari, A. Rendell, J. C. Burant, S. S. Iyengar, J. Tomasi, M. Cossi, J. M. Millam, M. Klene, C. Adamo, R. Cammi, J. W. Ochterski, R. L. Martin, K. Morokuma, O. Farkas, J. B. Foresman, and D. J. Fox, Gaussian, Inc., Wallingford CT, 2016. 19 A. D. Becke, *J. Chem. Phys.*, 1993, **98**, 5648–5652.

20 C. Adamo and V. Barone, *J. Chem. Phys.*, 1998, **108**, 664–675.

21 S. D. Wetmore, L. A. Eriksson and R. J. Boyd, *J. Chem. Phys.*, 1998, **109**, 9451–9462.

22 J. Campo, F. Palacio, J. Luzo, G. J. Mcintyre and J. M. Rawson, *Polyhedron*, 2005, **24**, 2579–2583.

23 J. M. Rawson, C. S. Clarke and D. W. Bruce, *Magn. Reson. Chem.*, 2009, **47**, 3–8.

24 S. Grimme, *J. Comput. Chem.*, 2004, **25**, 1463–1473.

25 S. Grimme, J. Antony, S. Ehrlich and H. Krieg, *J. Chem. Phys.*, 2010, **132**, 1–20.

26 A. J. H. Wachters, *J. Chem. Phys.*, 1971, **52**, 1033–1036.

27 S. Domagala, K. Kosc, S. W. Robinson, D. A. Haynes and K. Wozniak, *Cryst. Growth Des.*, 2014, **14**, 4834–4848.

28 G. B. Bacskay, *Chem. Phys.*, 1981, **61**, 385–404.

29 R. McWeeny, *Proc. Roy. Soc. (London).*, 1956, **A235**, 496.

30 S. J. Clark, M. D. Segall, C. J. Pickard, P. J. Hasnip, M. J. Probert, K. Refson and M. C. Payne, *Zeitschrift fuer Krist.*, 2005, **220**, 567–570.

31 B. Delley, *J. Chem. Phys.*, 1990, **92**, 508–517.

32 B. Delley, *J. Chem. Phys.*, 2000, **113**, 7756–7764.

33 S. Grimme, *J. Comput. Chem.*, 2006, **27**, 1787–1799.

34 J. P. Perdew, K. Burke and M. Ernzerhof, *Phys. Rev. Lett.*, 1996, **77**, 3865–3868.

35 B. Delley, *J. Phys. Chem. A.*, 2006, **110**, 13632–13639.

Chapter 3

Synthesis and characterisation of dithiadiazolyl cocrystals: An experimental and theoretical study

A novel third dithiadiazolyl (DTDA) cocrystal has been found, containing a co-former common to both previously-known DTDA cocrystals. Similar to the known cocrystals, the [4-phenyl-1,2,3,5-DTDA][4-(3'-fluoro-4'-trifluoromethyl)phenyl-1,2,3,5-DTDA] cocrystal was found to contain heterodimers, and was synthesised by co-sublimation of the co-formers.

3.1 Background

Dithiadiazolyl (DTDA) radicals have been the subject of much research in the field of molecular magnets[1], as well as in studies of their structure-property relationships (*vide supra*). These compounds possess a heterocyclic CNSSN• ring (Figure 3.1), with a singly-occupied molecular orbital (SOMO) nodal at the carbon, that appears to show little change in electronic structure when the R-group is changed[2]. This is interesting as one has more freedom to change the R-group in order to introduce specific interactions in the solid state. DTDAs also exhibit a large variety of packing motifs and binding modes which suggest that the structure-directing properties of the R-group are significant enough in the solid-state to be used as a tool to engineer the structure to achieve a desired outcome[3].

DTDA radicals tend to dimerise in the solid state (see chapter 1), in other words they spin-pair, resulting in a diamagnetic material. In fact, to date there are only six known monomeric (undimerised) DTDA structures[4–9]. The R-group versatility is once again an important feature of these compounds, since it can be varied in order to prevent dimerisation. Antorreno *et al.* and Banister *et. al.* (see refs. 5 and 6) hypothesised that strong cyano···sulfur interactions that compete with the out-of-plane dimerisation, as well as fluorine-fluorine repulsion between molecules are potentially two of the main driving forces

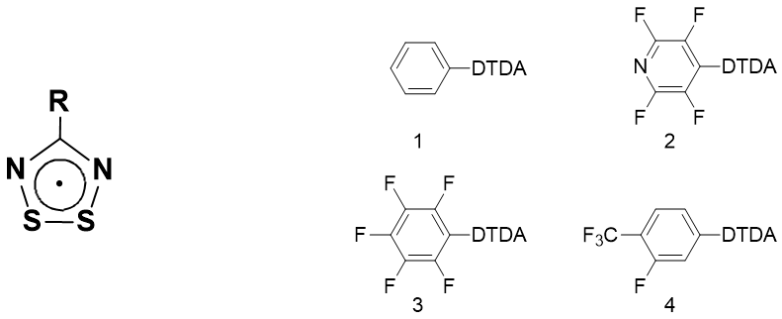

Figure 3.1. (Left) Dithiadiazolyl heterocycle structure. The R-group can be varied, (Right) DTDA co-formers for the three known cocrystals. Cocrystal **5**: composed of **1** and **2**; cocrystal **6**: composed of **1** and **3**; cocrystal **7**: composed of **1** and **4**.

behind the monomeric nature of these compounds. The appearance of undimerised DTDAs sparked increased interest the magnetic properties of these monomeric radicals[7,10], and in the efforts to hinder dimerisation, whilst simultaneously studying the effects that R-group modification has on the solid-state packing. [11]

Several methods have been employed to hinder dimerisation in radical compounds. Some of these methods include introducing electronegative species on the R-group in the ortho-position to the heterocyclic ring of DTDA radicals[12,11,13], as well as, more generally, bulky substituents like CF_3.[14,8] Introducing electronegative species, like halogens, into the ortho-position of the aromatic R-group has been shown to create a destabilising effect in the coplanarity of the two molecules of a dimer pair. The implication is that it potentially introduces more flexibility into the structure.[11] Bulky substituents serve to either protect the radical or introduce steric hindrance between the two molecules of a dimer pair. More recent attempts to prevent dimerisation in DTDAs include co-crystallising DTDAs with one another, where a second molecule is introduced into the structure, bearing different, and possibly structure-directing, functional groups. With this, the objective was to introduce interactions via the R-group that might weaken, and ultimately prevent dimerisation. However, to date only two DTDA cocrystals have been published, and both contain heterodimers.[15,16] In this study, a number of DTDA co-former combinations were attempted (see section 3.3 below), where the above-mentioned principles were applied as possible synthons (fluorinated *ortho*-positions, bulky substituents and strong potential cyano···sulfur interactions). However, although cocrystal formation was expected in some of these combinations due to the possibility for strong supramolecular synthon interactions, no cocrystals were successfully obtained.

The thermodynamics of the solid-state formation of radicals and their cocrystals, specifically DTDA radicals, remains a growing field.[17] A better understanding of the thermodynamics of cocrystal formation is crucial to elucidating the driving forces behind dimerisation. Once the driving forces behind the dimerisation interaction, as well as cocrystal formation, are better understood within these compounds, successful co-crystallisation may be something that could be predicted instead of left to serendipity. This could mean greater strides towards successfully hindering the dimerisation interaction. DTDA radicals pose a challenge to study computationally, especially periodically. This is due to the fact that, unlike neutral organics that do not show spin-pair dimerisation, a significant component of the lattice energy composition stems from the strong π^*-π^* dimerisation (spin-pairing interaction) between two monomers of a radical unit.[18,19] A number of studies on the ground-state electronic structure[20–22] as well as studies on the nature of the intradimer bond[11,22] have been reported on DTDAs. Recently, charge density studies have also been published on some DTDA cocrystals.[18,24] However, the driving force behind heterodimer/cocrystal formation is not yet fully understood.

As mentioned earlier, co-crystallisation has been used in an attempt to inhibit unwanted dimerisation. This makes use of a supramolecular synthon approach, where structure-directing interactions such as S-S···N, S-S···X (X=halogen) and S···NO_2, are introduced into the material via the R-group on the DTDA ring. This approach attempts to weaken, and ultimately prevent the π^*-π^* dimerisation by out-competing the spin-pairing interaction. The synthon approach has been successfully implemented in DTDA crystal engineering, whereby the above-mentioned interactions were exploited to yield monomeric structures. Very recently, an increase of intradimer S···S distances was observed for an increase in the size of the halogen in the 4-position of a 2-chloro-4-halophenyl-DTDA radical.[25] Intradimer S···S contacts of 4.58(2) – 4.69(2) Å [mean 4.64 Å] were reported for the 4'-(2-chloro-4-iodophenyl)-DTDA derivative, which could provide useful information towards

eventually preventing the π^*-π^* dimerisation.[25] Co-crystallisation with the aim of making monomeric species has not been as favourable as hoped, since all cocrystals currently known contain dimers, despite the presence of strong structure-directing interactions. The driving forces behind the formation of DTDA cocrystals, as well as understanding the lack of successful cocrystal formation with many other co-former partners, remain unanswered questions. Why did these specific cocrystals form, and not the multitude of other attempted partners? What drives the formation of the cocrystals in the gas- as well as solid states? Although more intensive topological charge density analysis has been carried out in order to start answering some of these questions, the data is limited due to the existence of only two DTDA cocrystals, both sharing a common co-former.

In this work, a third DTDA cocrystal, **7**, bearing the same common co-former, is reported. Computational results will also be presented, which entailed calculating gas-phase and periodic binding energies for the known cocrystals and their co-formers, with the aim of finding some observable trends in how these results relate to observed experimental results.

3.2 Results and Discussion

The route employed for the synthesis of **1** and **4** is based on a well-established procedure, described in chapter 2, and was performed in a standard Schlenk setup under inert conditions. Cocrystals of **7** were grown by co-sublimation of **1** and **4** *in vacuo*. Cocrystal **7** contains heterodimers of **1** and **4**.*

3.2.1 Crystal structure of [4-phenyl-1,2,3,5-DTDA][4-(3'-fluoro-4'-trifluoromethyl)phenyl-1,2,3,5-DTDA] (7).

Cocrystal **7** crystallises in the monoclinic space group P21/*n* (Table 3.1). The asymmetric unit contains one *cis*-cofacial dimer, with intradimer S···S interaction distances of 3.032(7) and 3.049(7) Å [mean

* **1**, **4**, and **7** were synthesised by J.P O'Connor in our laboratory. The structure of **7** has not been reported elsewhere.

3.041 Å]. This is in a similar range to the two previously known DTDA cocrystal S···S distances (2.957(5) Å to 3.069(7) Å), but appears to be on the lower range of typical intradimer S···S contacts in DTDA radicals (typically 2.796(1) Å to 4.196(3) Å, with an exceptional outlier at 4.700(7)[25] Å). The packing of **7** appears to be dominated by interdimer S···N contacts that propagate perpendicular to the *bc* plane in a side-on as well as tail-to-tail fashion [3.334(2) Å and 3.324(2) Å side-on and tail-to-tail, respectively] (Figure 3.2). Cocrystal **5** shows similar behaviour, with interdimer S···N contacts dominating the packing. These S···N contacts in **5** also propagate parallel to the *ab* plane through the heterocyclic nitrogen, varying in distance from 3.294(1) Å to 3.348(1) Å [mean 3.315 Å] along one sheet, and a second set of S-S···N contacts 2.294(1) Å in length, propagating along the *ac* plane as infinite chains, alternating in direction, with S···N contacts through the pyridyl nitrogen.

However, unlike **5** and **6** that show additional S···F contacts ranging from 3.056 Å to 3.242 Å, cocrystal **7** does not show any sulphur-halogen contacts within the sum of their van der Waals radii[26],

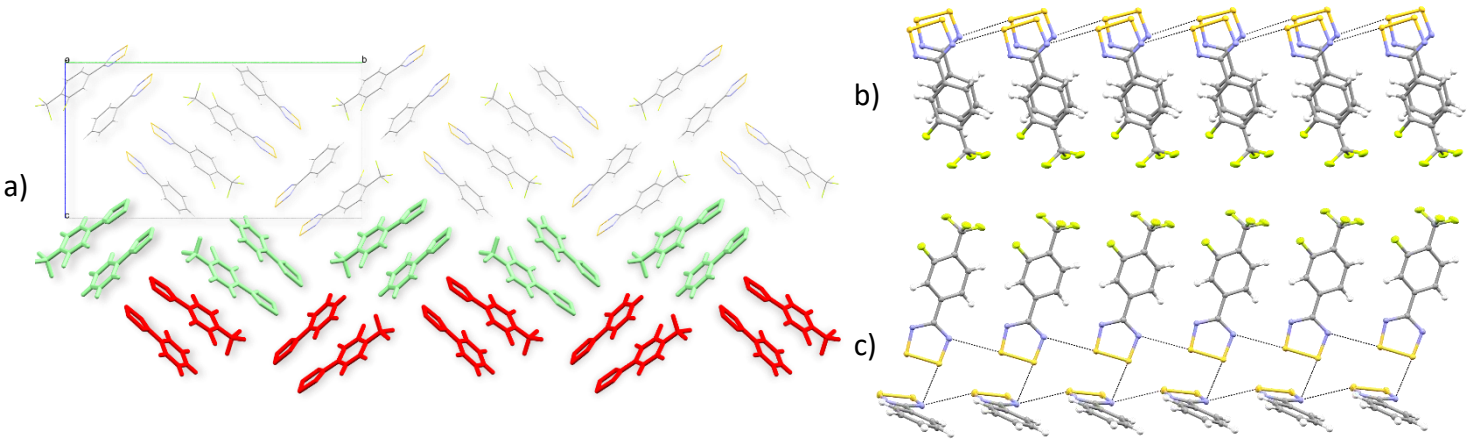

Figure 3.2. a) Herringbone packing along the *bc* plane in **7** (represented by the red and green layers), b) side on S···N contacts perpendicular to *bc* plane, c) tail-to-tail S···N contacts.

with the shortest S···F contact being 3.294(1) Å, being just outside the sum of the van der Waals radii. However, this is not necessarily an indication of the lack of an interaction since structure-directing S···N contacts are seen in the structures mentioned above that show distances just outside of the sum of their van der Waals radii.[26] Also note that none of the cocrystals or their co-formers show π-

Table 3.1. Crystallographic data for cocrystal **7**.

Empirical formula	$C_{15}H_8F_4N_4S_4$	
Formula weight	448.49	
Temperature (K)	100(2)	
Wavelength (Å)	0.71073	
Crystal system	monoclinic	
Space group	$P2_1/n$	
Unit cell dimensions (Å, °)	a = 5.7163(2)	α = 90
	b = 23.5674(10)	β = 94.673(2)
	c = 12.3602(6)	γ = 90
Volume (Å^3)	1659.6(1)	
Z	4	
Calculated density (g cm^{-3})	1.795	
Absorption coefficient (mm^{-1})	0.624	
F_{000}	904	
Crystal size (mm^3)	0.498 x 0.134 x 0.070	
q range for data collection (°)	1.728 to 28.319	
Miller index ranges	-7 ≤ h ≤ 7, -31 ≤ k ≤ 31, -16 ≤ l ≤ 16	
Reflections collected	45986	
Independent reflections	4131 [R_{int} = 0.0405]	
Completeness to q_{max} (%)	0.997	
Max. and min. transmission	0.7045 and 0.7457	
Refinement method	Full-matrix least-squares on F^2	
Data / restraints / parameters	4131 / 0 / 244	
Goodness-of-fit on F^2	1.094	
Final R indices [I > 2σ(I)]	R1 = 0.0344, wR2 = 0.0870	
R indices (all data)	R1 = 0.0392, wR2 = 0.0897	
Largest diff. peak and hole (e Å^{-3})	0.931 and -0.322	

stacking interactions, which is normally a prominent feature of aryl-perfluoraryl ring packing motifs.[27]

The distance between the centroids of the two molecules making up the heteromolecular unit in **7** (3.627 Å) aligns well with what is observed for that of the homomolecular dimers of **1** and **4** (3.579 and 3.810 Å, respectively) since the dimer unit must compensate slightly for the bulk of the -CF_3 group, which is absent in **1** and present on both partner molecules in **4**. The planes of the two molecules of the dimer of **7** are also bent slightly out-of-plane with respect to one another by 5.92°,

possibly due to the lower steric and electrostatic repulsion present in **4**, which has an out-of-plane bend of 8.06°).

Although previous work on DTDAs has shown that these radicals are often polymorphic[28,8,29], the co-formers involved in the formation of these three known DTDA cocrystals are, at least in our hands, not polymorphic. This is a curious observation, since it has been suggested that compounds that are polymorphic are more flexible, or at least have more than one stable low-energy structure, and would be more likely to adapt its geometry in such a way that it can accommodate a second co-former in the crystal packing motif.[11,30] In this, DTDA cocrystals are unusual since the co-formers do not appear to be polymorphic and yet readily form cocrystals, especially in the case of **1** which is a common co-former in all three. Additionally, an important observation in the cocrystal formation of both the two known cocrystals as well as the new cocrystal **7** is that 100% cocrystal formation is achieved by sublimation. There is no mixture of homo- and heterodimers in the bulk sample.

3.2.2 Computational results

In order to gain a deeper understanding of the formation of DTDA cocrystals, a computational study was carried out. A series of DFT calculations were performed on the known co-crystals **5** and **6** as well as novel cocrystal **7**, along with their individual co-formers **1**-**4** using the Gaussian09[31] software package. This was done in order to calculate binding energies (see section 3.2.2.1 below). Gas phase calculations were done on the homodimers and heterodimers (Figure 3.3) at the UB3LYP/6-311++G(d,p) level of theory, with counterpoise correction and Grimme's dispersion correction GD3.[32] All optimisations and single point energy calculations were done using a spin unrestricted method with singlet spin configuration, and all the dimers had *cis*-oid geometry, as in the experimentally determined crystal structures. Since the dimerisation between the radicals is a spin-pairing interaction, the radicals do not reside in individual orbitals but are rather paired up. This leads to a

singlet rather a triplet spin configuration. Periodic single point energy (SP) calculations were also performed using the Materials Studio 2016 software package, using the DMol[3] module with the GGA-PBE functional.[33]

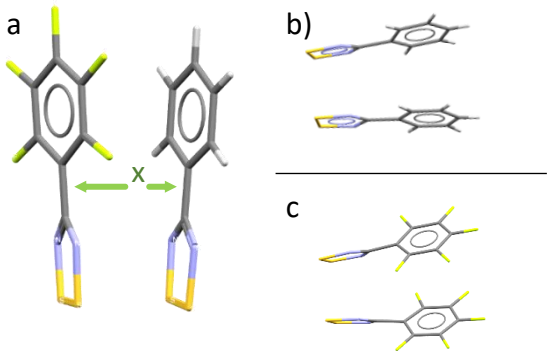

Figure 3.3. Representation of a heterodimer (a), composed of co-formers **1** (b) and **2** (c). The dimerisation energy calculated is the energy binding the two molecules of a heterodimer together (**x**).

All geometries, both for the periodic as well as gas-phase calculations, were extracted from the Cambridge Structural Database[34] and used without prior geometry optimisation (see Appendix A for refcodes), except that hydrogens were optimised to neutron distances prior to SP calculations. Fully optimised structures were confirmed to be minima by means of frequency calculations; frequencies were also calculated for structures not fully optimised, however, some small imaginary frequencies are present due to structures not being in absolute minimum energy geometries. The SP energies obtained in this way were then used in a series of further calculations in order to determine lattice and coupling energies.

3.2.2.1 Binding energies

Dimerisation (or binding) energy has been measured experimentally by electron spin resonance (ESR) and has been reported to be typically around -7 to -15 kcal/mol.[35] The binding energy calculated for the dimer pairs of **1** to **7** encompasses the spin-pairing energy between the two units, as well as interactions such as electrostatics, dispersion and other weaker interactions. In other words, the spin-pairing energy is a component of the binding energy (dimerisation) referred to here.

What is observed is that, in all cases, the binding energies (E_{bind}) of the homodimers of the co-formers are higher in energy than the heterodimers of the cocrystals, indicating that the cocrystal dimers are energetically more favourable than the dimers of the co-formers (Table 3.2).

Table 3.2. Results from gas-phase calculations on known cocrystals. Columns 2 and 3 contain the binding energies for the homodimers and heterodimers, respectively, whilst column 4 contains the coupling energy calculated as $E_{coup} = 2E_{hetero} - (E_{homo(A)} + E_{homo(B)})$. Numbers in brackets in column 3 indicate the cocrystal number.

	E_{bind}(XX) (kcal/mol)	E_{bind}(XY) (kcal/mol)	E_{coup} (kcal/mol)
1	-7.567		-5.555
2	-7.865	-10.493 (**5**)	
1	-7.567		-4.941
3	-8.953	-10.730 (**6**)	
1	-7.567		-2.780
4	-9.680	-10.013 (**7**)	

At first glance this makes sense intuitively, as one would expect the favourable formation of the cocrystals to be due to their being more energetically stable than their co-formers. These values are relatively consistent with experimental results for dimerisation energies of DTDA radicals. It can also be noted that the heterodimer binding energies (E_{bind}(XY)) differ by about 3 kcal/mol from that of their respective co-former homodimer (E_{bind}(XX)/(YY)) partners. The implication of this observation lies in that ideally there should be a strong thermodynamic driving force towards cocrystal formation. Previous thermodynamics studies have shown that, in fact, cocrystal formation in DTDAs is an entropically-driven process.[15]

The significant question is what happens in the gas phase that results in these materials packing as dimers. Do other intermolecular interactions dominate, bringing molecules closer together, and the dimerisation happens due to proximity and the sheer strength of the spin-pairing phenomenon, or do dimers (both homo- and heterodimeric) initially form in the gas phase, and the other intermolecular interactions are simply secondary?

Since the E_{bind}(XY) and E_{bind}(XX)/E(YY) values are relatively close in magnitude, it could be suggested that there is not any obvious strong driving force towards the formation of cocrystals over

simply having the individual components crystallise separately. It may then be possible that attempting to form cocrystals experimentally would be challenging, and more sensitive to precise experimental conditions. This is especially true, in our experience, with cocrystal **5**, where attempts to grow crystals of **5** do not consistently show cocrystal formation, but rather crystallisation of **1** and **2** separately. However, when material of the cocrystal is obtained, 100% cocrystal formation is always seen. Since the sublimation experiments for making these cocrystals are so sensitive to parameters such as temperature and vapour pressure, if there is no significant difference between the cocrystal binding energy and the binding energies of its co-formers this may result in erratic and sometimes irreproducible results.

Since the available data is limited to three known DTDA cocrystals, an investigation as to whether cocrystal formation is exclusive to this small sample set was conducted. To this end, binding energies were calculated for cocrystal combinations repeatedly tried experimentally that proved unsuccessful (*failed* combinations), to see whether there is an emerging pattern (Table 3.3[†],Figure 3.4). It was observed that the E_{bind}(XX) energies are of the same order as those of the co-formers making up the known cocrystals, although somewhat lower, ranging between -4.611 to -11.208 kcal/mol. One striking difference lies in that, in some cases, the binding energies of the heterodimers of the failed cocrystals differ much more from their co-formers than those that make up the known cocrystals. The results are somewhat irregular, suggesting that there is, in fact, no clear observable pattern by simply considering binding energies.

Another useful calculation is the coupling energy, as it gives a clearer indication of the relative favourability of the cocrystal formation as opposed to crystallisation of the co-formers separately, thereby giving an indication of the likelihood of cocrystal formation. Gas phase coupling energies

[†] A note on the layout of the table: perfluoro-PAHRIZ (f-PAHRIZ) has two E_{homo} values due to two possible orientations of the dimer (since it is not a symmetrical dimer). As a result, combinations with this radical (**F3** and **F4**) have either two or four E_{coup} values. Four in the case of **F3** since the heterodimer is also asymmetric and has two possible orientations, and two in the case of **F4** since the heterodimer is symmetrical, and therefore only has one possible *cis*-oid orientation.

were calculated for all three cocrystals as well (Table 3.2). The coupling energies were determined as follows:

$$E_{coup} = 2E(XY) - [E(XX) + E(YY)] \quad \text{Eq. (3.1)}$$

where E(XY) is the binding energy of the dimer in the gas phase and E(XX) and E(YY) refer to the binding energies of the co-former homodimer pairs. The gas phase coupling energies of the three cocrystals are negative, showing a larger stabilising contribution from the XY (heterodimer) pair – if the coupling energies were positive, then one would expect the likelihood of cocrystal formation to be lower, if not unlikely. Simply considering the binding energies, it is not immediately apparent what the driving force is behind cocrystal formation in the three cocrystals. However, considering the coupling energies along with the binding energies may suggest that, in the case of **5** which has the lowest coupling energy, the driving force behind cocrystal formation is, in fact, the stability of the heterodimer relative to both homodimers. Consequently, it is possible that in the gas phase, the heterodimer **5** may form first, followed by solid state packing and crystallisation, whereas this route may not necessarily be followed by **6** and **7**. However, more intensive analysis like pre-nucleation studies may need to be done.

Table 3.3. Results of binding energy calculations, determined for the series of *failed* cocrystal combinations. $E_{bind}(XX)$, $E_{bind}(XX)$ and E_{coup} are the same as determined above. Column two contains the REFCODES for the DTDA co-formers used.

	REFCODES	E_{bind}**(XX)** (kcal/mol)	E_{bind}**(XY)** (kcal/mol)	E_{coup} (kcal/mol)	
F1	UMAROP	-9.514	-10.569	-7.014	
	VUXZEU	-4.611			
F2	UMAROP	-9.514	-10.720	-2.668	-4.256
	OLOFOL	-9.258	-11.514		
F3	PAHRIZ	-11.208	-9.615	1.179	1.207
	f-PAHRIZ	-9.202 -9.230	-10.377	-0.345	-0.317
F4	PHTHAZ	-7.546	-11.275	-5.801	-5.774
	f-PAHRIZ	-9.202 -9.230			
F5	ZADVAB	-7.852	-9.619	-6.037	
	SAGMOD	-5.349			
F6	ZADVAB	-7.852	-9.838	-0.617	
	PAHRIZ	-11.208			
F7	PAHRIZ	-11.208	-9.090	-1.623	-2.422
	SAGMOD	-5.349	-9.490		

1: PHTHAZ
2: ZADVAB
4: UMAROP

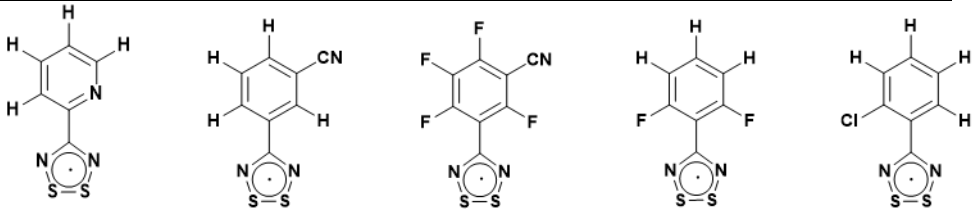

Figure 3.4. Structure of DTDAs used for the *failed* cocrystal calculations. PHTHAZ, ZADVAB and UMAROP are DTDAs **1**, **2** and **4**, respectively, from Figure 3.1.

It can also be noted that the coupling energy decreases steadily as the binding energy of the second co-former, partner to **1**, increases. This could simply indicate that, for these systems at least, as the binding interactions within a homodimer E(XX) pair becomes increasingly favourable, the formation of the heterodimer species becomes less favourable. This does not imply the cocrystal will not form, since other lattice interactions are also at play, but the conditions for obtaining a cocrystal may become more and more elusive.

The coupling energies of **F2**, **F3**, **F6** and **F7** are all in the range of 1.2 kcal/mol to -4 kcal/mol. If the coupling energies of the known cocrystals are an indication of the range where cocrystals are likely to be observed, then this may be an indication as to why of **F2**, **F3**, **F6** and **F7** are not seen – the coupling energy may simply not be favourable enough. For coupling energies > 0 it is

straightforward to assume that cocrystal formation is unlikely (as in **F3**). However, the coupling energy of **F5** may suggest that the combination warrants further investigation, especially considering the proximity of its E_{coup} to that of the known cocrystals. Although the energies of **F1** and **F4** indicate that these combinations are favourable and cocrystal formation likely, there may be other factors hindering cocrystal formation. In the case of **F4**, the perfluoro-PAHRIZ dimer was forced into the *cis*-oid dimer mode, where in actual fact it is a *trans*-antarafacial dimer in order to be able to compare it to the other systems, which are all *cis*-oid in nature. This could result in a falsely stabilising effect, meaning that although the combination seems favourable, the energies were calculated on a theoretical dimer mode of perfluoro-PAHRIZ. For **F1** successive attempts at cocrystal formation yielded no cocrystals, and this may simply be due to lack of strong-enough structure directing supramolecular synthons driving cocrystal formation, or the correct co-crystallisation conditions have simply not been found.

Table 3.4. Lattice, binding and other energy results from the periodic calculations of co-formers **1**-**4** and cocrystals **5**-**7**. E_{other} was obtained by subtracting the dimer energies from the energy of the unit cell.

Radical	E_{latt} ‡(kcal/unit)	E_{bind} (kcal/mol)	E_{other} (kcal/mol)
1	-94.58	-22.36 -24.34	-35.62
2	-103.46	-27.79	-37.83
3	-100.64	-27.60	-36.52
4	-106.79	-27.90 -26.55	-39.55
5	-105.96	-29.85 -25.54	-39.37
6	-102.93	-29.08	-36.93
7	-111.56	-28.95	-41.31

‡*E_{latt} is quoted per dimer pair, so the dimer is treated as the formula unit.*

Periodic calculations (Table 3.4), in other words calculations performed on the crystal structure, as opposed to a single dimer unit in the gas phase, were also performed on cocrystal **7** and two previously known cocrystals as well as their co-formers, to further probe other interactions in the lattice and their contribution towards cocrystal formation. The periodic binding energy was

calculated by subtracting the atomic energies of the two molecules making up the dimer from the atomic energy of the dimer. Differences in the magnitude of the binding energies calculated for that of the periodic and gas phase systems firstly stems from a difference in level of theory used to perform the calculations. Due to computational expense constraints associated with periodic systems at higher levels of theory, a lower, but comparable level of theory was used for the periodic calculations. Additionally, the periodic calculations were not corrected for zero-point vibrations. This is simply due to the fact that the periodic structures were not fully optimised, other than simple hydrogen position optimisations. As a result, the vibrational frequencies were largely positive since the structures are not in true minima. However, even though the absolute values are not comparable, the trends remain comparable between the two methods.

The challenge with periodic calculations on DTDA systems is finding an adequate way in which to account for the spin-pairing energy within the context of lattice energy, which we have yet to find. The periodic calculations performed on **1**-**7** show comparable results to that from the gas phase dimer calculations (Table 3.4). This is an encouraging result since this shows that some interactions that give the gas-phase dimers their relative stabilities also translate into the lattice (Table 3.1). The gas phase calculations ranked the energetic stabilities of the co-formers as **1**<**2**<**3**<**4** and the cocrystals as **7**<**5**<**6**, whereas the periodic calculations ranked the stabilities of the co-formers as **1**<**3**<**2**<**4** and the cocrystals as **6**<**5**<**7**. This may possibly be due to a difference in the levels of theory used for the gas phase and periodic calculations, or it may indicate that the *other* interactions provide additional stabilisation in some cases, like in co-formers **2** vs. **3** and cocrystals **6** vs. **7**.

The first thing to note is that, for every cocrystal combination, the lattice energy of the cocrystal is more stabilising than those of the two co-formers of that cocrystal. For example, cocrystal **5** has an E_{latt} = -105.96 kcal/unit, where its co-formers **1** and **2** have lattice energies of -94.58 and -103.46 kcal/unit, respectively. Radical **1** has no strong structure-directing electrostatic interactions

through the R-group, where the other radicals have additional strong electrostatic interactions through the heterocyclic ring as well as through the R-group. This is also reflected in the E_{other} value, where **1** has the lowest E_{other} amongst all the radicals. Here, E_{other} is essentially the interdimer interaction energy, as it encompasses all "packing" energy which is not dimerisation energy. The only strong interactions on the R-group are π-π interactions between two monomers of a dimer (no π-stacks present); the main structure-directing interactions are located around the DTDA heterocyclic ring. The relative E_{bind} energies of **5** and **6** reflect the strength and stabilising effect of the phenyl-perfluorophenyl π-stacking interaction[27] present in the dimers of **5** and **6**, and smaller in **7**. The magnitude of the binding energies when compared to the lattice energy also shows that in the solid state dimerisation energy is still enormously favourable and constitutes a large portion of the lattice stabilisation energy. It is then no surprise that attempts to prevent this dimerisation are not incredibly successful.

3.3 Additional co-crystallisation with DTDA radicals

Alongside the computational study on the known DTDA cocrystals (above), a simultaneous experimental co-crystallisation study was carried out on a number of DTDA radicals, as well as some small neutral organic compounds.

Since all compounds that were used during this project sublime, all initial co-crystallisations were done by sublimation. The general procedure involved weighing equimolar amounts of the two chosen co-formers and lightly grinding them together inside a thick crystallisation Schlenk under an atmosphere of nitrogen. Co-crystallisations were typically first attempted on a 20-100 mg scale, depending on the chosen co-formers. This Schlenk was then submerged into an oil bath set to a temperature, typically initially at a temperature closest to the highest sublimation temperature between the two co-formers, where after the Schlenk was evacuated and sublimation occurred under

vacuum onto the walls on the Schlenk. In order to further probe the sublimation co-crystallisation process, a number of parameters were varied for each co-crystallisation attempt:

1. Scale
2. Temperature
3. Dynamic vs static vacuum
4. Leaving sample to heat in oil bath under N_2(g) before applying vacuum

The biggest challenge with these sublimation experiments was the parameter of partial pressure for a number of reasons: 1) two compounds with (sometimes very) different sublimation temperatures are being heated in the same vessel to the same temperature, 2) even the smallest variation in mass of the sample will have an impact on the partial pressure of each component in the gas phase, 3) not every Schlenk has the exact same glass wall thickness, in turn affecting temperature in the Schlenk as well as on the glass wall, and 4) the temperature of the glass onto which crystals are nucleating is not the same with every experiment, due to ambient temperature fluctuations and seasonal changes. Some of these factors are easier to control, like the temperature of the glass wall and possibly the sample mass to a large extent, however variations in the glassware as well as the partial pressure in the gas phase are more challenging parameters to regulate. However, the scope of this project did not include fine-tuning such factors, and for the time-being it was accepted that these factors could result in erratic results as well as not seeing cocrystal formation where it possibly should be observed.

Co-crystallisation was also attempted from the melt. This was done by adding equimolar amounts of each co-former into a DSC pan, cycling it through a melt and observing the thermal events – specifically looking for events like a single melt endotherm on the second or third cycle, as opposed to two melts.

Due to time constraints, not many co-crystallisations were done where DTDAs were combined with other radicals, or neutral organics. This is also partially due to being unable to synthesise the *p*-NPNN radical (see chapter 2).

3.3.1 Attempted {DTDA}{DTDA} cocrystals

3.3.1.1 Sublimation experiments

A number of DTDAs were co-crystallised with another by co-sublimation of the co-formers (Table 3.5). All co-former combinations were attempted more than once, where scale and temperature was varied with each attempt. All scale and temperature variants showed the same result, for every combination.

Table 3.5. Summary table for DTDA cocrystal combinations that were attempted, both by sublimation and from the melt.

Co-former 1	Co-former 2	Result	Conditions
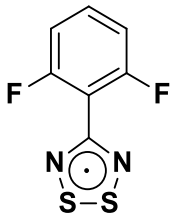	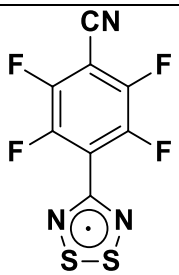	2**α** (see below for details)	Scale: 20-80 mg Temp: 80-105 °C Left under N_2 (g) for 5 minutes before applying vacuum
	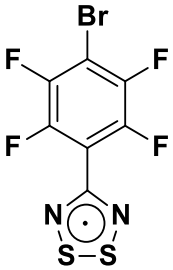	Co-formers crystallise separately	
	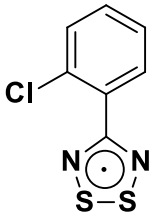	Co-formers crystallise separately	

	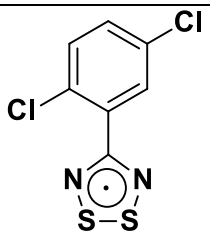	Co-formers crystallise separately	
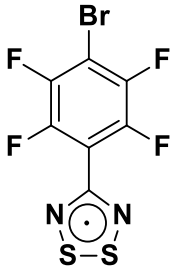	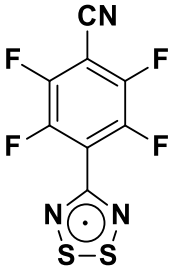	Co-formers crystallise separately	Scale: 20-30 mg
	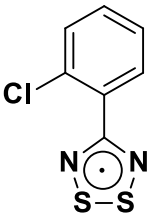	Co-formers crystallise separately	
	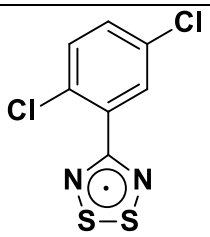	Co-formers crystallise separately	
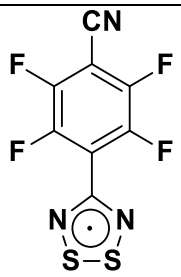	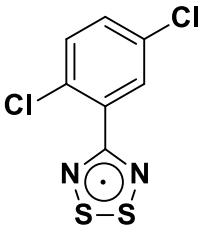	Co-formers crystallise separately	Scale: 20-30 mg
	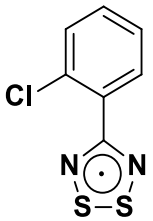	Co-formers crystallise separately	
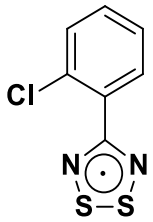	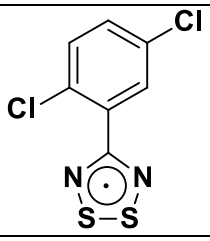	Co-formers crystallise separately	Scale: 20-30 mg

As seen in the above table, co-crystallisation attempts yielded no successful cocrystals, which were confirmed by unit cell determinations on crystals from many areas inside the Schlenk, using

SCXRD analysis. This included analysing crystals of all different colours and morphologies within the Schlenk to have a broad sample set. An interesting phenomenon was observed during the attempted sublimation co-crystallisation of radicals 4′-(4-cyanoperfluorophenyl)-DTDA (4-CNDTDA) and 4′-(2,6-difluorophenyl)-DTDA (F_2DTDA). Although no cocrystals were found during sublimation attempts, upon inspection of some larger rod-shaped crystals it was found that some crystals of the illusive ***α***-phase[11] of 4-CNDTDA formed. The reproducibility was tested in subsequent sublimations, and although the morphology of the ***α*-**(4-CNDTDA) crystals was not consistent, the procedure is reproducible – showing the formation of ***α*-**(4-CNDTDA) each time. According to previous attempts in literature, the ***α***-phase is typically produced either by rapid sublimation at 120 °C[9], or by sublimation onto a cold finger at -10 °C[36]. This was a purely serendipitous outcome. How exactly ***α*-**(4-CNDTDA) forms instead of the more common **β**-phase, is uncertain. However, it is clear that the presence of F_2DTDA in the vapour phase encourages preferred nucleation of ***α*-**(4-CNDTDA). It was also observed that the scale of the crystallisation, and in turn the vapour pressure, had an effect on the formation of ***α*-**(4-CNDTDA). This observation is made since, in the sublimation Schlenk used for the co-sublimation, a scale of 20-40 mg yielded ***α*-**(4-CNDTDA) whereas larger scale did not.

3.3.1.2 Co-crystallisation from the melt

DSC proved to be an unhelpful technique for studying co-crystallisation since it was observed to be irreproducible for compounds that sublime – see section below for notes on DSC of compounds that sublime. See Appendix A for DSC traces.

3.3.2 Other attempted cocrystals

As an initial study of cocrystal formation of DTDAs with other radicals and neutral organic compounds, two DTDAs were co-crystallised with non-DTDA compounds – one with TEMPO radical and one with *p*-benzoquinone (Table 3.6).

Table 3.6. Summary table of cocrystal attempts using DTDAs, a nitroxide radical in TEMPO, and a neutral organic compound in BQ. All co-crystallisations summarised here were attempted by sublimation.

Co-former 1	Co-former 2	Result	Conditions
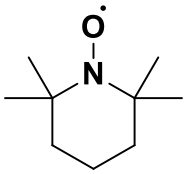	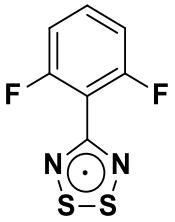	No crystals formed	**Short crystallisation schlenk:** **50-60 °C** **Static vacuum**
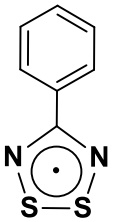	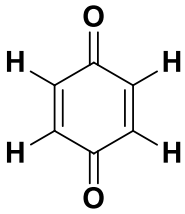	Co-formers crystallise out separately	**Specialised sublimation setup:** **Ph-DTDA: 90 °C** **BQ: 63 °C** **Dynamic vacuum** **Crystallisation schlenk:** **95 °C** **Static vacuum**

For the two co-crystallisation attempts shown in Table 3.6 no cocrystal formation was observed. In the case of the {4-phenyl-DTDA}{*p*-benzoquinone} combination, a possible reason for the lack of cocrystal formation may simply be an absence of any strong supramolecular synthons to drive the self-assembly of a cocrystal between those two components. Both molecules are unsubstituted, with the only possible interactions that could drive the formation of the cocrystal being S···O and some hydrogen bonding to the carbonyl oxygen on the quinone molecule. However, π*-π* dimerisation interactions in the PhDTDA would almost certainly out-compete these interactions. Similarly, for the {TEMPO}{ F_2DTDA } combination, the supramolecular synthons on these molecules may not be adequate to drive cocrystal formation, or the correct co-crystallisation conditions have not been found. However, a cocrystal using either TEMPO or benzoquinone along with a DTDA radical partner may be more likely to form given stronger supramolecular synthons on the DTDA ring, or even the benzoquinone, to drive co-crystallisation. For example, an iodine substituent on the DTDA radical could potentially halogen bond to the oxygen of either TEMPO or

benzoquinone (I···O) forming a cocrystal, however whether this DTDA will remain a dimer is a different question.

3.3.3 Description and characterisation of a novel radical cocrystal

Finally, co-crystallising radicals other than DTDAs with neutral organic compounds was investigated. The resulting materials may have some interesting magnetic or conducting properties, and will ultimately provide researchers commonly working with radical compounds with additional information towards a better understanding of the interactions within radical cocrystals and how best to apply the information to unknown systems (see Chapter 1).

A simple nitroxide radical, TEMPO (Figure 3.6a), was initially used as a co-former. The second

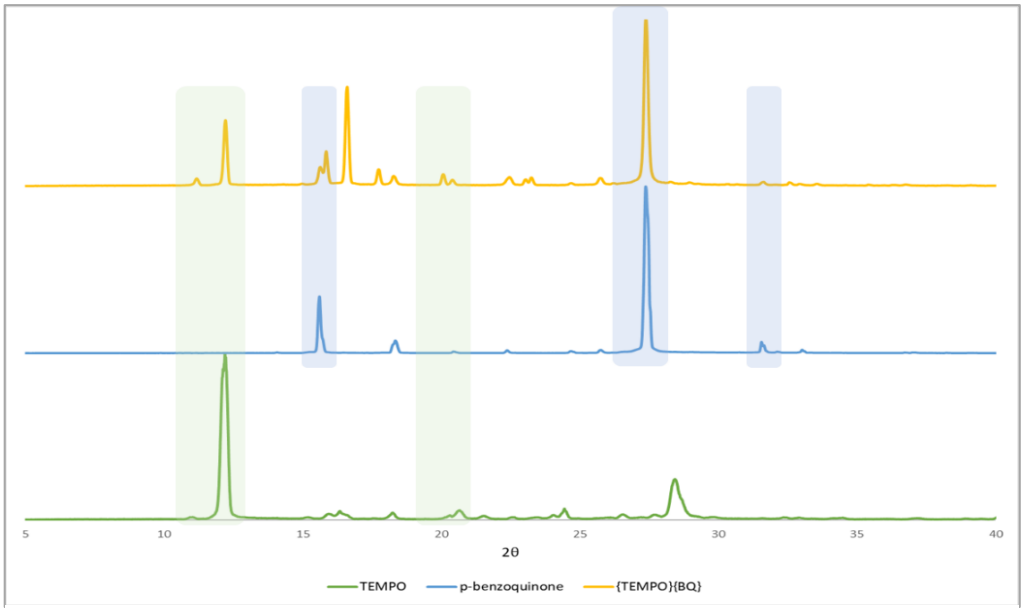

Figure 3.5. PXRD patterns collected for TEMPO, p-benzoquinone and the resulting physical mixture. Top) Physical mixture of TEMPO and BQ. Middle) experimental pattern for p-benzoquinone. Bottom) experimental pattern for TEMPO. Some of the main similarities are highlighted: blue) similarities with BQ, green) similarities with TEMPO

co-former was chosen from the family of *p*-benzoquinone compounds. These compounds are aromatic, promoting strong electrostatic interactions, and they are known to sublime. The first combination included TEMPO, and as the co-former, unsubstituted *p*-benzoquinone. Equimolar amounts of each compound were added to a crystallisation Schlenk and sublimed under static

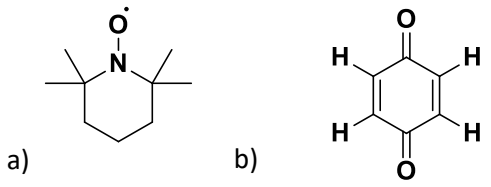

Figure 3.6. First cocrystal combination of a nitroxide radical with a neutral organic. a) TEMPO nitroxide radical as co-former 1, b) p-benzoquinone as co-former 2.

vacuum at 40-50 °C onto the wall of the Schlenk tube. Cocrystal formation was not seen, as co-formers crystallised out separately. Equimolar amounts of the two co-formers were also ground together, resulting in a yellow-orange powder. This powder was analysed by PXRD, which showed that it was simply a mixture of the two components (Figure 3.5).

Infrared analysis was done on the co-formers as well as the cocrystal in order to look for some characteristics that might indicate cocrystal formation i.e. peak shifts due to interactions and peak broadening due to hydrogen bonding (Figure 3.8). However, no such phenomena were seen, implying no cocrystal formation. The second quinone co-former chosen has *cyano*-substituents, which are known to be strongly structure-directing (Figure 3.7b). It also has *chloro*-substituents, providing opportunity for strong electrostatic interactions through halogen atoms. As previously, equimolar amounts of each component were ground together. An immediate colour change was observed as the coral TEMPO mixed with the yellow CCBQ, yielding a dark olive green coloured powder (Figure 3.9). The resulting green powder was analysed by PXRD, which indicated the possibility of cocrystal formation, since the pattern did not match that of either co-former 1 or 2

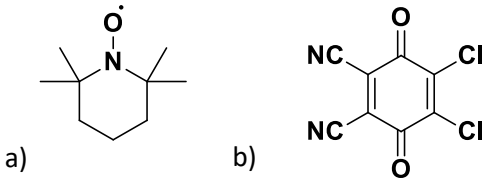

Figure 3.7. Second cocrystal combination of a nitroxide radical with a neutral organic. a) TEMPO nitroxide radical as co-former 1, b) 2,3-dichloro-5,6-dicyanobenzoquinone (**CCBQ**) as co-former 2.

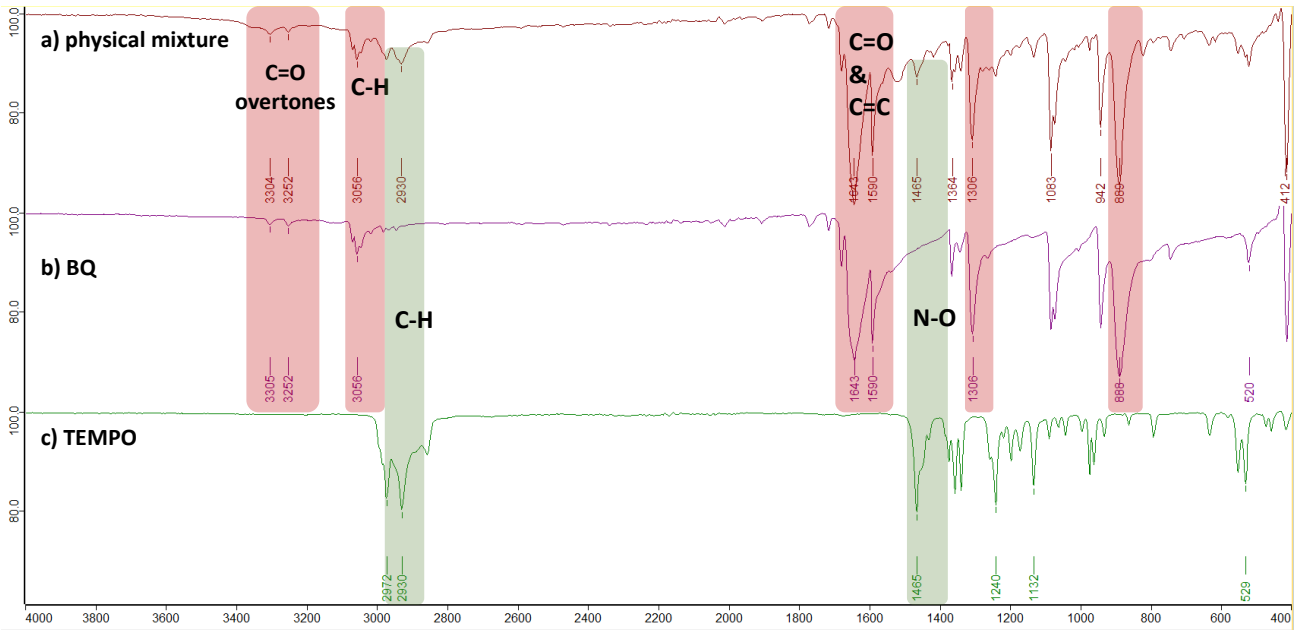

Figure 3.8. A comparison of the infrared spectra of the physical mixture of {TEMPO}{BQ}. a) TEMPO, b) BQ, c) physical mixture. Green and red bands highlight similarities in the spectra.

perfectly (Figure 3.10). To further confirm what was seen in the PXRD, a DSC trace was collected of the green ground sample. However, since the compounds used for this study all sublime, and some have very high vapour pressures, thermal analysis by way of DSC proved to be an irreproducible technique. As a result, DSC traces for the two cocrystal attempts with TEMPO will not be included

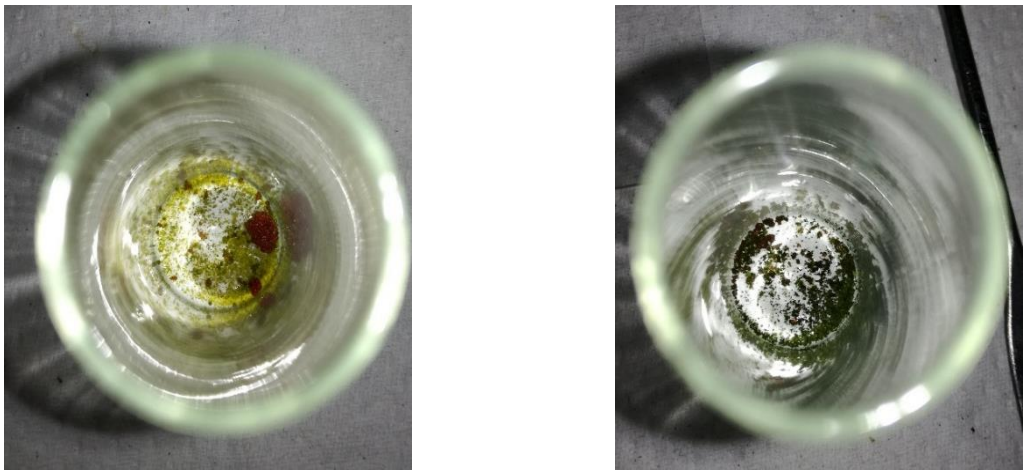

A) Immediately after combining co-formers

B) After 10 minutes, with no interference (such as grinding)

Figure 3.9. A representation of the colour change upon contact of the two co-formers. A) Immediately after addition and B) After standing for 10 minutes.

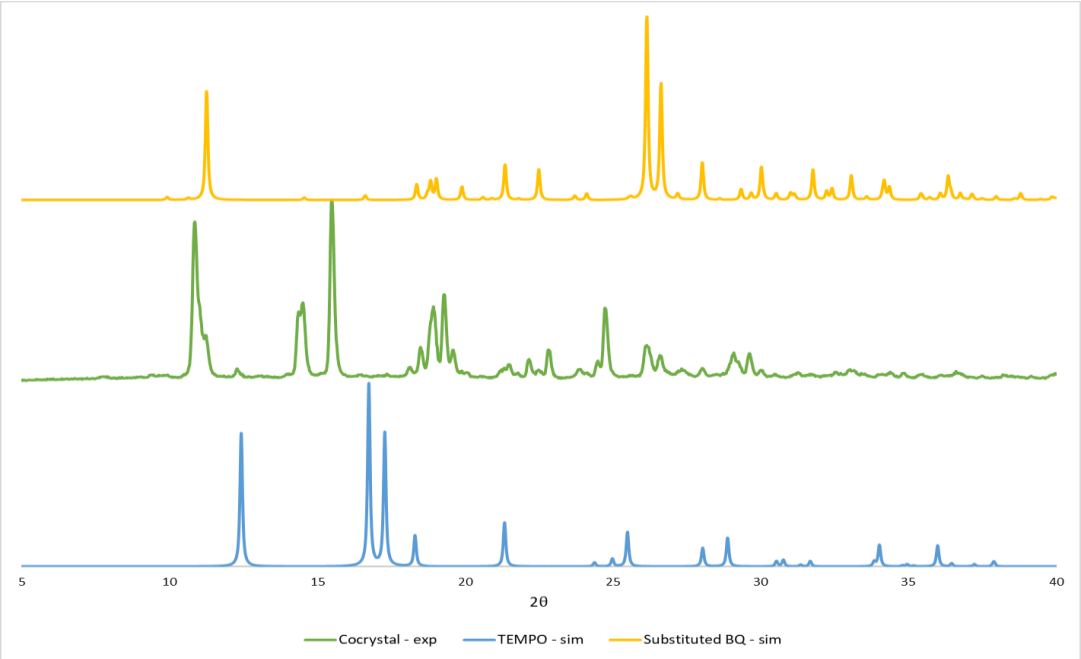

Figure 3.10. PXRD analysis comparison for co-crystallisation attempt of {TEMPO}{2,3-dichloro-5,6-dicyanobenzoquinone}. (Top) Simulated PXRD pattern for 2,3-dichloro-5,6-dicyanobenzoquinone, simulated from single crystal data, (middle) experimental powder pattern for the co-crystallisation attempt, (bottom) simulated PXRD pattern for the TEMPO radical, simulated from single crystal data.

here, since multiple subsequent runs resulted in very erratic and irreproducible results, even though parameters such as sample size and uniformity were kept as consistent as possible.

Firstly, as the sample is heated up in the closed DSC pan (hermetically sealed) either one or both of the components sublime. What could then happen is that some sample recrystallises on the lid of the pan, causing the second heating cycle to be irreproducible and an inaccurate representation of the true event. What could also happen is that, as it recrystallises, one crystal may fall off the lid back into the pan, resulting in false thermal events. Sample could also simply condense on the lid of the pan or along the sides, and does not crystallise completely, resulting in a false mass loss and eventually thermal events that could simply be a false change in heat capacity.

Infrared analysis was done on the co-formers as well as the cocrystal (Figure 3.11). Firstly, it is clear that there is a decrease in transmittance (or intensity) of some functional groups. This is a concentration effect, due to Beer's law (Eq. 3.1). In the cocrystal powder, the concentration of each

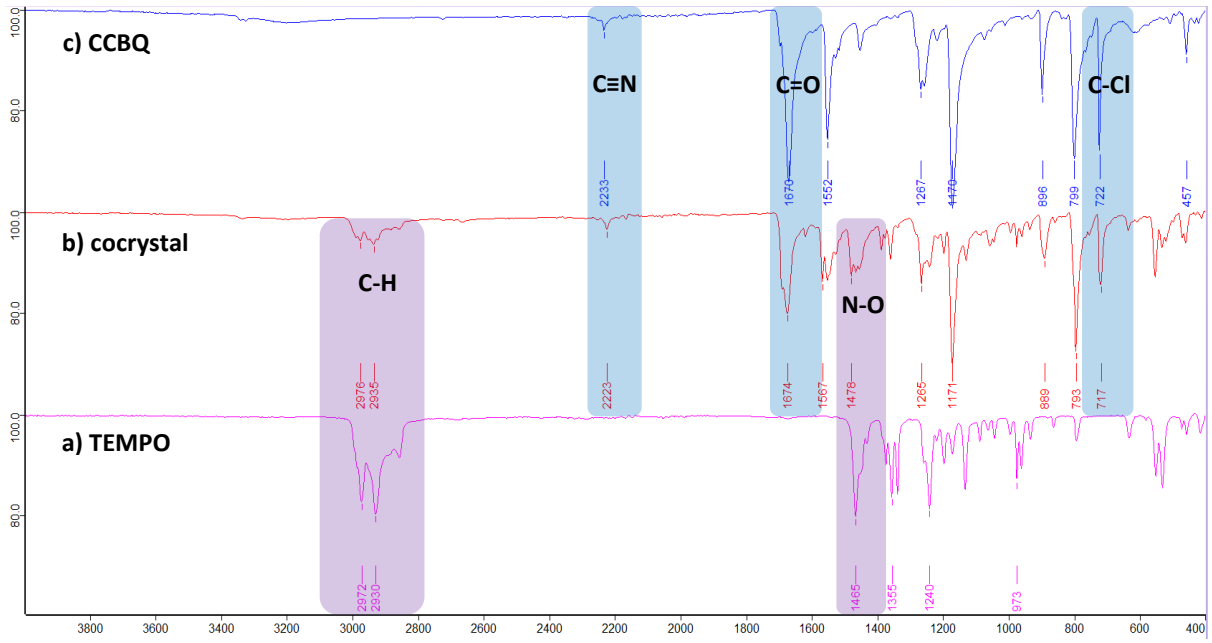

Figure 3.11. A comparison of the infrared spectra of the components of the cocrystal of TEMPO with CCBQ. a) TEMPO, b) cocrystal, c) CCBQ.

functional group is lower than in the single component. This is highlighted in the blue and purple sections.

What is also evident is a change in shape of some of the peaks. The effects are not huge, but some minor changes can be seen especially in the **N-O** and **C=O** bands. Comparing this spectrum with the one determined for the {TEMPO}{BQ} combination, which is hypothesised to not form a cocrystal, one can see clear peak shifts and shape changes, which indicates some sort of interactions happening, unlike in the {TEMPO}{BQ} combination.

The ultimate analytical technique which would solidify what we observe to be cocrystal formation would be SCXRD. As a result, sublimation and solution co-crystallisations were attempted in order to obtain some single-crystals for data collection. The sublimation experiment with this combination was done using the specialised sublimation apparatus described in chapter 5. The two components were added to the two ends of the sublimation setup and heated under applied vacuum (TEMPO: 36 °C, CCBQ: 210 °C). Thin orange-brown needles grew onto the glass wall within 24 hours, however analysis showed no cocrystals – only the CCBQ crystallised on its own. Crystallisations were

also set up in acetonitrile, $CHCl_3$/acetonitrile, and ethanol. However, no crystal growth has been observed as yet.

$$A = \varepsilon l c \qquad \text{Eq. (3.1)}$$

A = absorbance
ε = absorptivity
l = path length
c = concentration

3.4 Summary & conclusion

A third DTDA cocrystal has been found by co-sublimation of radicals **1** and **4**, with **1** currently being a common co-former in all three known DTDA cocrystals. The cocrystal was found to have *cis*-oid dimer geometry and lacked the common DTDA S···F interactions. A theoretical study was conducted on the three known cocrystals, as well as a series of *failed* cocrystals. The first thing that was considered was the magnitude of the binding energies of the co-formers. It was hypothesised that one might ideally look for co-formers that have high (less negative) relative binding energies, since they clearly do not bind as strongly as homodimers and might find a more likely partner in a molecule of a different compound. This, however did not seem to be the case since, amongst the co-formers that were used in unsuccessful attempts at cocrystal formation, there were ones with very small stabilising E_{bind} and yet would not form cocrystals with a chosen partner with a stabilising E_{bind}. It was, however, observed that for all three known cocrystals, E_{bind} for the heterodimer was consistently more stabilising than for the homodimers of the co-formers. Secondly, it was considered that larger negative coupling energies might be an indication of how easily a cocrystal of a

specific chosen pair might be obtained, however as seen above it is once again not that simple.

The periodic calculations seemed to agree relatively well with the gas-phase calculations in that the cocrystals are consistently more stable than their co-formers. The periodic calculations showed firstly that the completely fluorinated co-formers, **2** and **3**, had lower lattice energies than **1** which has no heteroatom substituents on the R-group, possibly due to the presence of strong electrostatic interactions both intradimer as well as between the heterocycle of one monomer and the fluorinated R-group of another. It is also clear that, in all cases, the binding energy constitutes a large portion of the total lattice energy. The periodic binding energies of the three cocrystals are all in the same range. The strength of the E_{other} energy of **7** is, however, somewhat of a curiosity since, simply considering the interactions present in the crystal structure of **7**, it lacks strong structure-directing electrostatic interactions on the R-group, other than a single F···H interdimer hydrogen bond, and yet it still has a very stabilising energy in comparison to the other cocrystals. More intensive computational analysis needs to be done on these cocrystals in order to determine why this may be the case. Since very little periodic computational work has been done on these compounds there is little by way of a benchmark, but, decidedly, looking at the periodic systems of DTDAs may just prove more informative than *in vacuo* studies have been able to in the past since not only can intradimer binding energy be obtained, but also information regarding the relative stability of the other lattice interactions. This may aid in picking appropriate cocrystal partners with strong supramolecular synthons for future co-crystallisation experiments.

A number of DTDA radicals were also co-crystallised with one another by two methods – sublimation and melt co-crystallisation, however no cocrystals were found. Whether this is due to an unfavourable combination or incorrect crystallisations conditions is uncertain, but warrants further research. Some combinations, for instance the {4'-(4-cyanoperfluorophenyl)-DTDA}{4'-(4-bromoperfluorophenyl)-DTDA} are combinations with the potential for strong synthon interactions (like Br···S, Br···N, CN···S) that could provide some structure-directing forces. Further study on this combination is encouraged.

A nitroxide radical, TEMPO, was then also co-crystallised with a DTDA radical, however no cocrystals were found from this experiment. This could possibly be due to the lack of strong structure-directing moieties on either molecule.

Lastly, some radicals were also co-crystallised with neutral organic molecules of the *p*-benzoquinone family. In the case of pure *p*-benzoquinone as a co-former, no cocrystals were found. This could again, be due to a lack of any strong structure-directing interactions on the BQ molecule, other than an aromatic system for π-stacking. However, a cocrystal was successfully made using 2,3-dichloro-5,6-dicyano-benzoquinone and TEMPO as co-former partners. A number of characterisation techniques indicate the formation of a cocrystal, including an immediate colour change upon mixing of the two co-formers. Without any single crystals for structural confirmation, cocrystal formation cannot be finally confirmed. Future work on this will include either solving the structure from PXRD data, or successfully growing single crystals for SCXRD analysis.

3.5 References

1 J. M. Rawson, A. Alberola, A. Whalley, J. Rawson and A. Whalley, 2006, 2560–2575.
2 A. J. Banister, J. M. Rawson and S. L. Birkby, *J. Chem. Soc. Dalt. Trans.*, 1991, 1099–1104.
3 D. A. Haynes, *CrystEngComm*, 2011, **13**, 4793–4805.
4 G. Antorrena, J. E. Davies, M. Hartley, F. Palacio, M. Jeremy, J. Nicholas, B. Smith and A. Steiner, *Chem. Commun.*, 1999, 1393–1394.
5 A. Alberola, R. J. Less, C. M. Pask, J. M. Rawson, F. Palacio, P. Oliete, C. Paulsen, A. Yamaguchi, R. D. Farley and D. M. Murphy, *Angew. Chem. Int. Ed.*, 2003, **42**, 4782–4785.
6 W. V. F. Brooks, N. Burford, J. Passmore, M. J. Schriver and L. H. Sutcliffe, *Chem. Commun.*, 1987, 69–71.
7 A. Alberola, R. J. Less, F. Palacio, C. M. Pask and J. M. Rawson, *Molecules*, 2004, **9**, 771–781.
8 A. Alberola, C. S. Clarke, D. A. Haynes, S. I. Pascu and J. M. Rawson, *Chem. Comm.*, 2005, **3**, 4726–4728.
9 A. J. Banister, N. Bricklebank, W. Clegg, M. R. J. Elsegood, C. I. Gregory, I. Lavender, J. M. Rawson and B. K. Tanner, *Chem. Commun.*, 1995, 679–680.
10 A. Alberola, R. J. Less, C. M. Pask, J. M. Rawson, F. Palacio, P. Oliete, C. Paulsen, A. Yamaguchi, R. D. Farley and D. M. Murphy, *Angew. Chem. Int. Ed.*, 2003, **42**, 4782–4785.
11 C. S. Clarke, D. A. Haynes, J. N. B. Smith, A. S. Batsanov, J. A. K. Howard, S. I. Pascu and J. M. Rawson, *CrystEngComm*, 2010, **12**, 172–185.
12 A. Alberola, E. Carter, C. P. Constantinides, D. J. Eisler, D. M. Murphy and J. M. Rawson, *Chem. Commun.*, 2011, **47**, 2532–2534.
13 C. P. Constantinides, D. J. Eisler, A. Alberola, E. Carter, D. M. Murphy and J. M. Rawson, *CrystEngComm*, 2014, **16**, 7298–7312.
14 R. A. Beekman, R. T. Boeré, K. H. Moock and M. Parvez, *Can. J. Chem.*, 1998, **93**, 85–93.
15 S. W. Robinson, D. A. Haynes and J. M. Rawson, *CrystEngComm*, 2013, **15**, 10205–10211.
16 C. Allen, D. A. Haynes, C. M. Pask and J. M. Rawson, *CrystEngComm*, 2009, **11**, 2048–2050.
17 R. G. Hicks, *Can. J. Chem.*, 2004, **82**, 1119–1127.
18 S. Domagala, K. Kosc, S. W. Robinson, D. A. Haynes and K. Wozniak, *Cryst. Growth Des.*, 2014, **14**, 4834–4848.
19 S. A. Fairhurst, K. M. Johnson, L. H. Sutcliffe, K. F. Preston, A. J. Banister, Z. V Hauptman and J. Passmore, *Dalt. Trans.*, 1986, 1465–1472.
20 A. W. Cordes, C. D. Bryan, W. M. Davis, R. H. de Laat, S. H. Glarum, J. D. Goddard, R. C. Haddon, R. G. Hicks, D. K. Kennepohl, R. T. Oakley, S. R. Scotf and N. P. C. Westwood, *J. Am. Chem. Soc.*, 1993, **115**, 7232–7239.
21 C. D. Bryan, A. W. Cordes, J. D. Goddard, R. C. Haddon, R. G. Hicks, C. D. MacKinnon, R. C. Mawhinney, R. T. Oakley, T. T. M. Palstra and A. S. Perel, *J. Am. Chem. Soc.*, 1996, **118**, 330–338.
22 J. Campbell, D. Klapstein, P. F. Bernath, W. M. Davis, R. T. Oakley and J. D. Goddard, 1996, **1669**, 4264–4266.
23 K. V Shuvaev, A. Decken, F. Grein, T. S. M. Abedin, L. K. Thompson and J. Passmore, *Dalt. Trans.*, 2008, 4029–4037.
24 S. Domagala and D. A. Haynes, *CrystEngComm*, 2016, 1–11.
25 C. P. Constantinides, E. Carter, D. Eisler, Y. Beldjoudi, D. M. Murphy and J. M. Rawson, *Cryst. Growth Des.*, 2017, **17**, 3017–3029.
26 A. Bondi, *J. Chem. Phys.*, 1964, **68**, 441–451.
27 L. M. Salonen, M. Ellermann and F. Diederich, *Angew. Chem. Int. Ed.*, 2011, **50**, 4808–4842.
28 A. J. Banister, N. Bricklebank, I. Lavender, J. M. Rawson, C. I. Gregory, B. K. Tanner, W. Clegg, M. R. J. Elsegood and F. Palacio, *Angew. Chem. Int. Ed. Engl.*, 1996, **35**, 2533–2535.
29 E. M. Fatila, M. C. Jennings, J. Goodreid and K. E. Preuss, *Acta Cryst.*, 2010, **C66**, 260–264.
30 A. Nangia, *Acc. Chem. Res.*, 2008, **41**, 595–604.
31 2016 Revision D.01, M. J. Frisch, G. W. Trucks, H. B. Schlegel, G. E. Scuseria, M. A. Robb, J. R. Cheeseman, G. Scalmani, V. Barone, G. A. Petersson, H. Nakatsuji, X. Li, M. Caricato, A. Marenich, J.

Bloino, B. G. Janesko, R. Gomperts, B. Mennucci, H. P. Hratc, .
32 S. Grimme, J. Antony, S. Ehrlich and H. Krieg, *J. Chem. Phys.*, 2010, **132**, 1–20.
33 J. P. Perdew, K. Burke and M. Ernzerhof, *Phys. Rev. Lett.*, 1996, **77**, 3865–3868.
34 C. R. Groom, I. J. Bruno, M. P. Lightfoot and S. C. Ward, *Acta Cryst.*, 2016, **B72**, 171–179.
35 S. A. Fairhurst, K. M. Johnson, L. H. Sutcliffe, K. F. Preston, A. J. Banister, Z. V. Hauptman and J. Passmore, *J. Chem. Soc., Dalt. Trans.*, 1986, 1465–1472.
36 Y. Beldjoudi, A. Arauzo, F. Palacio, M. Pilkington and J. M. Rawson, *J. Am. Chem. Soc.*, 2016, **138**, 4–11.

Chapter 4

Polymorphism in 4'-(2,6-difluorophenyl)-1,2,3,5-dithiadiazolyl

THE MOST BEAUTIFUL EXPERIENCE WE CAN HAVE IS THE MYSTERIOUS. IT IS THE FUNDAMENTAL EMOTION WHICH STANDS AT THE CRADLE OF TRUE ART AND TRUE SCIENCE.

-- ALBERT EINSTEIN

4.1 Background

Polymorphism is a common phenomenon in molecular crystals (see chapter 1). The question of whether there are compounds that are *not* polymorphic is becoming more common than whether a compound *is* polymorphic. The same is true for two of the six DTDAs used in this project, as they have two or more known polymorphs.[1–4] Although polymorphism can be frustrating and unpredictable, it is an important concept when working with molecular magnetic materials since different polymorphs can result in different magnetic responses in materials. One example of this is the two polymorphs of 4-cyanoperfluorophenyl-DTDA (Figure 4.1), where the **α**-phase showed paramagnetic behaviour at room temperature, and the

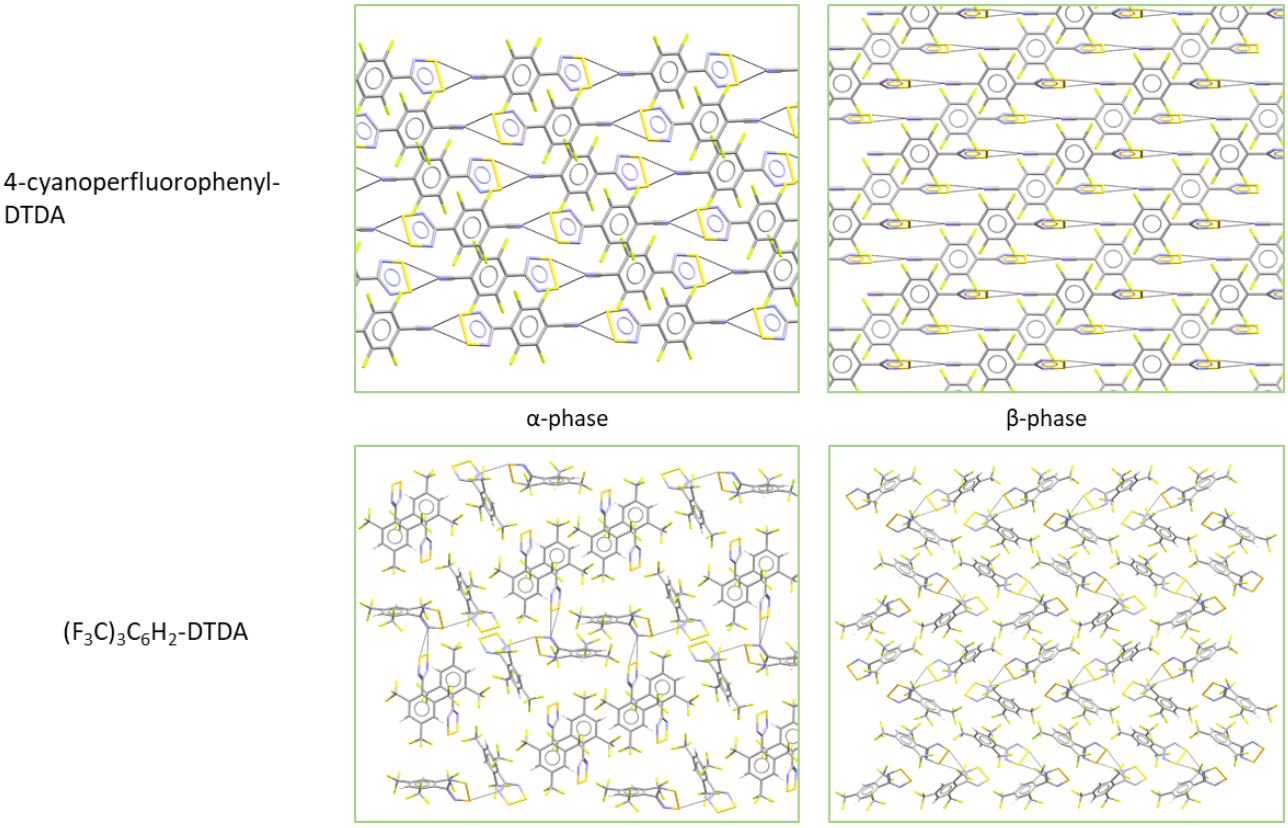

Figure 4.1. Crystal structure of the two polymorphs of 4-cyanoperfluorophenyl-DTDA (top) and $(F_3C)_3C_6H_2$-DTDA (bottom). Left and right are the alpha and beta polymorphs, respectively.

β-phase exhibits weak ferromagnetism at 36 K.[1,2] Another example is the $(F_3C)_3C_6H_2$-DTDA radical which has two polymorphs with different magnetic behaviour.[5]

In addition to exhibiting different magnetic behaviour, some DTDA polymorphs have been found that exhibit different dimerisation binding mode (see chapter 1, Figure 1.4) as well as displaying a mixture of monomers and π*- π* dimers in the same structure[4,5]. One such radical exhibiting a partially-dimeric polymorph is the ***γ***-phase of 2,6-difluorophenyl-DTDA. This compound is one of the DTDAs initially chosen for study during this project, and because of some interesting thermal analysis data that arose during characterisation of the polymorphs, further analysis was carried out.

4.1.1 A short overview of the structures of 3α, β and γ

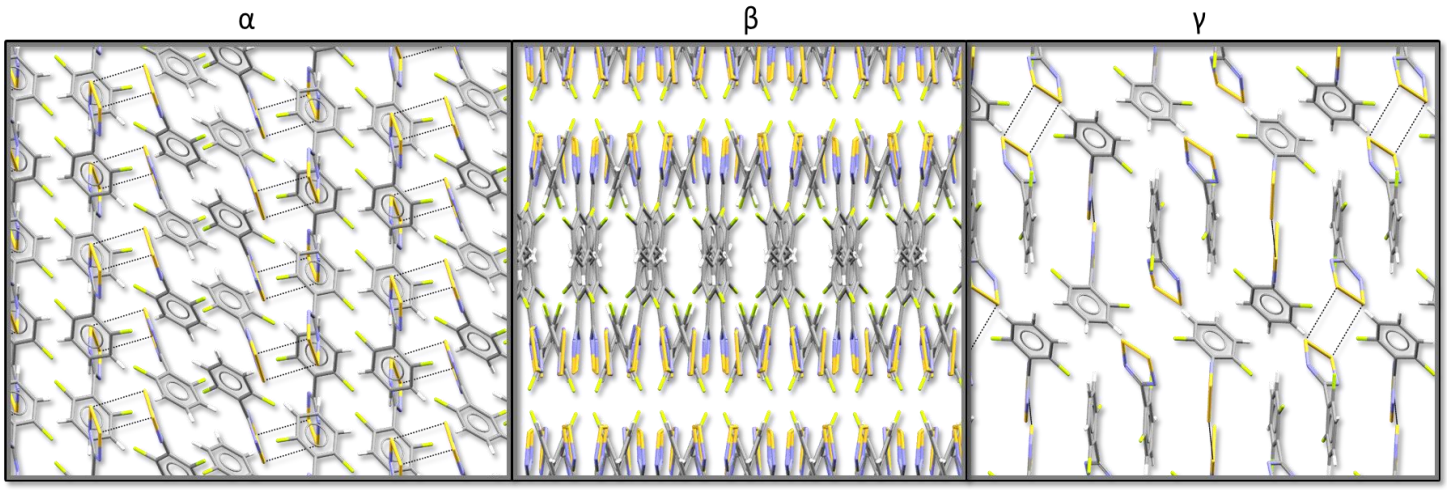

Figure 4.2. View down the *b*-axis of the three polymorphs of radical **3**. S-S···S-S interactions are displayed in the α and γ phases; the network is too complicated for display in β in this view. A mixture of monomers and dimers can clearly be seen in the γ-phase.

All three polymorphs of **3** have been known since 2010, when all three were found in the same year. The ***α***- and ***γ***-phases both crystallise in the monoclinic space group $P2_1/c$, although they are quite different. Where ***α*** is completely dimeric (*cis*-oid dimers) with S-S···S-S contacts of 3.069(3) and 3.129(3) Å [mean 3.099 Å], ***γ*** has sheets of dimers in between 1D layers of monomeric radicals, with the *trans*-antarafacial dimers having S-S···S-S contacts of

3.208(1) Å. The **β**-phase packs in the tetragonal space group $I4_1/a$, with a very large unit cell (Table 4.1) containing 16 dimer units with S-S···S-S contacts of 3.069(7) and 3.216(8) Å [mean 3.143 Å]. Like ***α***, the **β**-phase is also completely dimeric.

Table 4.1. A comparison of unit cell parameters for the three polymorphs of radical **3**.

	3α	**3β**	**3γ**
a /Å	16.885(4)	30.168(1)	10.3839(5)
b /Å	11.989(4)	30.168(1)	7.9745(3)
c /Å	8.207(4)	7.1749(2)	20.5463(8)
α /deg	90	90	90
β /deg	95.51(3)	90	109.846(2)
γ /deg	90	90	90
V /Å^3	1653.70	6529.94	1600.32

4.2 Synthesis and characterisation of three polymorphs of 4'-(2,6-difluorophenyl)-1,2,3,5-dithiadiazolyl radical (3)

The three polymorphs are made from bulk sample (vide infra) of **3**, the synthesis of which is described fully in Chapter 2. At least two methods for the synthesis of each polymorph have been reported in the literature[3,4]. This is unsurprising since these polymorphs are grown by sublimation and therefore there are a large number of parameters influencing nucleation and crystal growth, resulting in some irreproducibility. As far as possible, sublimation conditions, including scale, temperature, vacuum (dynamic vs. static), and laboratory space were kept constant in the current study. The vacuum pressure used for the growth of the polymorphs in this study differs somewhat from that stated in literature, which would affect sublimation results.

DSC traces of all polymorphs were determined in order to see whether these polymorphs undergo phase changes. PXRD patterns were not collected for each individual

phase since very little sample of each polymorph could be made, and PXRD is a destructive form of analysis for these air-sensitive compounds.

Synthesis of 3α: Fatila *et al.* reported crystals of the ***α***-phase isolated as purple-black blocks from sublimation at 50 °C (323 K) under a static vacuum of 10^{-2} Torr over several days[4], whilst Clarke *et al.* grew crystals of ***α***-phase at 110 °C (383 K)[3].

In our hands, crystals of the ***α***-phase were grown by adding ~40 mg of bulk **3** scraped off a cold finger into a thin schlenk under nitrogen. This was then kept under nitrogen atmosphere for about two minutes whilst heating in an oil bath to 35 °C. The sample was then sublimed onto the walls on the schlenk under static vacuum (1.7 Torr), and crystals of **3*α*** were isolated as green/black blocks of consistent morphology.

Synthesis of 3β: Fatila *et al.* reported crystals of the **β**-phase isolated as as green-bronze needles by sublimation at 35 °C (308 K) under a static vacuum of 10^{-2} Torr[4] within 24 hours, whilst Clarke *et al.* grew crystals of **β**-phase under 1/3 of an atmosphere of nitrogen at 95 °C (368 K)[3].

Crystals of the **β**-phase of radical **3** were more of a challenge to grow than either the ***α*** or ***γ*** phases. Several different crystallisation conditions were attempted, including varying the sublimation temperature between 35 and 95 °C, as well as using either vacuum or a partial pressure of nitrogen. Beautiful bronze/black needles of **3β** were finally grown by subliming 40 mg of freshly synthesised bulk sample of **3**[*] scraped directly from the cold finger into a smaller thin schlenk, at 75 °C under vacuum (1.7 Torr). Needles of **β**-phase grew onto the walls of the schlenk within 24 hours.

[*] Attempting to grow single crystals of 3**β** from sample that was not freshly synthesised consistently proved unsuccessful.

Synthesis of 3γ: Fatila *et al.* reported crystals of the **α**-phase isolated as blue-red blocks by sublimation at 80 °C (354 K) under a static vacuum of 10^{-3} Torr.[4] In our hands, crystals of **3γ** were obtained as purple/bronze blocks by subliming 100 mg of **3** onto the wall of a thin schlenk, under dynamic vacuum (1.7 Torr) at 70 °C. Attempts to grow single crystals of **3γ** during the colder months of winter were unsuccessful using a range of sublimation conditions.

Bulk sample that was sublimed onto the cold finger during purification was analysed by PXRD to evaluate the phase purity of the material obtained on the cold finger. The diffractogram showed a mixture of phases, where **β** and **γ** appear to be in excess, with indication of some **α** present (Figure 4.3).

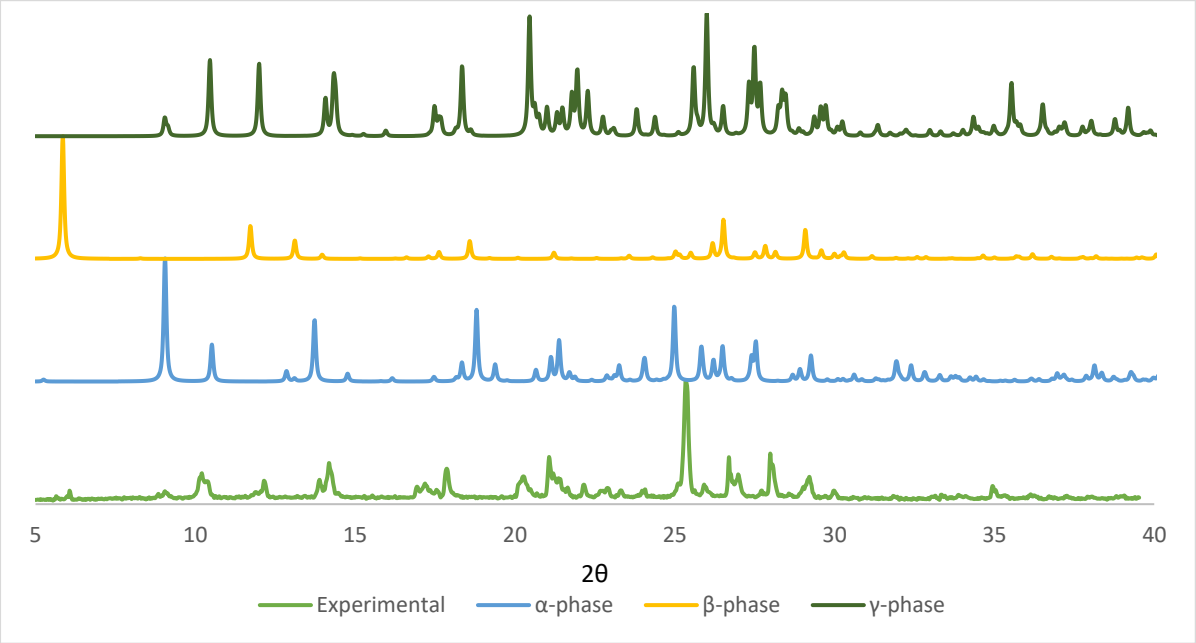

Figure 4.3. Powder X-ray diffractograms of radical **3**. Simulated patterns, generated using single-crystal data in Mercury[6], are presented for **α**, **β** and **γ**, with the bottom being the experimental pattern.

4.3 Thermal analysis

After working very closely with the three phases of **3**, as well as observing the behaviour of the sample when attempting to grow specific phases some initial hypotheses as to the relative stability of the three phases were developed. The **β**-phase was suspected to be a kinetically stable form, since single crystals of this phase could only be grown by immediately subliming

newly synthesised sample. However, speculating around the stability of the α and γ phases was more challenging, since 1) it was observed that the α-phase crystals converted to γ over time, and 2) γ is 50% monomeric, which is not a common occurrence in these materials. So, in order to begin establishing a relationship between the three polymorphs of **3**, thermal analysis was performed on the bulk sample as well as each individual phase. DSC traces of each phase were collected whilst cycling each sample through at least two runs (Figure 4.4).

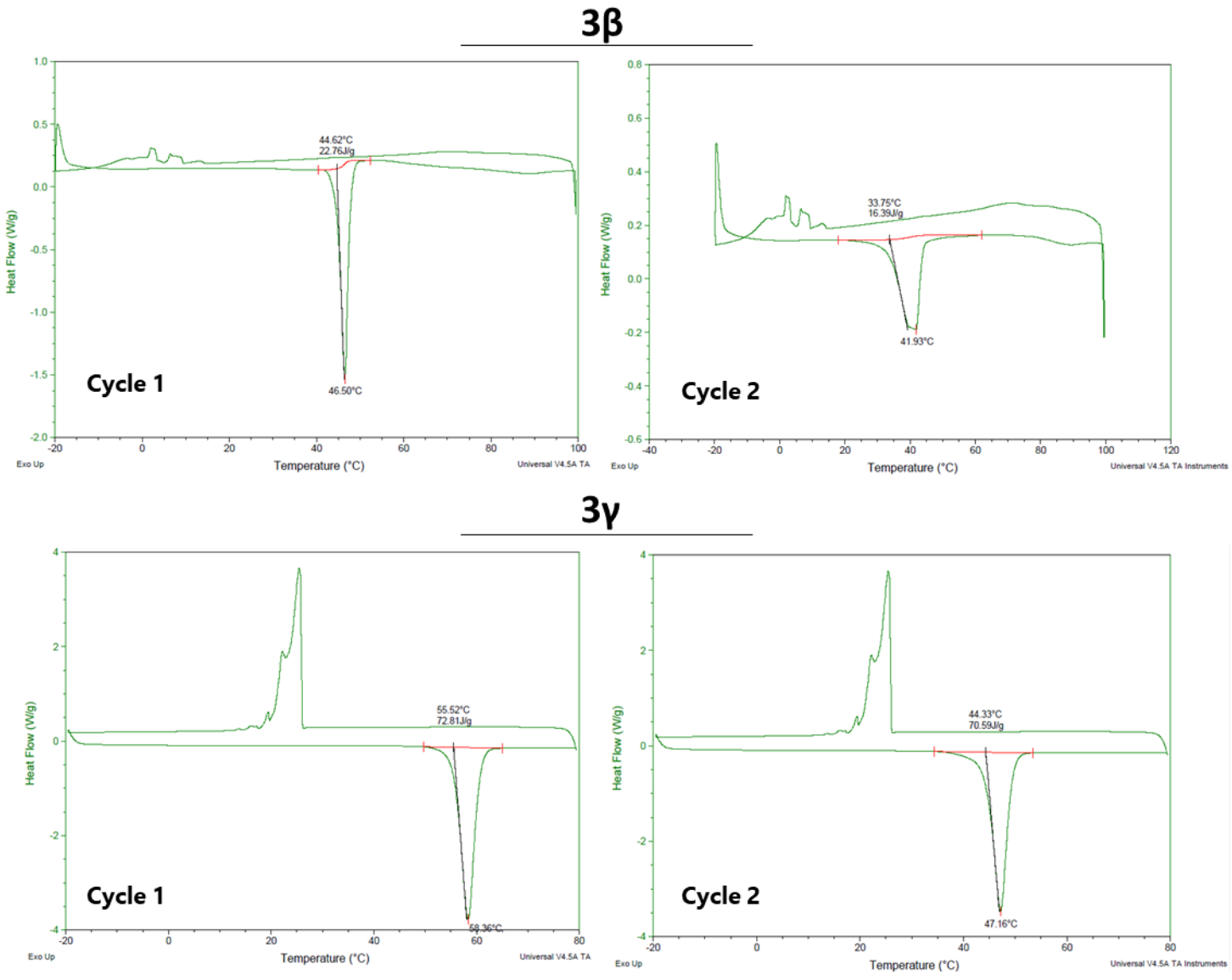

Figure 4.4. DSC traces of the **β** and γ phases of **3**. Top) **3β**, left: cycle 1 – event onset temperature of 44.62 °C (22.76 J/g), right: cycle 2 – event onset temperature of 33.75 °C (16.39 J/g). Bottom) **3γ**, left: cycle 1 – event onset temperature of 55.52 °C (72.81 J/g), right: cycle 2 – event onset temperature of 44.33 °C (70.59 J/g).

The first thing to be said about both **3β** and **3*γ*** is that both undergo clear changes on heating. The phases melt upon heating, however the melt endotherm in the second heating cycle that has a different onset temperature and enthalpy associated with it than in the first cycle. The first cycle of both samples distinctly showed two different phases in that **3β** showed a thermal event (melt) at 44.62 °C and an enthalpy of 4.94 kJ/mol whereas **3*γ*** showed a thermal event (melt) onset at 55.52 °C with an enthalpy of 15.82 kJ/mol. However, considering the second cycle of **3*γ*** – it shows a melt endotherm with an onset temperature of 44.33 °C. This corresponds very well with the endotherm on the first cycle of **3β** (see more clearly in Figure 4.5), showing a conversion to the **β**-phase. This could also possibly indicate that the **β**-phase is the thermodynamic form, at least between the **β** and ***γ*** phases.

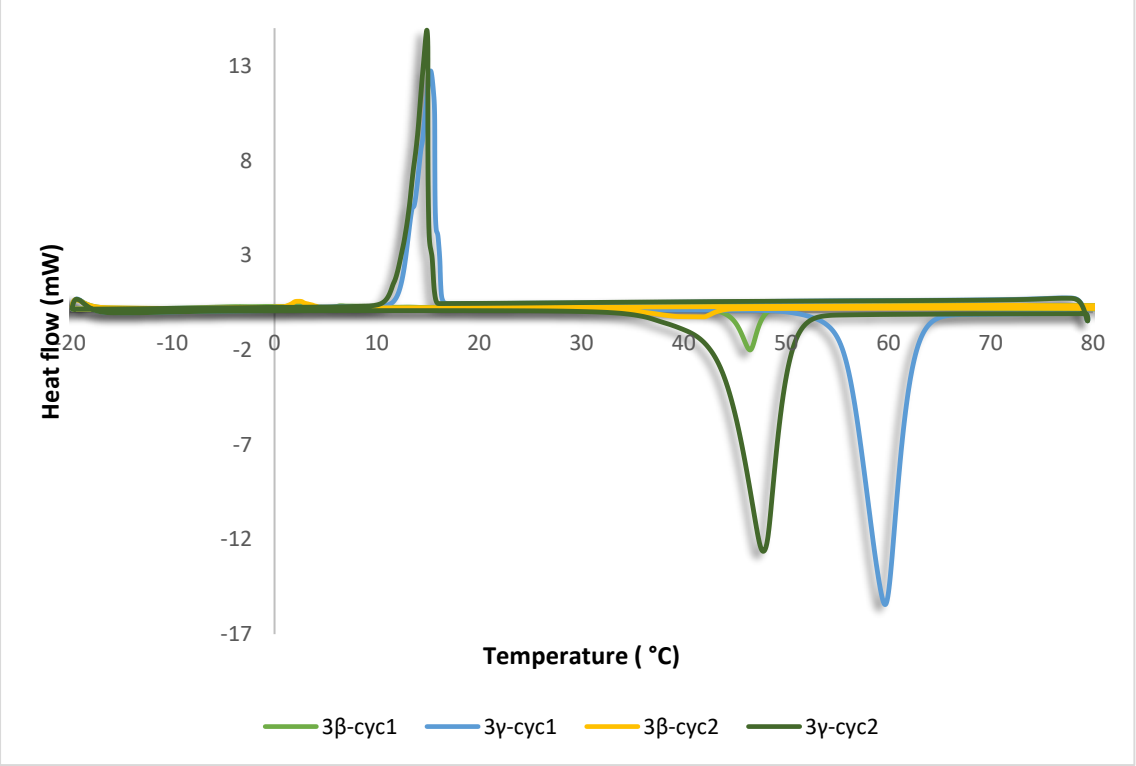

Figure 4.5. DSC trace overlay of the first two cycles of **3β** and **3*γ***. Onset temperatures of the endotherm in cycle 1 of **3β** and cycle 2 of **3*γ*** are 44.62 °C and 44.33 °C respectively.

To ensure that this was not a reversible transformation or to look for possible further conversion, **3*γ*** was cycled up to six times in the DSC, but no further changes were observed. The endotherm at 44 °C remains consistently for at least six cycles.

Variable-temperature PXRD (VT-PXRD) experiments were attempted in order to further investigate the stages of the phase transformation, however, some challenges arose during transfer of sample into the glass capillary for data collection. Sample of radical **3** becomes sticky and particles clump together when exposed to air, making it impossible to get into a capillary. Time unfortunately did not allow for more intensive study on the relative phase stabilities due to the challenges faced with getting phase-pure sample of the **α**-phase. Especially since it was observed by SCXRD that the **α**-phase converts to *γ* over some time. sample of **3*α*** could not be made in time for the completion of this section of the project, and full investigation of its phase change. As a result, conclusive analysis of the phase changes could not be made. Future work on this is imperative, as full analysis of the **α**-phase would provide the results needed to complete the polymorph study and allow for the a more in-depth analysis on the phase changes. In future, a solution to the VT-PXRD problem may be to use a capillary with a much larger internal diameter (2.5 mm vs. 0.5 mm, for example).

Charge density analysis has also recently been done on **3β** and **3γ** by a collaborator, Prof. K. Wozniak, and these results, alongside the experimental work in this study, may shed some light on the changes observed and the relative stability of the three polymorphs.

4.4 References

1 A. J. Banister, N. Bricklebank, W. Clegg, M. R. J. Elsegood, C. I. Gregory, I. Lavender, J. M. Rawson and B. K. Tanner, *Chem. Commun.*, 1995, 679–680.

2 A. J. Banister, N. Bricklebank, I. Lavender, J. M. Rawson, C. I. Gregory, B. K. Tanner, W. Clegg, M. R. J. Elsegood and F. Palacio, *Angew. Chem. Int. Ed. Engl.*, 1996, **35**, 2533–2535.

3 C. S. Clarke, D. A. Haynes, J. N. B. Smith, A. S. Batsanov, J. A. K. Howard, S. I. Pascu and J. M. Rawson, *CrystEngComm*, 2010, **12**, 172–185.

4 E. M. Fatila, M. C. Jennings, J. Goodreid and K. E. Preuss, *Acta Cryst.*, 2010, **C66**, 260–264.

5 A. Alberola, C. S. Clarke, D. A. Haynes, S. I. Pascu and J. M. Rawson, *Chem. Comm.*, 2005, **3**, 4726–4728.

6 C. F. Macrae, I. J. Bruno, P. R. Chisholm, P. Edgington, E. McCabe, L. Pidock, R. Rodriguez-Monge, J. Taylor, J. Van De Streek and P. A. Wood, *J. Appl. Cryst.*, 2008, **41**, 466–470.

Chapter 5

Diversity amidst uniformity in a series of charge transfer cocrystals with similar supramolecular architectures

Herein the preparation of a series of charge transfer cocrystals formed between *p*-benzoquinone and four *p*-halophenols using the methods of neat co-grinding, recrystallisation and co-sublimation is reported. The solid-state features of these charge transfer cocrystals using single-crystal X-ray diffraction were also investigated.

An analogous series of organic charge transfer complexes/cocrystals has been prepared and structurally characterised. The complexes consist of *p*-benzoquinone (BQ) as the electron-acceptor, and one of four monosubstituted *p*-halophenols (XP, where X represents the halogen) as electron donors. The cocrystals of 4-bromophenol (BrP) and 4-chlorophenol (ClP) with *p*-benzoquinone ({BrP}{BQ} and {ClP}{BQ}, respectively) were previously reported, and were shown to be isostructural to one another.[1,2] We report the preparation of two new cocrystals of BQ with 4-fluorophenol {FP}{BQ} and 4-iodophenol {IP}{BQ}. All of the cocrystal combinations {XP}{BQ} can be prepared in both 1:1 and 2:1 donor-acceptor ratios with the only exception being 4-iodophenol, which yielded only a 2:1 form. In the case of {FP}{BQ} and {IP}{BQ} different forms were isolated using different methods of crystallization namely: recrystallization from solution and co-sublimation.

5.1 Background

Halophenols (XPs) are interesting building blocks in crystal engineering and in the area of supramolecular recognition. These molecules have a variety of binding sites that allow for molecular recognition; they are able to form hydrogen bonds through the phenolic oxygen atom, as well as forming halogen bonds via the halogen atom also located on the benzene ring. Benzoquinone and its derivatives (including quinhydrone) are widely known as good electron acceptors owing to their large electron affinity.[3,4]

Cocrystals have received much attention from diverse areas such as chemical crystallography, crystal engineering, pharmaceutical chemistry, magnetochemistry,[5] and others.[6] The pharmaceutical industry has shown increased interest in cocrystals and cocrystal formation, since cocrystals of pharmaceutical compounds can have different biopharmaceutical properties to the individual drug molecules. For example, cocrystals may

have improved solubility, improved dissolution rates,[7,8] and therefore improved bioavailability (of drug compounds).[7] Crystal engineering using cocrystals has attracted more interest over the years as cocrystals provide a unique way to investigate the influence of specific synthons on the structure-property relationships of materials as well as a way to establish a hierarchy between interaction types.[9–13]

Polymorphism is another phenomenon that is pervasive throughout solid state chemistry, and can have both beneficial and detrimental outcomes (see chapters 1 and 4). There have been a number of alternate definitions of polymorphism over the years, as highlighted by Bernstein[14], showing that the term "polymorph" is not arbitrary to define. For this text, polymorphism will be described as a phenomenon where the same chemical compound exhibits at least two different crystal structures.[14–17] Polymorphs, much like different compounds, may have different physical properties that arise from the differences in their packing arrangements.[18] This is especially relevant in the pharmaceutical industry where control over the physical properties of compounds are of vital importance.[18] The use of cocrystals was at some stage proposed as a method to eliminate polymorphism during the manufacturing process; however, a number of polymorphic cocrystals have since been reported.[12]

Polymorphs of compounds have been found by simply using different crystallisation techniques, different conditions of crystallisation and different solvents.[11,19,20] Some of these techniques include neat grinding, liquid-assisted grinding, recrystallisation from solution, co-sublimation, etc.[11,21–24] Techniques such as neat grinding and liquid-assisted grinding emphasize the extent to which solvent molecules influence the polymorphic form obtained from experiment.[19]

As a continuation and extension of the series of the {XP}{BQ} cocrystals first reported in 1967, two additional analogues were investigated. 4-fluorophenol and 4-iodophenol were used as donor co-formers to the *p*-benzoquinone acceptor molecule (Scheme 5.1). These cocrystal analogues were made in an attempt to observe the influence that the halogens, iodine and fluorine, would have on the properties, form and structure of the resulting cocrystals. This series of cocrystals exhibits an array of interesting solid-state phenomena, including isostructurality, concomitant polymorphism, polarity, and a variety of competing synthons.

In this text, polymorphic forms and forms that simply have different stoichiometric ratios for the cocrystal (1:1 vs. 2:1) will be differentiated by using the symbols **α** and **β** for polymorphs, and the term "form" along with a number "1" or "2" in front of the donor molecule in the shorthand notation for the 1:1 form or the 2:1 form, respectively. For example, {1XP}{BQ} is the 1:1 form, whereas {2XP}{BQ} is the 2:1 form. Where the number is omitted, simply the cocrystal combination as a whole is being called (referring to both the 1:1 and 2:1 forms; also including the polymorphs).

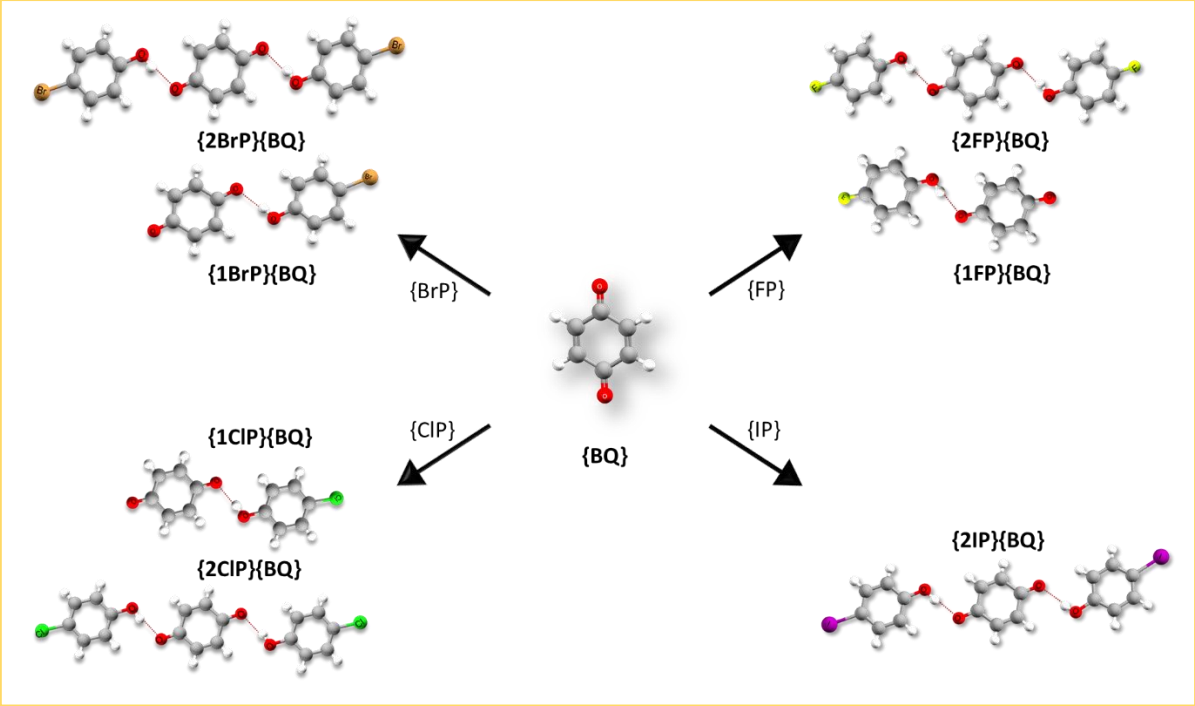

Scheme 5.1. Representation of cocrystal combinations as well as abbreviations used for cocrystals and co-formers. The donor-acceptor stoichiometric ratios, 1:1 and 2:1, are denoted by either the presence or absence of the number "2" in front of the acceptor molecule abbreviation.

5.1.1 Design of sublimation apparatus

One of the techniques used to investigate cocrystal formation was sublimation. In order to effectively co-sublime two different compounds with different sublimation temperatures, specialised apparatus was designed and built in-house (see Appendix A, Figure 13 for diagram). The apparatus has two sublimation chambers connected to a U-tube. Each chamber/bulb can be heated independently enabling dual-temperature sublimation in a single device and reducing the risk of decomposition of one of the components when the substances have significantly different sublimation temperatures. Furthermore, the device houses a cold-finger at the apex of the U-tube that is removable to collect sublimed crystals. In turn, the cold-finger also serves as a port for a removable stopcock that allows for the evacuation of the system.

The general procedure to carry out a sublimation experiment is described below. Firstly, the bulbs are loaded separately with the materials to be sublimed. Secondly, the whole system is evacuated. The system is sealed and left under static vacuum, while the two bulbs are heated independently to the sublimation point of each component using flexible heating mantles. As the vapour pressure of each compound rises they mix in the U-tube and crystallisation occurs. The sublimation temperatures for all the compounds in this section could not be found in the literature, so a temperature just below the melting points of each were chosen as a starting point. This seemed to be effective as cocrystal formation was readily seen. No further exploration was done on sublimation temperature variation as it was not within the scope of this study.

5.2 Cocrystal synthesis*

5.2.1 Known complexes

5.2.1.1 Synthesis of {1BrP}{BQ} and {2BrP}{BQ}.

Equimolar amounts of 4-bromophenol (16.6 mg, 0.093 mmol) and *p*-benzoquinone (10 mg, 0.093 mmol) were co-ground with a mortar and pestle, yielding a brown–orange powder of the cocrystal {1BrP}{BQ}. Crystals suitable for single-crystal X-ray diffraction (SCXRD) were obtained by recrystallisation from chloroform. A similar procedure was followed to generate the 2:1 form, {2BrP}{BQ}, using the relevant molar ratios for 4-bromophenol (32 mg, 0.185 mmol) and *p*-benzoquinone (10 mg, 0.093 mmol). The resulting powdered product had a deep brown-red colour.

* Phase purity for all compounds was established by PXRD analysis. See Appendix A for additional PXRD analysis not presented explicitly in this chapter.

Using the sublimation apparatus, both the {1BrP}{BQ} (orange) and {2BrP}{BQ} (dark red) forms were obtained concomitantly. The individual components were heated to 113 °C (BQ) and 64 °C (BrP). The 1:1 cocrystal, {1BrP}{BQ}, preferentially formed further from the heat source, whereas the 2:1 form, {2BrP}{BQ}, crystallised closer to the heat source (a flexible heating mantle).

IR (cm^{-1}) **{1BrP}{BQ}**: 3210 (OH), 1637 (C=O), 1586 (C=C), 1227 (C-O), **{2BrP}{BQ}**: 3211 (OH), 1636 (C=O), 1587 (C=C), 1228 (C-O).

5.2.1.2 Synthesis of {1ClP}{BQ} and {2ClP}{BQ}.

{1ClP}{BQ} was obtained by co-grinding of 4-chlorophenol (11.7 mg, 0.093 mmol) and *p*-benzoquinone (10 mg, 0.093 mmol) resulting in an orange powder. The powder was dissolved in chloroform and single crystals were obtained by slow evaporation. The same procedure was followed for {2ClP}{BQ}, where 2 equivalents of 4-chlorophenol (23.4 mg, 0.18 mmol) were used and the reaction yielded a dark brown/red product.

Using the sublimation apparatus, both the {1ClP}{BQ} (orange) and {2ClP}{BQ} (dark red) forms were obtained (concomitantly). BQ and ClP were heated to 113 °C and 44 °C, respectively. As with {BrP}{BQ}, the 1:1 complex preferred to form on cooler regions of the apparatus, whereas the 2:1 form {2ClP}{BQ} preferred to grow closer to the heat source.

IR (cm^{-1}) **{1ClP}{BQ}**: 3211 (OH), 1636 (C=O), 1587 (C=C), 1228 (C-O), **{2ClP}{BQ}**: 3252 (OH), 1635 (C=O), 1586 (C=C), 1218 (C-O).

5.2.2 New complexes

5.2.2.1 Synthesis of α-{1FP}{BQ}

α-{1FP}{BQ} was obtained by co-grinding *p*-benzoquinone (10 mg, 0.093 mmol) and 4-fluorophenol (10.3 mg, 0.093 mmol) using a mortar and pestle. The solid-state reaction yielded

a burnt-orange powder indicating the formation of a cocrystal. Crystals suitable for SCXRD were obtained by dissolution and subsequent recrystallisation from chloroform.

5.2.2.2 Synthesis of β-{1FP}{BQ} as well as {2FP}{BQ}

Co-crystallisation using the co-sublimation apparatus produced crystals of both **β-{1FP}{BQ}** and **{2FP}{BQ}** phases concomitantly. The sublimation chambers were loaded separately with *p*-benzoquinone (30 mg, 0.278 mmol) and 4-fluorophenol (31 mg, 0.278 mmol), and heated to 113 °C and 49 °C respectively; single crystals appeared after approximately 10 hours.

The **β**-phase of **{1FP}{BQ}** crystallises as bright-orange plates and tends to grow on cooler regions of the apparatus, i.e. further from the heat source, while the **{2FP}{BQ}** form grows as dark-crimson rod-shaped crystals nearer the heat source.

IR (cm^{-1}) **β-{1FP}{BQ}**: 3220 (OH), 1641(C=O), 1590 (C=C), 1195 (C-O), **{2FP}{BQ}**: 3272 (OH), 1633 (C=O), 1590 (C=C), 1195 (C-O).

5.2.2.3 Synthesis of α-{2IP}{BQ}

Co-grinding of *p*-benzoquinone (10 mg, 0.093 mmol) and 4-iodophenol (40.7 mg, 0.185 mmol) with a mortar and pestle yielded a coral-red powder. Crystals of **α**-{2IP}{BQ} suitable for SCXRD were obtained by slow evaporation from chloroform.

IR (cm^{-1}) **α-{2IP}{BQ}**: 3230 (OH), 1635 (C=O), 1576 (C=C), 1078 (C-O).

5.2.2.4 Synthesis of β-{2IP}{BQ}

p-Benzoquinone (30 mg, 0.278 mmol) and 4-iodophenol (122 mg, 0.56 mmol) were co-sublimed at 113 °C and 94 °C respectively, under dynamic vacuum. Small dark red crystals of **β**-{2IP}{BQ} formed within 12 hours while dark crimson rod-shaped crystals suitable for SCXRD were obtained within three days.

IR (cm^{-1}) **β-{2IP}{BQ}**: 3246 (OH), 1636 (C=O), 1575 (C=C), 1069 (C-O).

Crystals of a 1:1 form were not obtained, despite numerous efforts via both co-sublimation and solution crystallization. Despite starting with 1:1 ratios of the starting materials the reaction consistently yielded the 2:1 form.

5.3 Results and discussion

In the case of {ClP}{BQ} and {BrP}{BQ}, both the 1:1 and 2:1 forms have been previously reported by Shipley and Wallwork[1,2] (refcodes: BNQBRP, BNQCLP, BNQDBP and BNQDCP). For the purposes of this work, the data were recollected at 100 K since the original structural data were collected at room temperature or 283 to 303 K as reported (Table 5.1). The 1:1 complexes/cocrystals of {ClP}{BQ} and {BrP}{BQ} crystallise in the triclinic space group $P\bar{1}$ while the 2:1 cocrystals crystallise in the monoclinic space group $P2_1/c$. The asymmetric unit of the 1:1 cocrystals consists of a single complex unit made up of a molecule each of BQ and XP (X = Cl or Br). The BQ and XP molecules are arranged in an alternating fashion (mixed stacks) in columns along the *ab* diagonal and are hydrogen bonded to each other, across columns, via O-H···O interactions (Figure 5.1). For the 2:1 complexes the asymmetric unit consists of half a molecule of BQ and a single molecule of XP (X = Cl or Br). The BQ and XP molecules are arranged in offset alternating stacks parallel to the *a* axis. The BQ molecule is hydrogen bonded to two molecules of XP across the columns via O-H···O interactions (Figure 5.1).

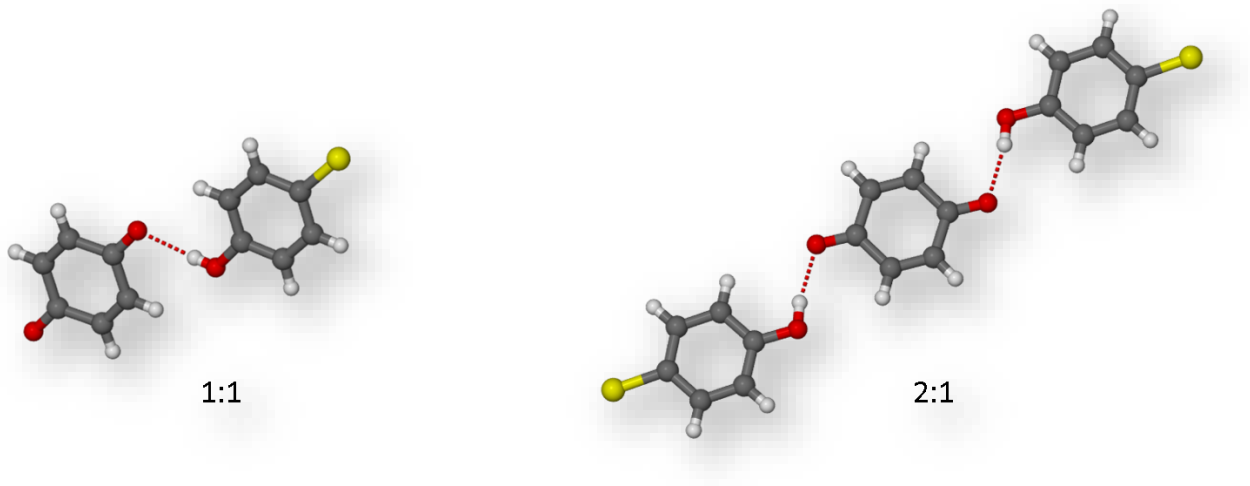

Figure 5.1. Example representation of the hydrogen bonded units present in the 1:1 (left) and 2:1 (right) forms of both {ClP}{BQ} and {BrP}{BQ}. Atoms in yellow represent halogen atoms (Cl or Br) while atoms coloured red and grey are oxygen and carbon atoms, respectively.

5.3.1 Result and discussion

5.3.1.1 Forms of **{FP}{BQ}.**

Two different forms of {FP}{BQ} were obtained using different methods of crystallization: sublimation and recrystallization, as described earlier. For the sake of clarity, the 1:1 cocrystal of {FP}{BQ} obtained by recrystallization from chloroform will be referred to as the **α**-phase, **α**-{FP}{BQ}, while the phase obtained from co-sublimation, having a different stoichiometric ratio, as the **β**-phase, **β**-{FP}{BQ} – essentially a solid solution.[25] Both forms have different structural aspects from {1ClP}{BQ} and {1BrP}{BQ}.

Structure of 1:1 α-{4-fluorophenol}{*p*-benzoquinone} (α-{1FP}{BQ}).

The ***α***-phase of {1FP}{BQ} crystallises in the triclinic crystal system with space group *P*1 where the molecules of the cocrystal have a polar arrangement (Figure 5.2). The asymmetric unit of ***α***-{1FP}{BQ} consists of a single molecule of both BQ and FP located in separate columns. The molecules form a 1:1 hydrogen-bonded dimer unit resulting in stacks linked by O-H···O

hydrogen bonds having a donor – acceptor (D···A) distance of 2.761(7) Å. The intra-stack distance, measured as the distance between the planes of the FP rings, is 3.340 Å.

The FP···BQ hydrogen bonded dimers pack to form 2D layers (see Figure 5.2[†]). Within these layers, dimers are connected by two different types of $R_2^2(8)$[‡] rings – one between two BQ molecules, involving only C=**O** as H-bond acceptors, and another between two FP molecules, with a fluorine and C-**OH** as H-bond acceptors (Figure 5.2a).[26] These layers are held together by an extensive hydrogen bonding network (Figure 5.2b and c).

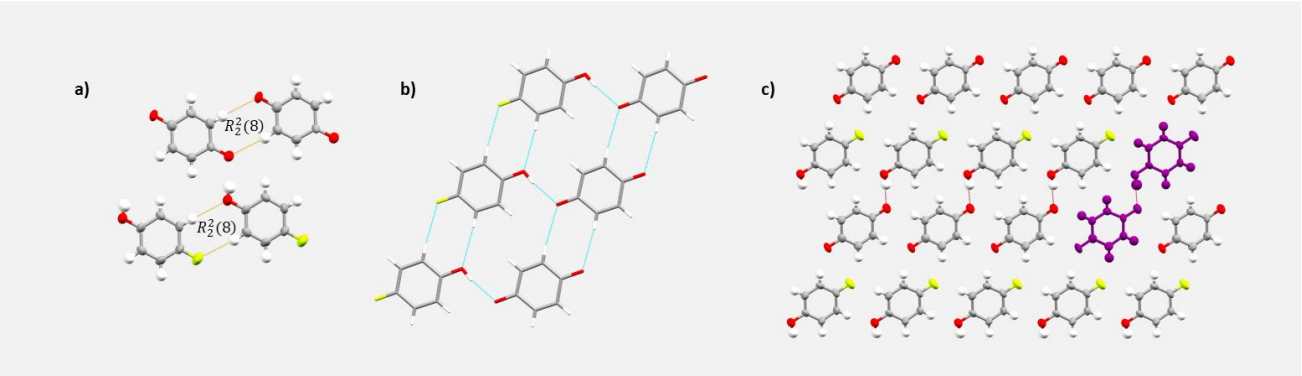

Figure 5.2. Packing in **α**-{1FP}{BQ}. (a) $R_2^2(8)$ hydrogen bonding between two BQ molecules as well as two FP units. (b) Hydrogen bonding network holding 1:1 units together in 2D layer. Hydrogen bonding contacts are displayed in cyan (c) Polar stacking arrangement (layer), viewed down the *a* axis. A dimeric unit is highlighted in purple.

Structure of β-{4-fluorophenol}{*p*-benzoquinone} (β-{1FP}{BQ}). Co-sublimation of FP and BQ resulted in a second polymorph[§] (for clarity) of the 1:1 form, **β**-{1FP}{BQ}, which crystallizes in the monoclinic space group $P2_1/c$. The asymmetric unit consists of a molecule of BQ and a molecule of FP superimposed on the same site and having a site occupancy ratio of 53:47 (FP:BQ) as determined by SCXRD analysis. The structure is therefore best described as a solid solution[25]. Co-sublimation experiments were repeated on this sample,

[†] See Appendix A for additional hydrogen bond parameter tables.
[‡] This is graph set notation for hydrogen bonding. Here, "R" is the design pattern (in this case, a ring), "8" is its degree (the numbers of atoms in the ring), "2" (top) is the number of donor atoms and "2" (bottom) the number of acceptor atoms.
[§] Since this structure is a solid solution, it is not a polymorph of {1FP}{BQ}, but rather a different form entirely. But since "forms" are also used to differentiate between 1:1 and 2:1 co-former stoichiometries, the solid solution form is simply referred to as a polymorph, form clarity.

however a solid solution was consistently obtained. This is not entirely surprising, as the size and shape of the two molecules are very similar and can therefore be substituted for one another. Surprisingly, this phenomenon is not observed for crystals grown from solution. The solvent therefore plays an important role in how the molecules pack in 3D.

To establish which polymorph of {1FP}{BQ} is produced when the components are co-ground, a PXRD pattern of the ground sample (1:1) was measured and compared to the patterns simulated from the single-crystal X-ray diffraction data. From a visual comparison it appears that the ground sample is the **β** polymorph. (Figure 5.3). Slight peak shifts may be due to temperature differences, since the experimental pattern was collected at room temperature whereas the simulations based on data collected at 100 K. Additional peaks not belonging to **β**-{1FP}{BQ}, one below 15 degrees and another between 25 and 30, match similar peaks in the PXRD pattern of 4-fluorophenol, since BQ is very volatile and sublimes out of the sample quite rapidly.

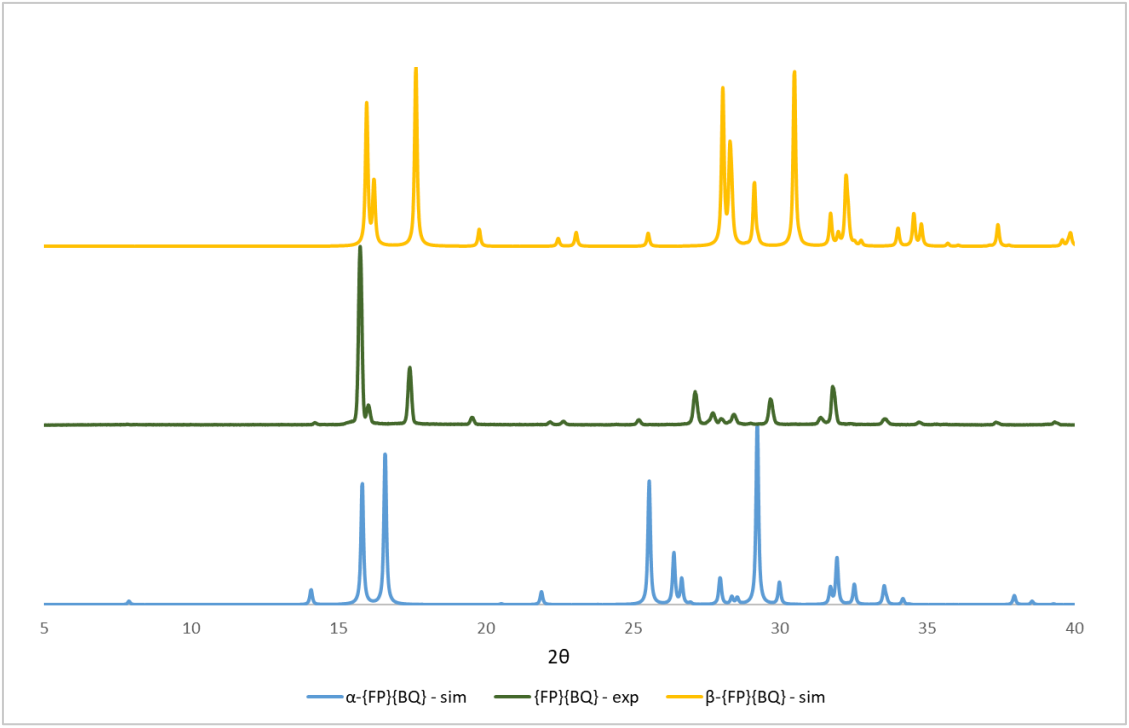

Figure 5.3. Comparison of the cocrystal material of {1FP}{BQ} prepared by neat co-grinding with the simulated PXRD patterns for the two forms, where (top) **β**-{1FP}{BQ}, (middle) {1FP}{BQ} and (bottom) **α**-{1FP}{BQ}.

Since the 1:1 forms of the previously-known cocrystals {ClP}{BQ} and {BrP}{BQ} were shown to be isostructural[1,2], the **α**- and **β**-{1FP}{BQ} forms were compared to these known forms to determine whether they, too, were isostructural to {1ClP}{BQ} and {1BrP}{BQ} (Figure 5.4). The simulated PXRD patterns of **α**- and **β**-{1FP}{BQ} forms were used for the comparative check since the experimental co-ground pattern shows evidence of a mixture of phases.

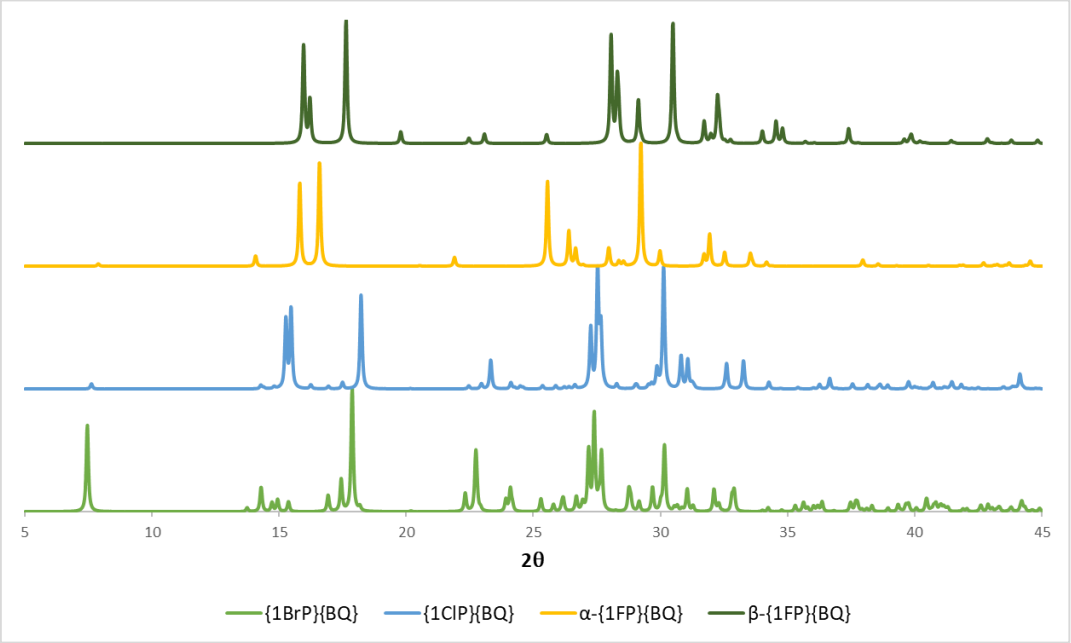

Figure 5.4. A comparison of the simulated PXRD patterns of **α**- and **β**-{1FP}{BQ} with the simulated patterns of {1ClP}{BQ} and {1BrP}{BQ}. This shows that neither **α**- nor **β**-{1FP}{BQ} are isostructural to {1ClP}{BQ} or {1BrP}{BQ}.

It was observed from the PXRD patterns that neither **α**- nor **β**-{1FP}{BQ} are isostructural to {1ClP}{BQ} and {1BrP}{BQ} (also see Table 5.1 for crystal structure comparison). This is evidenced by the fact that the PXRD patterns do not compare very well, and very few similarities can be observed between the patterns.

5.3.1.2 Structure of 2:1 {4-fluorophenol}{*p*-benzoquinone} ({2FP}{BQ}).

The 2:1 form of {FP}{BQ} crystallises in the monoclinic crystal system in the space group $P2_1/c$, with the asymmetric unit consisting of half a molecule of BQ and complete molecule of FP. The hydrogen bonded unit is made up of a BQ molecule linked to two FP molecules, which are

arranged along diagonal planes criss-crossing the unit cell. These trimers stack in columns along the *a* axis. Within each trimer, OH···O contacts are 2.737(1) Å in length, which is only slightly longer than those observed in the structures of {2ClP}{BQ} and {2BrP}{BQ} (2.725(1) and 2.720(1) Å, respectively). The columns are held together by van der Waals interactions as well as parallel displaced π-interactions. The trimers are also oriented in such a way that the hydroxyl moiety (C–O(H)) of the FP molecule in one layer lies over the centre of a BQ ring in the layer above and below (C-O(H)···π 3.226 Å), and similarly the carbonyl moiety C=O of the BQ lies over the centre of an FP ring in the layers above and below (C=O···π 3.033 Å) (Figure 5.5b). These are electrostatically-driven interactions, where the electronegative regions on the F/O atoms are interacting with the electropositive region over the centre of the aromatic rings.

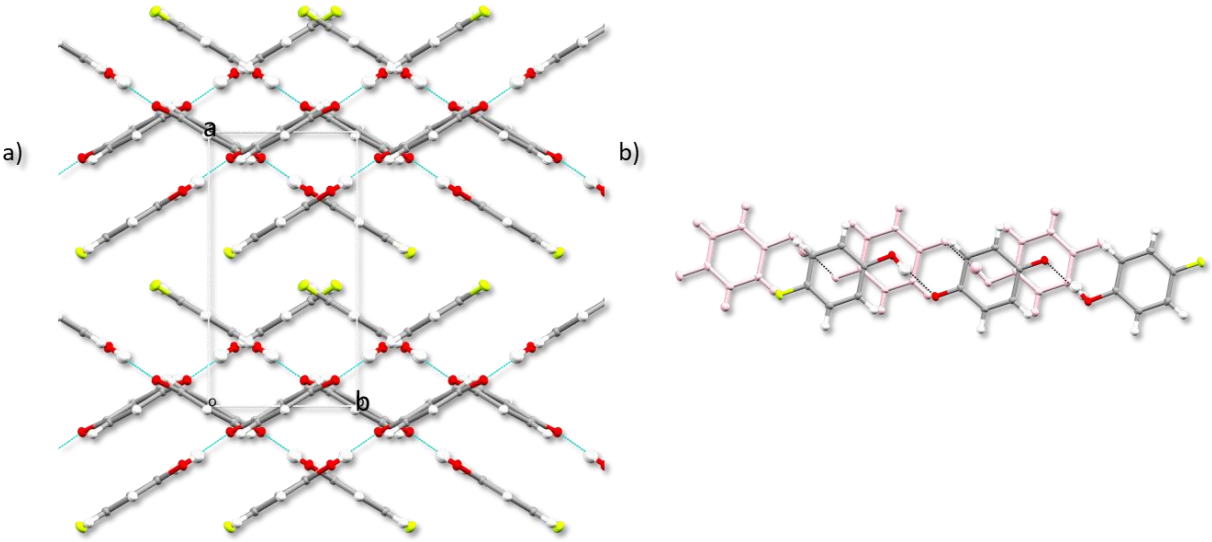

Figure 5.5. a) Trimer stacks down the *a* axis. b) Slipped orientation between two trimers, with the C-OH bond over the centre of a BQ ring, and a C=O bond over the centre of an FP ring.

5.3.1.3 Structures of the different polymorphs of the 2:1 form of {4-iodophenol}{*p*-benzoquinone} ({2IP}{BQ})

Two polymorphs of {2IP}{BQ} were isolated: **α**-{2IP}{BQ} from solution, and a second, **β**-{2IP}{BQ}, from co-sublimation. Both the **α** and **β** polymorphs crystallise in the monoclinic crystal system, with **α**-{2IP}{BQ} crystallising in $P2_1/n$, and **β**-{2IP}{BQ} in $P2_1/c$ (See Table 5.1).

Structure of 2:1 α-{4-iodophenol}{*p*-benzoquinone} (α-{2IP}{BQ}). The structure of **α**-{2IP}{BQ} has a similar packing arrangement to that of {2ClP}{BQ}, {2BrP}{BQ} and {2FP}{BQ} (Figure 5.6), although significant differences such as space group and unit cell dimensions prevents **α**-{2IP}{BQ} from being classed as isostructural to the aforementioned cocrystals (Figure 5.7). The asymmetric unit consists of one molecule of BQ and two molecules of IP, with each of the three molecules located in separate columns. The three molecules form a 2:1 hydrogen-bonded trimer. The two IP molecules are symmetry independent and are not arranged symmetrically around the BQ molecule. The mean plane through one of the IP molecules is tilted with respect to the mean plane through the BQ molecule (Figure 5.6b). As a result, the hydrogen bond lengths in the hydrogen bonded unit are not symmetrical. The OH···O contact to the more inclined IP is 2.771(3) Å in length whereas the hydrogen bond length is 2.722(3) Å for the other IP molecule. Though the difference is small, it affects the extended network of the overall structure, compared to the other 2:1 forms, where the hydrogen bonds are symmetrical on either side of the BQ molecule. Unlike all the other 2:1

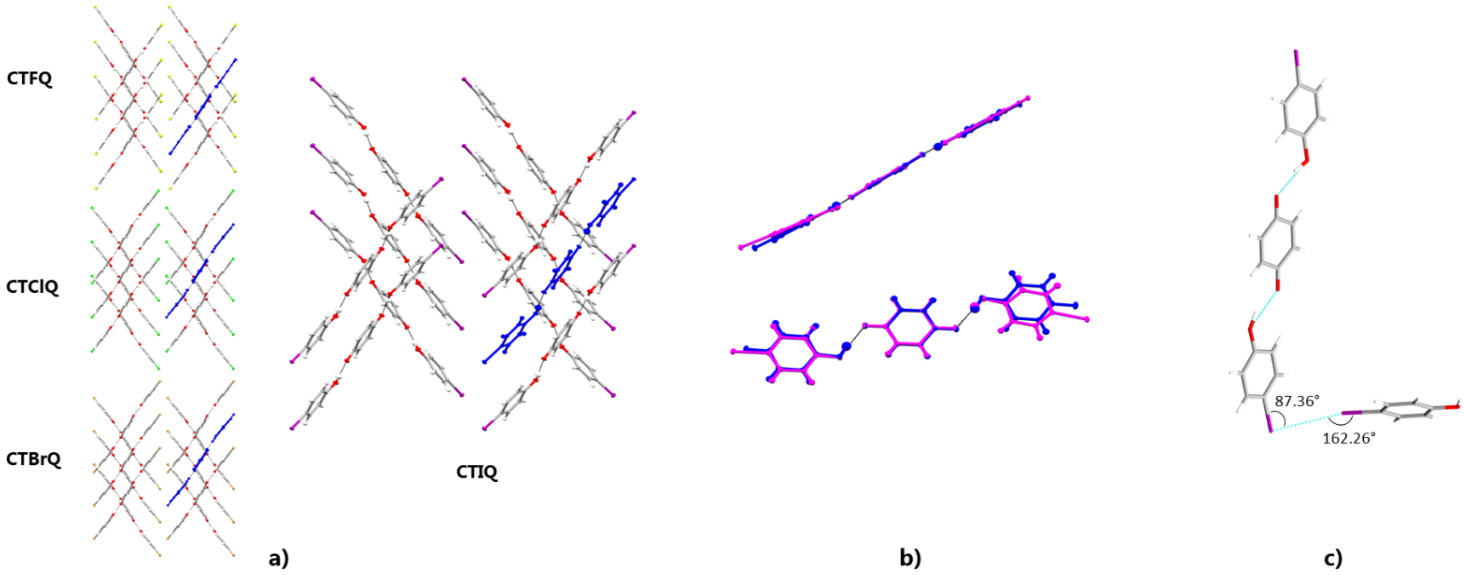

Figure 5.6. a) A representation of some of the structural similarities between the 2:1 forms of the four cocrystal combinations. Trimer unit is displayed in blue – the *S*-shape becomes more pronounced with increase in halogen size b) overlay of the **α**-{2IP}{BQ} (pink) and {2FP}{BQ} (blue) trimer, with the S-shape more visible in {2IP}{BQ} owing to one IP molecule being tilted out-of-plane (top), as well the second IP slightly rotated in the plane of the dimer due to halogen bonding contacts (bottom), c) Type-II halogen bonding between two adjacent IP molecules.

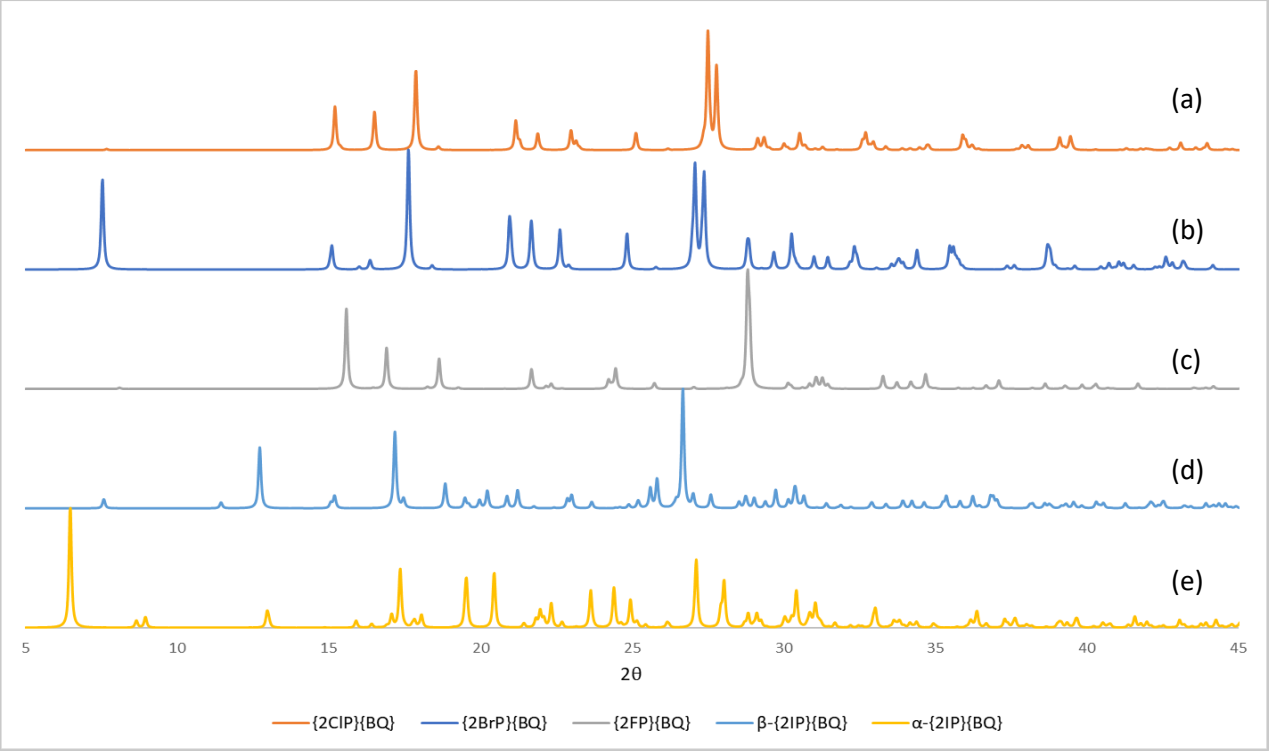

Figure 5.7. Experimental PXRD patterns for the 2:1 forms of (a) {2ClP}{BQ}, (b) {2BrP}{BQ}, (c) {2FP}{BQ}, (d) β-{2IP}{BQ} and (e) α-{2IP}{BQ}. Once again, the patterns of {2ClP}{BQ} and {2BrP}{BQ} show isostructurality in (a) and (b) respectively, whilst neither α-{2IP}{BQ} nor β-{2IP}{BQ} are isostructural to each other or {2ClP}{BQ} and {2BrP}{BQ}. {2FP}{BQ} also appears to be isostructural to {2ClP}{BQ} and {2BrP}{BQ}, with some peaks less pronounced due to possible preferred orientation and different atoms in the unit cell.

forms, the structure for **α**-{2IP}{BQ} possesses extensive I···I halogen bonding interactions (Figure 5.6c). There are no halogen bond or halogen-halogen contacts in the F- and Cl-analogues, and only the {1BrP}{BQ} structure has Br···O contacts (the orientation is wrong for halogen bonds).

A feature of the **α**-{2IP}{BQ} structure is that the mean planes passing through the IP molecules are inclined, to different extents, to the mean plane through the BQ molecule, resulting in a very subtle, *S*-shape of the hydrogen bonded trimer; a feature less visible in the other three 2:1 cocrystal analogues. The inclination of the mean plane of the IP molecule is about 9.30° to the mean plane of the BQ molecule. One of the IP molecules is also involved in Type II halogen bonding[27] with an iodine atom belonging to an IP molecule in an adjacent layer (Figure 5.6c, Figure 5.8). The extensive type II I···I halogen bonding interactions present in this structure are responsible for the distortion of the hydrogen bonded trimer stacks,

potentially resulting in this compound not being isostructural to the 2:1 complexes of the known cocrystals.

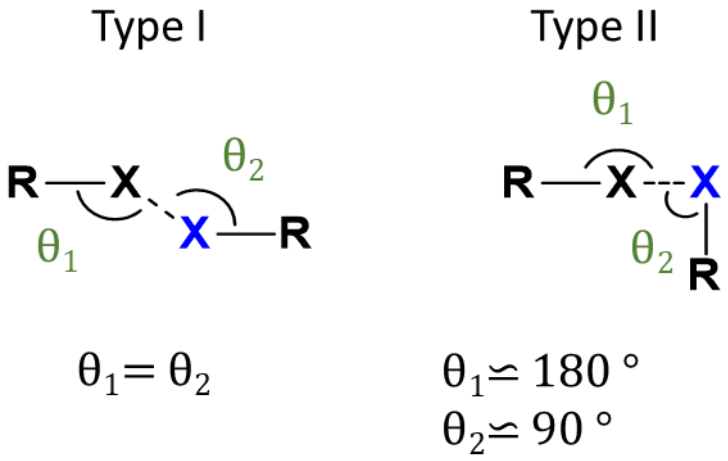

Figure 5.8. Type I and type II halogen-halogen contacts (adapted from ref 27).

Structure of 2:1 β-{4-iodophenol}{*p*-benzoquinone} (β-{2IP}{BQ}). The **β**-polymorph crystallises in the monoclinic crystal system in space group $P2_1/c$, similar to {2BrP}{BQ}, {2ClP}{BQ} and {2FP}{BQ}. However, the packing motif is very different from the other 2:1 forms. The only similarity between these cocrystals lies in the presence of a hydrogen-bonded trimer in the 2:1 complexes. The asymmetric unit consists of a molecule of BQ (two halves) and one molecule of IP. The molecules are arranged in alternating stacks or columns parallel to the *ac* diagonal. The structure also has single layers of BQ molecules that are arranged in a way such that they section trimer motifs from one another (Figure 5.9). The BQ layers are held in place by I···O halogen bonds to both the carbonyl moieties on the BQ molecule. Thus, an infinite hydrogen- and halogen-bonded chain propagates throughout the structure.

The OH···O contact distance in the trimer is 2.749(2) Å, which is slightly longer than most of the H-bonding distances of the same type in the other 2:1 cocrystals. As

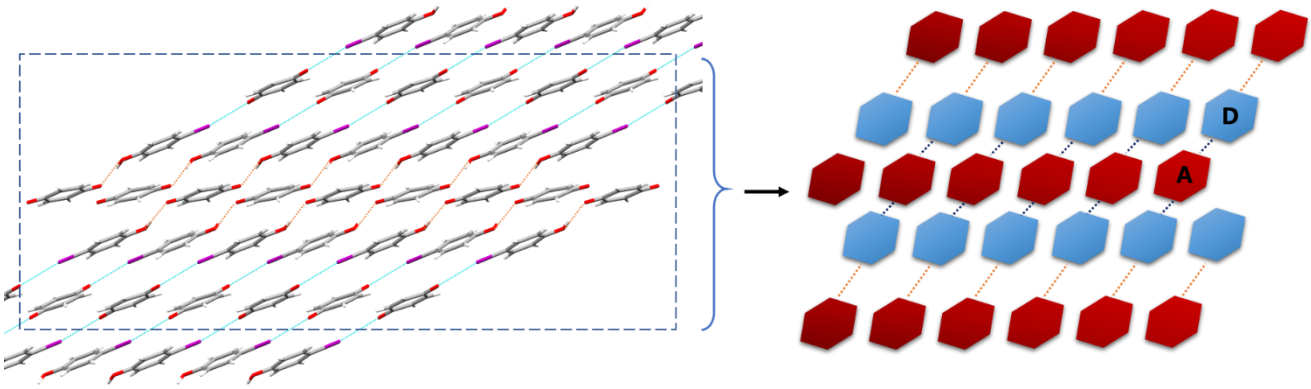

Figure 5.9. Representation of the view down the *c* axis of **β**-{2IP}{BQ}, showing trimers separated by a layer of BQ molecules. Light blue hexagons represent donor IP molecules, red hexagons represent acceptor BQ molecules. Orange contacts show halogen F···O halogen bonding, dark blue contacts show 2:1 H-bonding.

with the rest of the structures, the mean plane of the phenol ring in **β**-{2IP}{BQ} is slightly inclined out of the BQ plane, by 6.08°.

Once again, in order to establish which polymorph is produced by co-grinding the IP and the BQ, a PXRD pattern of a ground sample was collected and compared to simulated patterns of **α**-{2IP}{BQ} and **β**-{2IP}{BQ}**.** It appears as if the **β**-phase forms upon co-grinding of the co-formers, which is also the polymorph obtained by sublimation (Figure 5.10). Additional peaks may be due to a small fraction of the **α**-phase or some residual starting material. Peaks around 25° correspond to unreacted IP, as displayed in Figure 5.10.

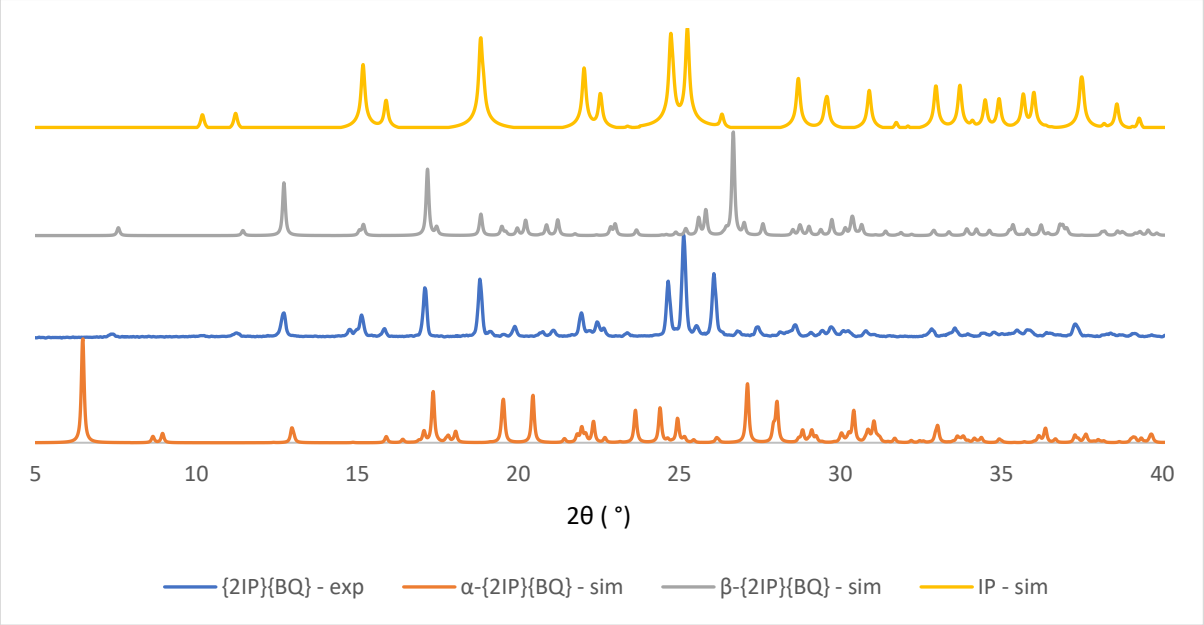

Figure 5.10. A comparison of the {2IP}{BQ} cocrystal produced by neat co-grinding with the simulated PXRD patterns for the two polymorphs **α**-{2IP}{BQ} and **β**-{2IP}{BQ}. It appears as if the polymorph made by neat co-grinding is largely the **β**-phase, the same form as obtained by sublimation.

5.3.2 Structural similarities in {2FP}{BQ}, {2ClP}{BQ} and {2BrP}{BQ}

As mentioned earlier the structures of {2FP}{BQ}, {2ClP}{BQ} and {2BrP}{BQ} have some similarities in their packing arrangements. From the PXRD patterns in Figure 5.7 it is clear that (a) and (b) are isostructural while (c) may be included upon closer inspection of the PXRD patterns. This can be complemented by considering the tabulated unit cell data (Table 5.1). The differences between the PXRD patterns of (c) ({2FP}{BQ}) and (a) ({2ClP}{BQ}) and (b) ({2BrP}{BQ}) are essentially due to the differences in the unit cell dimensions. The unit cell of (c) is marginally smaller than that of (b) and (c), and this is reflected in the PXRD pattern as a shift of peaks to higher 2θ. When the structures of {2FP}{BQ}, {2ClP}{BQ} and {2BrP}{BQ} are overlaid the differences in the atomic positions are observable, but it also shows the similarity in the packing arrangements (viewed along the *b* axis, Figure 5.11). Also shown in Figure 5.11 is the

overlay of the hydrogen bonded trimer for the three cocrystals. All three are superimposable as shown.

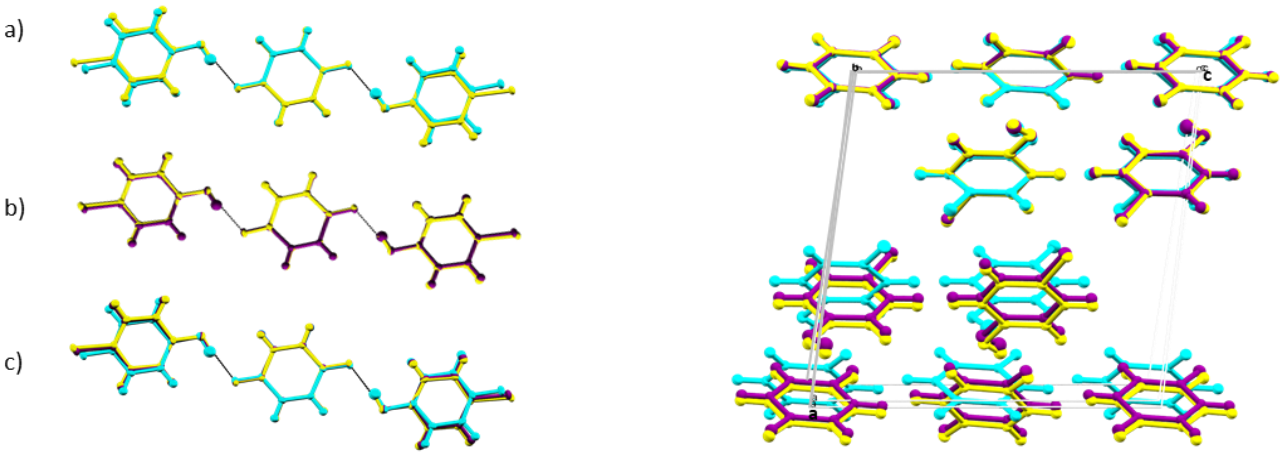

Figure 5.11. Left: overlay of the hydrogen-bonded trimers of the 2:1 forms {2FP}{BQ} (light blue), {2ClP}{BQ} (purple) and {2BrP}{BQ} (yellow) where (a) is an overlay of {2FP}{BQ} and {2BrP}{BQ} with an rms. of 0.0783, (b) an overlay of {2BrP}{BQ} and {2ClP}{BQ} with an rms. of 0.0206 and (c) an overlay of all trimers. Right: An overlay of the unit cells of {2FP}{BQ}, {2BrP}{BQ} and {2ClP}{BQ}. {2BrP}{BQ} and {2ClP}{BQ} overlay with an rms. of 0.0879, whereas {2FP}{BQ} overlays with {2ClP}{BQ} at an rms. of 0.280.

Table 5.1. Crystallographic data for all cocrystals discussed in this chapter.

	α-{1FP}{BQ}	β-{1FP}{BQ}	{1ClP}{BQ}	{1BrP}{BQ}	{2FP}{BQ}
Empirical formula	C_{12} H_9 F O_3	C_{12} H_9 F O_3	C_6H_5ClO,$C_6H_4O_2$	C_6H_5BrO,$C_6H_4O_2$	$C_9H_7FO_2$
M	220.19	219.83	236.64	281.1	166.15
Crystal system	triclinic	monoclinic	triclinic	triclinic	monoclinic
Space group	P1	P21/c	P-1	P-1	P21/c
a (Å)	3.607(4)	3.8511(2)	6.8353(4)	6.8467(5)	11.0335(7)
b (Å)	6.446(8)	5.6370(2)	7.0972(4)	7.1170(5)	5.9058(4)
c (Å)	11.35(1)	22.192(1)	12.2879(7)	12.5065(9)	11.4954(7)
α (°)	91.77(2)	90	93.639(2)	94.746(2)	90
β (°)	98.42(2)	90.522(2)	106.001(2)	104.692(2)	98.597(2)
γ (°)	102.19(2)	90	112.347(2)	112.515(2)	90
V (Å^3)	254.483	481.74(4)	520.40(5)	533.41(7)	740.64(8)
Z	1	2	2	2	4
T (K)	296(2)	100(2)	100(2)	100(2)	100(2)
ρ_{calc} (g cm^{-3})	1.437	1.516	1.51	1.75	1.49
μ(Mo Kα)/mm^{-1}	0.115	0.121	0.353	3.84	0.121
θ range (°)	1.818-28.513	1.835-26.097	3.161-28.348	3.163-28.420	3.787-28.335
Refns.(all)/unique refns.	1861/1077	894/871	2446/2430	2610/2558	1805/1728
R_{int}	0.0464	0.0503	0.0295	0.0148	0.0439
R1	0.0887	0.0511	0.0297	0.0153	0.0461
wR2 (all data)	0.1295	0.1119	0.083	0.0371	0.1108
GoF, S	1.054,1.053	1.074,1.085	1.178,1.178	1.104,1.104	1.103,1.103

	{2ClP}{BQ}	{2BrP}{BQ}	α-{2IP}{BQ}	β-{2IP}{BQ}
Empirical formula	C_6H_5ClO, 0.5($C_6H_4O_2$)	C_6H_5BrO, 0.5($C_6H_4O_2$)	2(C_6H_5IO),$C_6H_4O_2$	C_6H_5IO,$C_6H_4O_2$
M	182.6	227.06	548.09	328.09
Crystal system	monoclinic	monoclinic	monoclinic	monoclinic
Space group	P21/c	P21/c	P21/n	P21/c
a (Å)	11.6009(7)	11.8101(4)	10.805(2)	11.6713(4)
b (Å)	6.0460(3)	6.0966(2)	6.1007(12)	10.3145(4)
c (Å)	11.7339(7)	11.8626(4)	27.322(6)	9.4247(3)
α (°)	90	90	90	90
β (°)	96.987(2)	96.849(1)	92.845(3)	92.9010(10)
γ (°)	90	90	90	90
V (Å^3)	816.89(8)	848.03(5)	1798.9(6)	1133.13(7)
Z	4	4	4	4
T (K)	100(2)	100(2)	100(2)	100(2)
ρ_{calc} (g cm^{-3})	1.485	1.778	2.024	1.923
μ(Mo Kα)/mm^{-1}	0.417	4.798	3.515	2.814
θ range (°)	3.724-26.078	3.460-27.189	2.86-27.06	2.93-27.15
Refns.(all)/unique refns.	1489/1477	1768/1690	3400/2931	2379/2272
R_{int}	0.0312	0.0176	0.0209	0.0134
R1	0.0314	0.0186	0.0257	0.0146
wR2 (all data)	0.076	0.0444	0.0448	0.0332
GoF, S	1.160, 1.160	1.068, 1.068	1.039, 1.039	1.083, 1.083

5.4 Summary

In the late 1960s, two organic charge transfer cocrystals were reported, each having 1:1 and 2:1 ratios, where 4-chlorophenol and 4-bromophenol are electron donors and *p*-benzoquinone is the electron acceptor. In this work, two new cocrystal combinations, each having different forms, are reported, completing the halophenol series with 4-fluorophenol and 4-iodophenol. The {4-fluorophenol}{BQ} cocrystal, {FP}{BQ} yielded a solid solution, a 1:1 cocrystal {1FP}{BQ} and a 2:1 cocrystal {2FP}{BQ}, while the iodophenol derivative yielded only a 2:1 form, {2IP}{BQ}, which has two polymorphs.

Different polymorphs were obtained using different crystallisation techniques – solvent recrystallisation and co-sublimation. Both the 1:1 and 2:1 forms of the two previously reported cocrystals are isostructural: {1ClP}{BQ} to {1BrP}{BQ} and {2ClP}{BQ} to {2BrP}{BQ}. According to the PXRD analysis, the 2:1 form of {FP}{BQ} is isostructural to the 2:1 forms of {ClP}{BQ} and {BrP}{BQ}. However, neither of the forms of {IP}{BQ} are isostructural to the known cocrystals or the new {2FP}{BQ} cocrystal. SCXRD analysis revealed that the **α**-{1FP}{BQ} form has a polar arrangement of the molecules. Type-II halogen···halogen interactions were observed in **α**-{2IP}{BQ}, a feature absent in all other structures in this series of cocrystals. The {1BrP}{BQ} cocrystal does, however, show Br···O halogen bonding. The different forms of {1FP}{BQ} and {2IP}{BQ} emphasises the influence of the solvent molecules on the packing arrangement of the molecules. As a result, liquid-assisted grinding with chloroform (LAG) should be investigated as a co-crystallisation technique whether the polymorphs obtained by recrystallisation from chloroform can be made by LAG with chloroform.

Finally, we were able to produce a range of diverse forms by co-sublimation and recrystallization of a uniform series of halophenols with *p*-benzoquinone. The in-house

designed sublimation apparatus also proved to be of great use since it allowed for the discovery of new forms and polymorphs in the co-crystallisation experiments.

5.5 References

1 G. G. Shipley and S. C. Wallwork, *Acta Cryst.*, 1967, **22**, 585–592.
2 G. G. Shipley and S. C. Wallwork, *Acta Cryst.*, 1967, **22**, 593–601.
3 C. Guo, W. Wang, W. Feng and P. Li, *RSC Adv.*, 2017, **7**, 12775–12782.
4 F. H. Herbstein, *Crystalline Molecular Complexes and Compounds: Structures and Principles*, Oxford University Press Inc, New York, 2005.
5 C. Allen, D. A. Haynes, C. M. Pask and J. M. Rawson, *CrystEngComm*, 2009, **11**, 2048–2050.
6 I. Miroshnyk, S. Mirza and N. Sandler, *Expert Opin. Drug Deliv.*, 2009, **6**, 333–341.
7 N. Qiao, M. Li, W. Schlindwein, N. Malek, A. Davies and G. Trappitt, *Int. J. Pharm.*, 2011, **419**, 1–11.
8 C. B. Aakeroy, S. Forbes and J. Desper, *J. Am. Chem. Soc.*, 2009, **131**, 17048–17049.
9 L. Loots, H. Wahl, L. van der Westhuizen, D. A. Haynes and T. le Roux, *Chem. Commun.*, 2012, **48**, 11507–11509.
10 G. P. Stahly, *Cryst. Growth Des.*, 2009, **9**, 4212–4229.
11 A. V. Trask, J. Van De Streek, W. D. S. Motherwell and W. Jones, *Cryst. Growth Des.*, 2005, **5**, 2233–2241.
12 S. Aitipamula, P. S. Chow and R. B. H. Tan, *CrystEngComm*, 2014, **16**, 3451.
13 C. B. Aakeroy, M. Baldrighi, J. Desper, P. Metrangolo and G. Resnati, *Chem. Eur. J.*, 2013, **19**, 16240–16247.
14 J. Bernstein, *Polymorphism in Molecular Crystals*, Oxford University Press Inc., New York, 2007.
15 G. R. Desiraju, *Cryst. Growth Des.*, 2008, **8**, 3–5.
16 A. J. Cruz-cabeza, S. M. Reutzel-Edens and J. Bernstein, *Chem. Soc. Rev.*, 2015, **44**, 8619–8635.
17 J. Bernstein and A. J. Cruz-Cabeza, *Chem. Rev.*, 2014, 2170–2191.
18 H. G. Brittain, Ed., *Polymorphism in Pharmaceutical Solids*, Informa Healthcare USA, Inc., New York, 2009, vol. 192.
19 A. M. Belenguer, G. I. Lampronti, A. J. Cruz-Cabeza, C. A. Hunter and J. K. M. Sanders, *Chem. Sci.*, 2016, **7**, 6617–6627.
20 R. Kuroda, T. Sato and Y. Imai, *CrystEngComm*, 2008, **10**, 1881–1890.
21 J. W. Steed and J. L. Atwood, Eds., *Encyclopedia of Supramolecular Chemistry*, Taylor & Francis Group, LLC, Boca Raton, USA, 1st edn., 2004.
22 D. Tan, L. Loots and T. Friščić, *Chem. Commun.*, 2016, **52**, 7760–7781.
23 T. J. Chiya and A. Lemmerer, *CrystEngComm*, 2012, **14**, 5124–5127.
24 S. Skovsgaard and A. D. Bond, *CrystEngComm*, 2009, **11**, 444–453.
25 P. Dechambenoit, S. Ferlay, N. Kyritsakas and M. W. Hosseini, *Chem. Commun.*, 2009, 1559–61.
26 M. C. Etter, J. C. MacDonald and J. Bernstein, *Acta Cryst.*, 1990, **B46**, 256–262.
27 P. Metrangolo and G. Resnati, *IUCrJ*, 2014, **1**, 5–7.

Chapter 6

Summary, Conclusion and Future Work

BE NOT THE FIRST BY WHOM THE NEW ARE TRIED,
NOR YET THE LAST TO LAY THE OLD ASIDE.

-- ALEXANDER POPE

In an investigation into cocrystal formation of organic (magnetic) materials, a series of dithiadiazolyl radicals were synthesised and co-crystallised with one another. Two co-crystallisation methods were employed - sublimation and melt co-crystallisation, however no {DTDA}{DTDA} cocrystals were found using the DTDA combinations chosen for the co-crystallisation experiments in this study. Whether this is due to an unfavourable co-former combination or incorrect crystallisation conditions is uncertain. In addition to the experimental co-crystallisations, a parallel computational study was conducted on both the pre-existing cocrystals as well as co-former combinations that proved unsuccessful in the past. Theoretical gas-phase binding energies (E_{bind}) were calculated, using the Gaussian09 software, of the two previously known {DTDA}{DTDA} cocrystals as well as the new third one, found by a fellow colleague James P. O'Connor, reported in this text. This was done to study the favourability of the homodimers of the co-formers compared to the heterodimers of the cocrystals, and try to answer the question – "homodimer or heterodimer?" The same theoretical gas-phase binding energies were calculated for a series of attempted/*failed* cocrystal combinations, which were modelled as *cis*-oid dimers (like the known cocrystals). For all the above-mentioned combinations, *failed* and known, the coupling energy was calculated. This gives an indication of the relative stability of the cocrystal to the co-formers: a negative coupling energy indicates that the heterodimer is more stable than the respective homodimers.

It was firstly observed that for all three known cocrystals, E_{bind} for the heterodimers (cocrystals) was consistently more stabilising than for the homodimers of the co-formers, and all the coupling energies were strongly stabilising and in the range of -2.8 to -5.6 kcal/mol. This was encouraging, since it was evident that the cocrystals are more stable as dimers than their co-formers. The *failed* cocrystal results were a little more challenging to interpret in that, in 6 cases out of 7, heterodimer energies were more stabilising than the homodimers of the

co-formers, and in all cases $E_{coup} < 0$, implying that heterodimer (cocrystal) formation should be favourable. If the coupling energies of the known cocrystals are an indication of the range where cocrystals are likely to be observed (favourable) for these DTDAs, then this may be an indication as to why these combinations are not seen – the coupling energy may simply not be favourable enough.

Since the last cocrystal to be found had the lowest coupling energy (-2.78 kcal/mol), it could be postulated that cocrystal formation would ideally be seen in combinations with coupling energies lower than -2.8 kcal/mol. This may be why a cocrystal is not seen for the combinations **F2, F3**, **F6** and **F7**, since their coupling energies are all less favourable than this. Although the energy of **F4** indicates that this combination is favourable and cocrystal formation likely, there may be other factors hindering cocrystal formation. For example, the perfluoro-PAHRIZ dimer was forced into the *cis*-oid dimer mode, in order to be able to compare it to the other systems, which are all *cis*-oid in nature, where in actual fact it is a *trans*-antarafacial dimer in the solid-state structure. This could result in a false stabilising effect. Lack of observed cocrystal formation in the combination **F1** may be due to the lack of strong-enough structure directing interactions, or the right co-crystallisation conditions have simply not been found. Then, that leaves **F5**. The energies observed for this combination indicates that possibly it warrants further investigation. Not only does it have a stabilising coupling energy (-6.037 kcal/mol), but the R-group on these two radicals shows the potential for very favourable pyridyl···perfluoropyridyl stacking interactions.

Periodic calculations (calculations on the crystal structure as opposed to a simple dimer in the gas phase) were also carried out on the known DTDA cocrystals, in order to study additional interactions, present in the overall stabilisation of the structure, that may influence cocrystal formation. The results compared well with the gas-phase energies in that the

cocrystals are consistently more stabilising than their co-formers. It can be seen that the interactions that stabilise the dimers in the gas phase also translate into the crystal structure. The gas phase calculations ranked the energetic stabilities of the co-formers as **1**<**2**<**3**<**4** and the cocrystals as **7**<**5**<**6**, whereas the periodic calculations ranked the stabilities of the co-formers as **1**<**3**<**2**<**4** and the cocrystals as **6**<**5**<**7**. Although these differences could be attributed to differences in the level of theory used to calculate these values, it could also mean that, especially in the case of radicals **2**, **3**, **6** and **7**, the lattice interactions which are not intra-dimer binding energies may have a larger influence on the self-assembly of these structures than in the case of **1**, **4** and **5** (whose relative order does not change from the gas phase to the periodic system). Radicals **2**, **3**, **6** and **7** should be studied more carefully to establish whether there are interactions present that could be exploited for further DTDA co-crystallisation studies.

The fact that all the heterodimers (gas phase) and cocrystals (periodic) are very stable, and more so than their co-formers, may in fact not be a desired result for these systems. It was mentioned in Chapters 1 and 3 that these radicals tend to dimerise (spin-pair) undesirably in the solid state, as do all the known cocrystals, which results in the material losing its magnetic properties. So, perhaps a favourable dimer is not the desired scenario? Perhaps more attention should be given where *cis*-oid dimers are unfavourable, since that material/co-former combination would potentially prefer to be monomeric. If the *cis*-oid dimer is unfavourable, then potentially the co-formers prefer to not pack that way, and may arrange themselves in the solid state, through other strong structure-directing interactions, to be monomeric (like radicals **1** and **2**), or even *trans*-antarafacial (which could be a step in the direction towards a monomeric species).

Two DTDAs were also co-crystallised with the TEMPO radical and *p*-benzoquinone as a starting point to investigate co-crystallisation of DTDAs with other radical or radical-forming compounds that do not show the same potential to spin-pair as {DTDA}{DTDA} combinations do. Both co-crystallisations were done by sublimation. The combination {4-phenyl-DTDA}{*p*-benzoquinone} simply resulted in the co-formers crystallising out separately, and was not investigated any further since cocrystal formation seemed unlikely. The combination {4'-(2,6-difluorophenyl)-DTDA}{TEMPO} behaved similarly, and no cocrystal formation was seen. The TEMPO radical was then co-crystallised with *p*-benzoquinone and 2,3-dichloro-5,6-dicyanobenzoquinone. Although {TEMPO}{*p*-benzoquinone} yielded no cocrystal, a new cocrystal was formed from the {TEMPO}{2,3-dichloro-5,6-dicyanobenzoquinone} combination. The cocrystal was also successfully made by co-grinding of the co-formers. A number of characterisation techniques indicate the formation of cocrystal, including an immediate colour change on mixing the two co-formers. Clear changes were also observed in the PXRD pattern and IR spectra. However, cocrystal formation still needs to be confirmed by SCXRD when single crystals for this combination are obtained.

Some {DTDA}{DTDA} combinations, for instance the {4'-(4-cyanoperfluorphenyl)-DTDA}{4'-(4-bromoperfluorphenyl)-DTDA}, show the potential for strong synthon interactions (like Br···S, Br···N, CN···S) that could provide some structure-directing forces for cocrystal formation of a (potentially) monomeric cocrystal. Further study on this combination is encouraged. Additionally, calculations on some *failed* cocrystal combinations indicated that the {4'-(2,3,5,6-tetrafluoropyrid-4-yl)-DTDA}{4'-(pyrid-2-yl)-DTDA} (**F5**) combination warrants further investigation, possibly altering co-crystallisation conditions more carefully, since cocrystal formation is likely. Future work should also focus on obtaining single crystals of the {TEMPO}{2,3-dichloro-5,6-dicyanobenzoquinone} cocrystal combination to compare with

PXRD data and confirm cocrystal formation. If single crystals cannot be obtained, attempts should be made to solve the structure from the powder data*.

Radical **3** (4'-(2,6-difluorophenyl)-DTDA) is known to be polymorphic, with three reported polymorphs. To our knowledge, no work has been published on the behaviour of these polymorphs in terms of possible phase changes or relative stabilities. Since interesting results were observed during full characterisation of these three polymorphs, further investigation was carried out. DSC thermograms clearly indicated a phase change of **3γ** to **3β** upon heating. Heating and cooling of a sample of **3γ** was cycled up to six times to establish whether this phase change is reversible, or whether conversion to another phase might be observed, however, the **3β** melt isotherm remains for at least six cycles. Analysis on **3α** could not be carried out since, although sample of **3α** was indeed successfully synthesised, it is suspected that **3α** undergoes a phase change to **3γ** either due to air exposure or over time. This resulted in a batch of **3α** left in a schlenk for a few days yielding only crystals of **3γ** in the same schlenk. Due to challenges with the synthesis of **3**, and time constraints, material of **3α** could not be obtained in time to complete the full study on the polymorphic conversion.

In order to complete the analysis on the three polymorphs of radical **3**, future work will entail making more sample of **3α** to collect thermal data (DSC) on it, in order to establish whether conversion to **3γ** does take place upon heating, and if not, what factors cause the conversion. VT-PXRD experiments also need to be conducted on all three phases, this time with a glass capillary with a larger internal diameter (for example 2.5 mm instead of 0.5 mm), to follow the polymorph conversion over the temperature range established by the DSC trace.

* Since writing this chapter as well as chapter 3, single crystals were found and co-crystallisation confirmed using SCXRD. However, analysis is still ongoing and the data will therefore not be presented in this thesis, due to time constraints.

A series of cocrystals between *p*-benzoquinone (BQ) and a range of halogenated phenols (XP) was also investigated. In 1967 the first two cocrystal in this series were reported – {4-chlorophenol}{BQ} ({ClP}{BQ}) and {BQ}{4-bromophenol} ({BrP}{BQ}). Both combinations had cocrystals with both a 1:1 and 2:1 donor-acceptor ratio, and were observed to be isostructural in the case of both the 1:1 and 2:1 forms. To complete this series and investigate the influence of the halogen on the structure, BQ was co-crystallised with 4-fluorophenol (FP) and 4-iodophenol (IP). A 1:1 and 2:1 cocrystal were obtained for the fluorinated derivative ({1FP}{BQ} and {2FP}{BQ}), and only a 2:1 form for the iodated derivative ({2IP}{BQ}). {1FP}{BQ} and {2IP}{BQ} were both found to be polymorphic, each having two polymorphs – unlike the previously reported cocrystals, which are not known to be polymorphic. The two polymorphs were obtained using two different crystallisation techniques – solvent crystallisation and sublimation. XRD analysis also revealed a solid solution in **β**-{1FP}{BQ}, and **α**-{1FP}{BQ} was found to be a polar structure. Type-I as well as type-II halogen contacts were observed in **α**-{2IP}{BQ}, a feature absent in all other structures in this series of cocrystals. The {1BrP}{BQ} cocrystal does, however, show Br···O halogen bonding. Although the two previously-reported cocrystals are isostructural to one another, in both the 1:1 and 2:1 forms, neither the **α** nor **β** polymorphs of {1FP}{BQ} or {2IP}{BQ} were found to be isostructural to the known cocrystals, despite **α**-{2IP}{BQ} showing some striking structural similarities to the known cocrystals. {2FP}{BQ} was, however, found to be isostructural to {2ClP}{BQ} and {2BrP}{BQ} It is clear that, although a series of structures may appear to be similar in their molecular architecture, a range of diverse properties can still be observed.

Future work on the {BQ}{XP} cocrystals should include VT-PXRD analysis to characterise any possible phase changes in the novel cocrystal combinations. UV/Vis analysis also needs to be carried out to quantify the charge-transfer character of these cocrystals. Additionally, some

experiments on {FP}{BQ}, {BrP}{BQ} and {ClP}{BQ} should be carried out to determine whether interconversion between the 1:1 and 2:1 phases is possible by mechanochemical methods. This will be done by adding a molar equivalent of the appropriate component and grinding, whereafter PXRD analysis will be used to establish whether a 1:1→2:1→1:1… conversion can be observed. Selectivity experiments will also be carried out mechanochemically, to establish whether BQ shows preferential cocrystal formation with one of the four halogenated derivatives.

Overall, this study showed us that cocrystal formation, especially in the gas phase, is something not yet fully understood. However, preliminary experimental and computational results on the co-crystallisation of DTDAs are a step in the right direction towards understanding the driving forces of cocrystal formation. It has also become clear that, potentially co-crystallising DTDAs with one another may not be the best option for preventing dimerisation since, as the periodic lattice energy calculations showed, a very significant portion of the lattice energy comes from the binding energy. This may only be overcome by providing a DTDA co-former with a partner not able to dimerise with it. From the structure property relationship study on the {*p*-XP}{BQ} cocrystals, we observed great versatility in the structures where fluorines and iodines are used as supramolecular synthons. The effect of these two halogens on the structure of a material could also be further exploited in cocrystal formation with DTDAs since they may provide unique results for the crystal engineering of DTDA cocrystals, as well as cocrystals in general.